8-2-2003

The Design and Evaluation of a Continuous Photocatalytic Reactor Utilizing Titanium Dioxide in Thin Films of Mesoporous Silica

Transito Lynne Macias

THE DESIGN AND EVALUATION OF A CONTINUOUS PHOTOCATALYTIC REACTOR UTILIZING TITANIUM DIOXIDE IN THIN FILMS OF MESOPOROUS SILICA

By

Transito Lynne Macias

A Thesis
Submitted to the Faculty of
Mississippi State University
in Partial Fullfillment of the Requirements
for the Degree of Master of Science
in Chemical Engineering
in the Dave C. Swalm School of Chemical Engineering

Mississippi State, Mississippi

August 2003

THE DESIGN AND EVALUATION OF A CONTINUOUS PHOTOCATALYTIC

REACTOR UTILIZING TITANIUM DIOXIDE IN THIN FILMS

OF MESOPOROUS SILICA

By

Transito Lynne Macias

Approved:

_____	_____
Irvin A. Jefcoat Professor of Chemical Engineering (Director of Thesis)	Mark E. Zappi Graduate Coordinator for the Dave C. Swalm School of Chemical Engineering Professor of Chemical Engineering (Committee Member)
_____	_____
Kirk H. Schulz Director of the Dave C. Swalm School of Chemical Engineering Professor of Chemical Engineering (Committee Member)	R. Mark Bricka Associate Professor of Chemical Engineering (Committee Member)

_____

Wayne Bennett
Dean of the College of Engineering

Name: Transito Lynne Macias

Date of Degree: August 2, 2003

Institution: Mississippi State University

Major Field: Chemical Engineering

Major Professor: Dr. I. Atly Jefcoat

Title of Study: THE DESIGN AND EVALUATION OF A CONTINUOUS PHOTOCATALYTIC REACTOR UTILIZNG TITANIUM DIOXIDE IN THIN FILMS OF MESOPOROUS SILCA

Pages in Study: 125

Candidate for Degree of Master of Science

Titanium dioxide (TiO_2) is an established photocatalyst utilized for the photo-oxidation of organics in wastewater. Aqueous suspensions of TiO_2 require expensive recovery and re-suspension steps to be utilized on an industrial scale. To harness the photocatalytic power of TiO_2 and avoid recovery and re-suspension mechanisms, Mr. William Adams and Dr. Martin G. Bakker immobilized titanium dioxide within the mesoporous structure of thin films of silica at the University of Alabama. The objective of this thesis was to design and evaluate a bench-scale, continuous, photocatalytic reactor utilizing the thin films of titanium dioxide in mesoporous silica as developed at the University of Alabama. This was accomplished in two phases of work: (I) batch reactions and (II) continuous reactions. Experimental conditions were as follows: medium-pressure, ultra-violet light (UV); TiO_2 in either 0.05 wt% suspensions (slurry) or thin films of mesoporous silica (film); and/or 750 ppm hydrogen peroxide (H_2O_2).

In batch and continuous experiments the UV/H_2O_2 and UV/TiO_2(slurry)/H_2O_2 system were the most successful with respect to the oxidation of 2,4-dichlorophenol (2,4-DCP). The loss of 2,4-DCP in continuous UV/TiO_2(film) systems was not significantly different from continuous UV only systems. However, the continuous UV/TiO_2(film)/H_2O_2 systems degraded more 2,4-DCP than systems utilizing UV light alone.

DEDICATION

This thesis is dedicated to the two men without whom it would not have been possible: Dr. Irvin A. Jefcoat and Dr. David E. James. Without them, this project would not be complete and I would not have retained the little sanity with which I have been blessed. I will forever be indebted to both of them for their patience, support, guidance, motivation, and love throughout my graduate career, when I needed it the most.

ACKNOWLEDGMENTS

First, I must thank all of those who have funded this project: the Alliance for Graduate Education in Mississippi (AGEM), the National Consortium for Graduate Degrees for Minorities in Engineering and Science (GEM), Eastman Chemical, Hunter Henry, and the Gulf Coast Hazardous Substance Research Center. I must also express my sincere gratitude to my committee members, namely, Dr. R. Mark Bricka, Dr. Kirk Schulz, and Dr. Mark Zappi, for sharing their expertise throughout the development of this project, and to Dr. Martin Bakker and Mr. William Adams, for all of their efforts towards the realization of this thesis. Further, I owe a very special thanks to Dr. Rafael Hernandez, an analytical Yoda, Tieling Xie, a great person with whom to share a lab, and the undergraduates who have worked so diligently on this project: John McGillivray, Trent Jefferies, Scott Junkin, Christopher Robinson, Erica Huntley, Kenyatta Veals, Krystal Gage, and, most especially, Otho Barnes, Jr., who has worked on this project since its inception. I must acknowledge all of my friends who have given me unending support, understanding, courage, and, most especially, perspective: Julie, Steven, Stephen, Rochelle, Lee, Katriana, Chuck, and Katherine. I must also thank my parents for giving me the faith on which I survive and my brothers who, through all of their actions, inspire me to be a better person. I cannot over emphasize my appreciation for Dr. and Mrs. Jefcoat, whom have both left an indelible mark on my soul. Finally, it is impossible to articulate the impact of Dr. David James, who gives each day more meaning.

TABLE OF CONTENTS

LIST OF TABLES

LIST OF FIGURES

LIST OF SYBMOLS AND ABBREVIATIONS

2,4-DCP: 2,4-dichlorohpenol, the model compound

[DCP]: the concentration of 2,4-dichlorophenol in solution

$[DCP]_o$: the initial concentration of 2,4-dichlorophenol in solution

H_2O_2: hydrogen peroxide

k: the Langmuir-Hinshelwood specific reaction rate constant

K: the Langmuir-Hinshelwood adsorption equilibrium constant

k_{p-1}: pseudo-first order reaction rate constant

ppm: parts per million; equivalent to milligrams of a given species per liter of water

TiO_2: titanium dioxide from Degussa Corporation

TiO_2(slurry): aqueous solutions of 0.05 wt% TiO_2 in suspension

TiO_2(film): a thin film of titanium dioxide in mesoporous silica as developed at the University of Alabama

UV: ultra-violet light

CHAPTER I.

INTRODUCTION

This thesis is part of a collaborative project between Mississippi State University and the University of Alabama. The end goal of this collaborative endeavor is the realization of a continuous, industrially applicable, photochemical reactor utilizing immobilized titanium dioxide (TiO_2) capable of degrading wastewater contaminants to mineralization products. Titanium dioxide is a well-established photocatalyst that has been utilized for the photo-oxidation of a wide range of organics in wastewater (Chang et al., 2000; Bahnemann, 1999; EPA, 1998; Suri et al., 1993). Titanium dioxide is most often suspended in batch solutions, which would require expensive recovery and re-suspension steps to be utilized on an industrial scale. In an effort to simultaneously harness the photocatalytic power of titanium dioxide and avoid costly recovery and re-suspension mechanisms, Mr. William Adams and Dr. Martin G. Bakker have immobilized titanium dioxide within the mesoporous structure of thin films of silica at the University of Alabama. Having established the photoreactivity of these films of titanium dioxide in mesoporous silica, parameters currently being evaluated at Alabama include the effect of film thickness and titanium dioxide loading on photoreactivity. Work at Mississippi State has focused on the design and evaluation of a

bench-scale, continuous, photo-catalytic reactor utilizing the thin films of titanium dioxide in mesoporous silica being developed at Alabama. Both institutions are evaluating their work based on the degradation of 2,4-dichlorophenol (2,4-DCP). 2,4-DCP was chosen as a model compound because its chlorinated aromatic structure is representative of many toxic, recalcitrant contaminant species present in hazardous waste and ground water. Additionally, the analysis of 2,4-DCP via high-pressure liquid chromatography is consistent and reliable.

This thesis details the bench-scale work completed at Mississippi State towards the development of a continuous, industrially applicable reactor employing ultra-violet (UV) light and immobilized titanium dioxide to degrade wastewater contaminants to mineralization products.

CHAPTER II.

LITERATURE REVIEW

As environmental regulations continue to become more stringent, technologies capable of destroying hazardous compounds gain more attention (Bahnemann, 1999; Hoffman et al., 1995). Traditional separation mechanisms, such as carbon absorption and air stripping, both magnify the associated hazardous compound's risk and require further treatment of concentrated contaminant streams (landfilling, carbon regeneration, recovery) (Jardim et al., 1997; Hoffman et al., 1995). The ability of Advanced Oxidation Processes (AOPs) to treat a wide range of hazardous wastes has brought this technology to the forefront of research over the last twenty years (Rupert and Bauer, 1994; Ku and Hsieh, 1992; Ollis and Turchi, 1990). Utilizing the hydroxyl radical (OH*), a powerful oxidizing species, AOPs can degrade hydrocarbon fuels, halogenated solvents, explosives and their byproducts, phenols, aromatic carboxylic acids, simple aromatics, aliphatic alcohols, microbes, surfactants, and pesticides to mineralization products: carbon dioxide (CO_2), water, and mineral salts (Chang et al., 2000; EPA, 1998; Bahnemann, 1999; Suri et al., 1993).

Advanced Oxidation Processes (AOPs)

Advanced Oxidation Processes (AOPs) exploit highly reactive but transient radicals to non-selectively degrade low levels of contaminants in aqueous and gaseous systems (Chang et al., 2000; EPA, 1998; Suri et al., 1993). Although the formation of several different radicals is possible, the success of AOPs is attributed specifically to the hydroxyl radical (OH*) (Suri et al., 1993). As illustrated in Table 2.1, the hydroxyl radical is one of the most powerful oxidizing species available (EPA, 1998; Legrini et al., 1993). Utilization of this oxidation power results in reactions that are a billion times faster than reactions with typical oxidants such as ozone (O_3) or hydrogen peroxide (H_2O_2) (EPA, 1998).

The oxidation mechanisms associated with AOPs may be homogeneous or heterogeneous (Suri et al., 1993). Homogeneous systems utilize some combination of hydrogen peroxide, ozone, and ultra-violet (UV) light while heterogeneous advanced oxidation reactions make use of UV light and a semiconductor such as titanium dioxide (TiO_2), strontium titanium dioxide ($SrTiO_2$), iron oxide (Fe_2O_3), cadmium sulfide (CdS), zinc sulfide (ZnS), or zinc oxide (ZnO) (Bahnemann, 1999; EPA, 1998; Hoffman et al., 1995; Suri et al., 1993). Homogeneous and heterogeneous processes that include ultra-violet light are described as photochemical processes (EPA, 1998).

Photocatalysis

Semiconductors are photo-reactive metal oxides employed in heterogeneous, photochemical AOPs for the eradication of contaminants and are referred to as photocatalysts (Munter et al., 2001; EPA, 1998; Suri et al., 1993). Semiconductors are characterized by a filled, low-energy valence band and an empty, high-energy conduction band (Bahnemann, 1999; EPA, 1998). Electrons cannot exist in the band-gap region between the valence band and the conduction band (EPA, 1998). When exposed to the appropriate wavelength of ultra-violet light, electrons in the low-energy valence band will absorb the photon's energy, become excited, and move into the high-energy conduction band (EPA, 1998). The result of this electron excitation is a hole, or positive charge, in the valence band (h^+_{VB}) and an electron in the conduction band (e^-_{CB}) (EPA, 1998). This electron-hole pair is in an unstable, excited state and will revert to its original state within nanoseconds, releasing the energy of the absorbed photon as heat (EPA, 1998). However, the semiconductor's unique band gap region slows recombination long enough to allow both the electron and the hole to react with species adsorbed on the semiconductor's surface (EPA, 1998).

Titanium Dioxide (TiO_2)

Due to its high level of photoconductivity, ready availability, and low cost, titanium dioxide is the most frequently employed semiconductor in

heterogeneous, photocatalytic AOPs (EPA, 1998; Legrini et al., 1993; Munter et al., 2001). Further, titanium dioxide/UV systems have been developed for a variety of chemical species with much success (Legrini et al., 1993). However, the fatal flaw of heterogeneous titanium dioxide/UV AOPs is photocatalyst recovery: suspended titanium dioxide particles have a very slow settling rate and must be centrifuged or microfiltered, neither of which are economically advantageous separation mechanisms (Legrini et al., 1993; Chang et al., 2000; Matthews, 1987; Hoffman et al., 1995). To establish a viable titanium dioxide/UV system, the photocatalyst must be immobilized; options for immobilization include both the integration of titanium dioxide within thin films, mesh structures, or ceramics in plug-flow reactors and titanium dioxide covered supports, such as glass beads or tubes, in fluidized-bed reactors (Chang et al., 2000; Legrini et al., 1993; Hoffman et al., 1995).

Three crystalline configurations of titanium dioxide exist: anatase, rutile, and brookite (EPA, 1998). The rate of formation of the hydroxyl radical is dependent upon the crystalline forms of titanium dioxide present (EPA, 1998). Of the three possible configurations of titanium dioxide, the anatase form has the highest level of photoconductivity with a band gap of 3.2 electron volts (EPA, 1998; Munter et al., 2001). Rutile is considered much less photo-reactive than anatase (Bahnemann, 1999; Munter et al., 2001). This is attributed to a more efficient recombination of the electron-hole pair and a smaller surface area in the rutile structure (Munter et al., 2001). Some

research has indicated that there may be an optimum combination of rutile and anatase crystals for photocatalysis (Ollis and Turchi, 1990). Degussa P25 is a commercially available 70:30 mixture of anatase and rutile crystals and is generally accepted as the standard photocatalytic form of titanium dioxide (Bahnemann, 1999; Hoffman et al., 1995; Legrini et al., 1993). Degussa P25 has an average surface area of 55 +/- 15 square meters per gram and crystalline sizes range from 30 nanometers to 0.1 millimeters in diameter.

The key to semiconductor-induced reactions is a light source that will emit photons at the optimum wavelength for excitation of valence band electrons, an optimum that varies between semiconductors (EPA, 1998). To excite titanium dioxide's valence band electrons, a light source must have a wavelength shorter than 387.5 nanometers to overcome the band-gap energy (EPA, 1998; Munter et al., 2001; Bahnemann, 1999). Medium-pressure, ultra-violet lamps provide the most effective source of photons for titanium dioxide systems, emitting wavelengths concentrated in the 200 to 400-nanometer range. Wavelengths shorter than 387.5 nanometers are emitted by the sun but in a much less concentrated and consistent manner, making the utilization of solar energy possible but much less advantageous than artificial sources (Legrini et al., 1993).

Photochemical Oxidation via TiO_2

Oxidation is the mechanism whereby a chemical species loses electrons (Kotz and Treichel, 1996). To maintain balance within a system, the loss of electrons in an oxidation reaction must be complemented by the gain of electrons in a reduction reaction; "redox" refers to this pair of reactions. The proposed mechanism by which organic contaminants are photochemically oxidized via titanium dioxide is outlined in Table 2.2. This mechanism was proposed by Turchi and Ollis (1990) and is referenced throughout literature (Serra et al., 1994; Suri et al., 1993).

Photochemical oxidation is initiated when TiO_2 particles absorb photons of ultra-violet light and become excitated (Turchi and Ollis, 1990; EPA, 1998; Bahnemann, 1999). When excited by photons of UV light, an electron-hole pair will form within the semiconductor as expressed by reaction 1 in Table 2.2 (Turchi and Ollis, 1990; Suri et al., 1993). The electron-hole pair will then either (i) recombine, returning to its original, unexcited state, and release the absorbed photon's energy as heat (reaction 5) or (ii) migrate to the surface and react with adsorbed species (Turchi and Ollis, 1990; Hugul et al., 2002). The electron-hole pair are very powerful reagents: versus a normal hydrogen electrode, the conduction-band electron has a reducing power of +0.5 to -1.5 volts and the valence-band hole has an oxidizing power of +1.0 to +3.5 volts (Bahnemann, 1999; Hoffman et al., 1995). To prevent

recombination, the electron-hole pair must be separated: the electron (e_{CB}^-) or hole (h_{VB}^+) must be "trapped" by surface adsorbates (Turchi and Ollis, 1990).

In aqueous solutions, dissociated and molecular water will readily bind to the surface of titanium dioxide (Reactions 2a, & 2b) (Turchi and Ollis, 1990; EPA, 1998). Adsorbed hydroxide ions and water molecules form hydroxyl radicals through an oxidation mechanism whereby they "trap" holes, as in reactions (6a) and (6b), initiating a complex sequence of redox reactions at the solid-liquid interface.

To promote the oxidation of titanium dioxide and thereby increase its photocatalytic activity, irreversible electron acceptors must be present (EPA, 1998). Irreversible electron acceptors are reducible species that will enhance system efficiency by maintaining a charge balance within the system and preventing recombination of the critical electron-hole pair (Munter et al., 2001; EPA, 1998; Hoffman et al., 1995). Both oxygen and hydrogen peroxide are excellent irreversible electron acceptors and can be easily added to the photocatalytic system matrix. As illustrated in Reactions 8b and 13, the oxidation of titanium results in superoxide ions, which are further reduced to hydrogen peroxide (Turchi and Ollis, 1990). When added to the ultra-violet light/titanium dioxide system, hydrogen peroxide will both inhibit the recombination of the electron-hole pair and generate an additional hydroxyl radical by consuming the conduction band electron (16) (EPA, 1998).

$$H_2O_2 + e^-_{CB} \rightarrow OH^- + OH^* \qquad (16)$$

It should be noted that hydrogen peroxide could also absorb photons from ultra-violet light to produce two hydroxyl radicals via photolysis, as in reaction 17 (Legrini et al., 1993; EPA, 1998; Bahnemann, 1999; Hoffman et al., 1995):

$$H_2O_2 + h\nu \rightarrow 2OH^* \qquad (17)$$

Reaction 17 does not involve titanium dioxide and can be utilized as its own advanced oxidation process (Bahnemann, 1999).

In addition to dissociated and molecular water molecules, contaminant species will also adhere to the surface of TiO_2 particles (Reaction 3) (Turchi and Ollis, 1990). However, non-aqueous UV/TiO_2 systems (organic solutions without water) have been unsuccessful, and therefore the direct interaction between the hole and organic molecule (Reaction 7) is not considered significant. Further, the abundant nature of the hydroxide ions and water molecules in aqueous solutions makes Reactions 6a and 6b much more probable.

While it is clear that hydroxyl radicals are produced at the titanium dioxide surface, the radicals may either remain adsorbed on the titanium dioxide surface or diffuse into solution. The hydroxyl radical could oxidize the organic contaminant molecule in one of four pathways (Turchi and Ollis, 1990):

- *Case I* (Reaction 9): The hydroxyl radical will remain adsorbed on or within close proximity of the titanium dioxide surface and will attack an adsorbed contaminant molecule.

- *Case II* (Reaction 10): The hydroxyl radical will diffuse into solution and attack an adsorbed contaminant molecule.
- *Case III* (Reaction 11): The hydroxyl radical will remain adsorbed on or within close proximity of the titanium dioxide surface and attack a nearby contaminant molecule in solution.
- *Case IV* (Reaction 12): The hydroxyl radical will diffuse into solution and attack a contaminant molecule also in solution.

The highly reactive nature of the hydroxyl radical makes it difficult to distinguish between Cases I and II. If the radical does diffuse into solution, as in Case II, it will react so rapidly that the net effect is the same as in Case I (Turchi and Ollis, 1990). The appearance of degradation byproducts consistent with those that appear via the degradation of aromatics by known sources of hydroxyl radicals further supports the hydroxyl radical formation theory (Bahnemann, 1999; Matthews, 1987).

The nature of the contaminant species dictates the hydroxyl radical's initial attack: in the case of alkanes and alcohols, the radical will abstract a hydrogen atom to form water (18) or in the case of aromatic compounds, the radical will attach itself to the contaminant species (Munter et al., 2001). In the case of hydrogen abstraction, organic radicals will combine with molecular oxygen to yield peroxyl radicals (19) which will in turn initiate chain reactions of oxidative degradation eventually leading to mineralization products.

$$HO^* + RH \rightarrow R^* + H_2O \qquad (18)$$

$$R^* + O2 \rightarrow RO^* \quad (19)$$

Research by Turchi and Ollis (1990) indicates that aromatic molecules adsorb to surface hydroxyls rather than directly to the titanium dioxide surface thereby implying that aromatic species are attacked via Reaction 11. Some contaminant species may seem to be instantaneously mineralized, while larger, more complex contaminant species (for example, halogenated aromatics) involve several intermediates before mineralization is realized. Most partially oxidized intermediates are alcohols, which are strongly attracted to titanium dioxide and can therefore be easily oxidized by hydroxyl radicals on or near the surface of the titanium.

Kinetics

Chemical kinetics describe the study of both the mechanism and rate of a chemical reaction (Smith, 1970; Hill, 1977). A chemical reaction occurs when a chemical species' identity is lost via a change in the number and/or type of atoms present and/or a change in its molecular structure (Fogler, 1999). A reaction mechanism describes each event required to produce a given chemical reaction (Smith, 1970). The reaction rate, r_A, is the molar quantity of a chemical species that is produced or consumed in a chemical reaction per unit time per unit volume; heterogeneous reaction rates are often expressed in units of catalyst weight or surface area instead of volume (Smith, 1970; Fogler, 1999). The appearance and disappearance of species

A are differentiated by positive and negative values of r_A, respectively (Fogler, 1999). Reaction rate depends on the concentrations of the chemical species present, temperature, pressure, and catalyst, if any, but is independent of the type of reaction system (i.e., batch or continuous) (Fogler, 1999). The relationship between the reaction rate and concentration must be determined experimentally and can often be written as a product of the reaction rate constant and a function of the concentrations of the reactant species (Fogler, 1999). Given reaction 20, a rate law describing the disappearance of species A may be written in terms of its reactants as shown in equation 21:

$$aA + bB \rightarrow cC + dD \quad (20)$$

$$-r_A = k_A C_A^{\alpha} C_B^{\beta} \quad (21)$$

In reaction 20, lowercase letters represent stoichiometric coefficients, and capital letters represent the chemical species being consumed and produced. The stoichiometric coefficients balance the number and type of reactant atoms with the number and type of atoms produced. In equation 21, C_A and C_B are the concentration of species A and B, respectively, and their superscripts, α and β, are the order of the reaction with respect to each species. (Fogler, 1999). The sum of the superscripts α and β is the overall order of the reaction: if α is 2 and β is 0.5, the reaction would be of order 2.5; α and β must be determined experimentally (Fogler, 1999; Smith, 1970). The reaction rate constant, k_A, is specific to species A, as denoted by the subscript A (Fogler, 1999). Further, k_A is constant with respect to reactant

concentration but varies strongly with temperature, as described by the Arrhenius equation:

$$k_A (T) = A \exp(-E/RT) \quad (22)$$

where A is the pre-exponential or frequency factor, E is the activation energy, R is the ideal gas constant, and T is absolute temperature (Fogler, 1999; Smith, 1970). As stated above, the units of reaction rate are moles disappearing (or appearing) per unit time per unit volume or catalyst weight; the units of the reaction rate constant must be determined from the order or the reaction such that the units of r_A are appropriate (Fogler, 1999).

Most often, reaction rate is determined by measuring the concentration of reacting species throughout the course of the reaction (Smith, 1970). A zero-order reaction is independent of concentration, as illustrated in Equation 23, and will result in a linear relationship between concentration and time (Fogler, 1999; Smith, 1970).

$$-r_A = k_A \quad (23)$$

Reactions of zero order can occur when one species is in such excess that its change in concentration is negligible: in this instance, the dependency of r_A on concentration cannot be detected, resulting in an apparent zero-order rate equation (Fogler, 1999). In the case of zero-order reactions, the reaction rate constant and the reaction rate have the same units. Equation 24 illustrates a first-order rate law for the disappearance of species A:

$$-r_A = k_A C_A \quad (24)$$

Here, the reaction rate constant is the slope of the plot of $\ln\{[A]/[A]_o\}$ versus time, where [A] is the concentration of A and $[A]_o$ is the initial concentration of A; the units of k_A in a first-order reaction are inverse time. A pseudo-first order reaction rate will occur when the reaction rate depends on the concentration of two species, as in Equation 25, but one species is in large excess and may be combined with the reaction rate constant to form k_A' as illustrated in Equation 26. Equation 25 may then be written as a first order reaction rate, as in equation 27.

$$-r_A = k_A C_A C_B \quad (25)$$

$$k_A' = k_A C_B \quad (26)$$

$$-r_A = k_A' C_A \quad (27)$$

Pseudo-first order reaction rate constants are determined via the same method as first-order reaction rate constants. Pseudo-first order reaction rates are reported for the photocatalytic degradation via titanium dioxide of pentachlorophenol, 2,4-dichlorophenol, 3,5-dichlorophenol, 2,3,5-trichlorophenol, 2-chlorophenol, 4-chlorophenol, salicylic acid, and 2,4,6-trichlorophenol (Hugul et al. 2002; Jardim et al. 1997; Chang et al., 2000; Matthews, 1987).

The photocatalytic oxidation of most contaminant species via titanium dioxide can be described with Langmuir-Hinshelwood kinetics (Matthews, 1990; Turchi and Ollis, 1990; Hugul et al., 2002; Ollis and Turchi, 1990; Ku and Hsieh, 1992; Hoffman, 1995; Serra et al., 1994; Chang et al., 2000).

Langmuir-Hinshelwood kinetics utilize both a reaction rate constant, k, and an adsorption equilibrium constant, K, to describe heterogeneous surface reactions (Hugul et al., 2002). The Langmuir-Hinshelwood model assumes that the initial rate of a surface reaction (R_i) is proportional to the fractional coverage (θ) and that the adsorption equilibrium of the solute follows a Langmuir isotherm Equations 28 and 29, respectively,

$$R_i = \frac{dC_i}{dt} = \frac{kKC_i}{1 + KC_i} \tag{28}$$

$$\Theta = \frac{KC_i}{1 + KC_i} \tag{29}$$

where C_i is the initial concentration of solute (i.e., contaminant species) (Serra et al., 1994; Hugul et al., 2002). The values of both rate constants, k and K, can be determined from a plot of $1/R_i$ vs $1/C_i$ as illustrated in equation 30.

$$\frac{1}{R_i} = \frac{1}{kKC_i} + \frac{1}{k} \tag{30}$$

It should be noted that the initial rate of the surface reaction, R_i, must be determined experimentally at various levels of initial concentration, C_i, as described previously. The Langmuir-Hinshelwood specific reaction rate constant, k, has units of molar concentration over time, and the adsorption equilibrium constant, K, has units of inverse molar concentration (Hugul et al., 2002). Both k and K depend on the catalyst utilized and the disappearing species.

The law of the conservation of mass dictates that the initial and final mass of a system must be equal (neglecting the conversion of mass to energy). A change in the number of moles in a reactive system may occur so long as the total mass of the system remains constant. The evaluation of any reactive system begins by defining the boundaries of the system and then performing a mole balance on each species (Fogler, 1999). The mole balance of any chemical species within a defined system may be written as:

$$\text{In} + \text{Generation} - \text{Out} = \text{Accumulation}$$

$$F_{jo} + G_j - F_j = (dN_j/dt) \qquad (31)$$

Where F_{jo} is the rate of flow of species j into the system in moles per unit time; F_j is the rate of flow of species j out of the system in moles per unit time; G_j is the rate of generation of species j by chemical reaction within a system in moles per unit time, and (dN_j/dt) is the rate of accumulation of species j within the system in moles per unit time (Fogler, 1999). F_{jo} is the product of the inlet concentration, C_{jo}, and the inlet volumetric flow rate, v_o (32).

$$F_{jo} = C_{jo}\, v_o \qquad (32)$$

In instances of uniform distribution of temperature and concentration throughout the reaction system, the generation of species j, G_j, is simply the product of the reaction volume, V, and the reaction rate, r_j:

$$G_j = V * r_j \qquad (33)$$

If the distribution of temperature and concentration vary with respect to location within the system, the generation of species G must be calculated from Equation 34.

$$G_j = \int^V r_j dV \tag{34}$$

It is often desirable to design a reactor that will achieve a specified conversion. The conversion of species A, X_A, can be calculated from equation 35.

$$X_A = \frac{moles\ of\ A\ reacted}{moles\ of\ A\ fed} \tag{35}$$

A batch reactor is a closed vessel in which a reaction takes place with no flux of material into or out of the vessel. Using Equation 31, the mole balance for a constant-volume batch reactor becomes:

$$G_j = (dN_j/dt) \tag{36}$$

Assuming a perfectly mixed system, Equations 33 and 36 can be combined as in Equation 37.

$$G_j = V * r_j = (dN_j/dt) \tag{37}$$

In systems that are operated batch-wise, reactants will be consumed until they are completely exhausted or achieve equilibrium with their products. The design equation for a batch reactor in terms of conversion is:

$$N_{jo} \frac{dX_j}{dt} = -r_j V \tag{38}$$

where N_{jo} is the number of moles of species j at time zero. To calculate the time required to achieve a specific conversion of reactants in a batch reactor, the reaction rate must be known as a function of conversion.

Continuous, or flow, reactors are those vessels through which the flow of reactants and products occurs simultaneously with reaction. A tubular reactor in which flow is always turbulent is one type of continuous reactor and is often referred to as a plug-flow reactor (PFR). A PFR is advantageous because concentration will not vary radially, greatly simplifying the design equations associated with the design of a tubular reactor. Once at steady state, the accumulation term for all continuous reactors is zero. The mole balance for a PFR, therefore, reduces to Equation 39:

$$F_{jo} + G_j - F_j = 0 \tag{39}$$

Because the rate of reaction, r_j, is a function of concentration, which will vary along the length of the PFR, the generation term in equation 38 should be solved via equation 34. Equation 34 can be integrated over very small, spatially-uniform sub-volumes of the reactor resulting in equation 40.

$$G_j = \int^{\Delta V} r_j dV = r_j \Delta V \tag{40}$$

Equation 41 is one form of the design equation for plug-flow reactors that will result from the combination of equations 39 and 40 and the definition of an integral.

$$\frac{dF_j}{dV} = r_j \tag{41}$$

To calculate the volume required to achieve a specific conversion of reactants in a flow reactor, the reaction rate must be known as a function of conversion, which is almost always directly proportional to the volume of a flow reactor. Equation 42 is the design equation for plug-flow reactors in terms of conversion.

$$C = F_{jo} \int_0^X \frac{dX}{-r_A} \tag{42}$$

Photocatalytic Reactors Utilizing UV Light and TiO_2

Most bench-scale ultra-violet/titanium dioxide systems utilize suspensions of titanium dioxide particles and are operated in batch mode (Hoffman et al., 1995; Serra et al., 1994; Hugul et al., 2002; Ku and Hsieh, 1992; Jardim et al., 1997; Almquist et al., 2003). These systems are an effective means to screen contaminant species for UV/TiO_2 applicability, to determine specific reaction rate constants, and to optimize operating conditions such as contaminant concentration, TiO_2 loading, and use of oxidant. However, the suspended titanium dioxide must be recovered from the effluent via centrifuge, filtration, or coagulation and flocculation, none of which are applicable at a larger scale (Hoffman et al., 1995). An industrially applicable UV/TiO_2 system will have to immobilize titanium dioxide particles to avoid expensive recovery and re-suspension mechanisms.

To immobilize TiO_2, Matthews (1987) employed the inherent ability of Degussa P25, a standard photocatalytic form of TiO_2, to stick to glass surfaces. Two reactor configurations were evaluated. The first configuration utilized titanium dioxide immobilized on the surface of glass mesh. The glass mesh was wrapped around a 20 watt NEC blacklight fluorescent tube and then inserted in a 39-millimeter inside diameter glass tube. The second configuration consisted of 7.5 meters of 6-millimeter inside diameter quartz tubing coiled 65 times around the same 20 watt NEC blacklight. In the second configuration, titanium dioxide was immobilized on the inner surface of the quartz tubing by evaporating 6 cubic centimeters of a suspension containing 75 milligrams of TiO_2 to dryness, under vacuum. The resulting film of titanium dioxidie particles in the second reactor could not be removed by water alone. Under identical operating conditions, the second reactor was more successful than the first. Matthews (1987) attributed the greater level of oxidation of the second reactor to a longer contact time between the contaminant species and the titanium dioxide particles.

The Matrix is a commercially available UV/TiO_2 system (EPA, 1992). The Matrix system consists of 2 units in series; each unit contains 12 wafers in which 6 reactor cells are located. Each reactor cell has a diameter of 4.5 centimeters and consists of a 75-watt, 254-nanometer, ultra-violet light, 1.6 meters in length, surrounded by 8 layers of fiberglass mesh bonded with anatase TiO_2 and is enclosed in a stainless-steel housing. Each reactor cell

is rated for a flow rate of 0.8 liters per minute, but the configuration of cells within a wafer allows for a total maximum flow rate of 2.4 liters per minute. To enhance the efficiency of the UV/TiO_2 reaction, 70 milligrams per liter of hydrogen peroxide are injected at various locations within a Matrix unit. The estimated cost of groundwater remediation via a Matrix system is $18 per cubic meter of water treated.

2,4-Dichlorophenol (2,4-DCP)

Chlorinated phenols (chlorophenols) are introduced to the environment as a result of the seepage of industrial effluents, waste incineration, uncontrolled use of biocides and water disinfection via chlorine (Hugul et al., 2002; Jardim et al., 1997). Chlorophenols may also form in the environment as a result of the partial oxidation of naturally occurring aromatic compounds by chlorine in water (Ku and Hsieh, 1992). Chlorophenols are toxic, resist biodegradation, and bioaccumulate in plant and animal species, affecting the entire food chain (Hugul et al., 2002; Ku and Hsieh, 1992; Trapido et al., 1998). While there is evidence to support the application of AOPs to degrade chlorophenols, the efficiency of AOPs is specific to each species and must be determined prior to application (Trapido et al., 1998).

Several chlorinated phenols are listed as priority pollutants by the United States Environmental Protection Agency (EPA); one such priority pollutant is 2,4-dichlorophenol (2,4-DCP) (Trapido et al., 1998). 2,4-DCP is

produced as an intermediate in both the pulp and paper and fine chemical industries and will form in the environment via the degradation of chlorophenoxy herbicides (Serra et al., 1994). The molecular structure of 2,4-DCP is illustrated in Figure 2.1, and some chemical properties are listed in Table 2.3. 2,4-DCP is a suspected carcinogen that attacks the eyes and kidneys. It is readily absorbed through the skin, will cause burns and blindness if it comes in contact with eyes, will attack mucous membranes and upper respiratory tract if inhaled, and may be fatal if swallowed. Overexposure to 2,4-DCP can cause burning sensations, headache, nausea, gastrointestinal disturbances, and blindness (Acros, 2002; Sigma-Aldrich, 2002; Supelco, 2002).

The Photo-Oxidation of 2,4-Dichlorophenol via TiO_2

The application of ultra-violet/titanium dioxide technology to batch 2,4-dichlorophenol systems has been evaluated by Serra et al. (1994), Hugul et al. (2002), Ku and Hsieh (1992), and Jardim et al. (1997). A summary of their experimental conditions and rate constants is outlined in Table 2.4. All of the authors who studied the photo-oxidation of 2,4-DCP emphasized the balance between titanium dioxide loading, initial 2,4-DCP concentration, and UV-light penetration required to optimize this matrix (Serra et al., 1994; Hugul et al., 2002; Ku and Hsieh, 1992; Jardim et al., 1997). The discrepancies between optimal titanium dioxide loadings reported in each work can be attributed to

differences in experimental apparatuses; reactor volume alone varied between 40 and 800 milliliters.

Serra et al. (1994) and Jardim et al. (1997) utilized 125-watt high-pressure mercury vapor lamps. Serra et al. (1994) filtered all but 365nm wavelengths and did not encounter a significant loss of 2,4-DCP due to photolysis alone but did report a loss of 45% of the initial 2,4-DCP concentration after 30 minutes of irradiation in a titanium dioxide matrix. Jardim et al. (1997) did not filter the UV spectrum emitted by the ultra-violet light source utilized in their experiments. All of the results reported by Jardim et al. have been corrected to compensate for the destruction of 2,4-DCP due to UV exposure alone (photolysis). In systems combining ultra-violet light and 0.1 grams of titanium dioxide per liter of 2,4-DCP solution, Jardim et al. reports the total disappearance of 20 milligrams of 2,4-DCP per liter of water (20 ppm 2,4-DCP) after 90 minutes of exposure. Hugul et al. (2002) employed a 125 W Phillips HPK medium-pressure mercury vapor lamp with a wavelength range of 240 to 570 nanometers exhibiting maximum quantum efficiency at 254 nanometers. As denoted in Table 2.4, Hugul et al. reported a pseudo-first order rate constant of 0.0066 per minute for the destruction of 2,4-DCP in systems employing only ultra-violet light (no titianium dioxide, no oxidant). Hugul et al. further reported the destruction of 50% of the initial concentration of 2,4-DCP after 50.7 minutes of irradiation with 0.1 grams of titanium dioxide per liter of 2,4-DCP solution. Ku and Hsieh (1992) report the

loss of approximately 25% of the initial 2,4-DCP concentration after 3 hours of exposure to low-pressure ultra-violet light. The addition of 1.4 grams of anatase titanium dioxide per liter 2,4-DCP solution resulted in a loss of 70-80% of the initial 2,4-DCP concentration after 3 hours of exposure to the same low-pressure UV light.

Both chlorohydroquinone and 4-chlorophenol were identified as byproducts of the UV/TiO_2 oxidation of 2,4-DCP (Serra et al., 1994). The formation of chlorohydroquinone was much more significant than that of 4-chlorophenol, which was attributed to the dechlorination of the phenolic ring as evidenced by an increased level of chloride ions. Hugul et al. (2002) confirm the appearance of quinones and organic acids during the photocatalytic oxidation of 2,4-DCP. Jardim et al. (1997) were not able to establish the identity of the byproducts formed during the photo-oxidation of 2,4-DCP but did report a plateau in un-identified byproduct formation between 30 and 90 minutes of UV exposure and a constant level of toxicity to *Photobacterium phosphoreum* and *Escherichia coli* throughout experimentation.

Utilizing systems with both ultra-violet light alone and ultra-violet light with hydrogen peroxide, Trapido et al. (1998) also investigated the degradation of 2,4-dichlorophenol via photolysis and photo-oxidation, respectively. Trapido et al. reported significantly enhanced reaction rates in systems that included H_2O_2. The loss of 90% of the initial 2,4-DCP

concentration after a few hours in systems with UV light and H_2O_2 occurred in batch systems exposed to UV light at 254 nanometers. This is attributed to the low molar extinction coefficient of H_2O_2 (19.6 per molar per second), which allows for good penetration of UV light and thus the efficient production of hydroxyl radicals via reaction 17 as well as the simultaneous photolysis of 2,4-DCP.

Taking into consideration continuous reactor design elements from Matthews (1987) and the results of 2,4-dichlorophenol degradation via ultra-violet/titanium dioxide in batch systems (Table 2.4), experimental work in this thesis continued towards the development of a bench-scale continuous photocatalytic reactor utilizing titanium dioxide in thin films of mesoporous silica.

Table 2.1. Oxidation Potentials of Some Oxidants (Legrini et al., 1993)

Species	Oxidation Potential (V)
fluorine	3.03
hydroxyl radical	2.80
atomic oxygen	2.42
ozone	2.07
hydrogen peroxide	1.78
perhydroxyl radical	1.70
permanganate	1.68
hypobromous acid	1.59
chlorine dioxide	1.57
hypochlorous acid	1.49
hypoiodous acid	1.45
chlorine	1.36
bromine	1.09
iodine	0.54

Table 2.2. Mechanism for Photochemical Oxidation via Titianium Dioxide by Ollis and Turchi (1990).

Excitation	$TiO_2 \xrightarrow{h\upsilon} e^- + h^+$	1
Adsorption		
	$O_L^{2-} + Ti^{IV} + H_2O \longleftrightarrow O_L H^- + Ti^{IV} - OH^-$	2a
	$Ti^{IV} + H_2O \longleftrightarrow Ti^{IV} - H_2O$	2b
	$site + R_1 \longleftrightarrow R_{1,ads}$	3
	$OH^\bullet + Ti^{IV} \longleftrightarrow Ti^{IV} \int OH^\bullet$	4
Recombination		
	$e^- + h^+ \longrightarrow heat$	5
Trapping		
	$Ti^{IV} - OH^- + h^+ \longleftrightarrow Ti^{IV} \int OH^\bullet$	6a
	$Ti^{IV} - H_2O + h^+ \longleftrightarrow Ti^{IV} \int OH^\bullet + H^+$	6b
	$R_{1,ads} + h^+ \longleftrightarrow R^+_{1,ads}$	7
	$Ti^{IV} + e^- \longrightarrow Ti^{III}$	8a
	$Ti^{III} + O_2 \longrightarrow Ti^{IV} - O_2^{\bullet -}$	8b
Hydroxyl Attack		
Case I	$Ti^{IV} \int OH^\bullet + R_{1,ads} \longrightarrow Ti^{IV} + R_{2,ads}$	9
Case II	$OH^\bullet + R_{1,ads} \longrightarrow R_{2,ads}$	10
Case III	$Ti^{IV} \int OH^\bullet + R_1 \longrightarrow Ti^{IV} + R_2$	11
Case IV	$OH^\bullet + R_1 \longrightarrow R_2$	12
Reactions of Other Radicals		
	$e^- + Ti^{IV} - O_2^{\bullet -} + 2(H^+) \longleftrightarrow Ti^{IV}(H_2O_2)$	13
	$Ti^{IV} - O_2^{\bullet} + (H^+) \longleftrightarrow Ti^{IV}(HO_2^\bullet)$	14
	$(H_2O_2) + (OH^\bullet) \longleftrightarrow (HO_2^{\bullet -}) + (H_2O)$	15

*Note: Species in parentheses may be adsorbed or in the aqueous phase.

O_L denotes one lattice oxygen

R_1 is the organic contaminant molecule, R2 is the resulting organic molecule.

Figure 2.1. Molecular Structure of 2,4-Dichlorophenol (2,4-DCP).

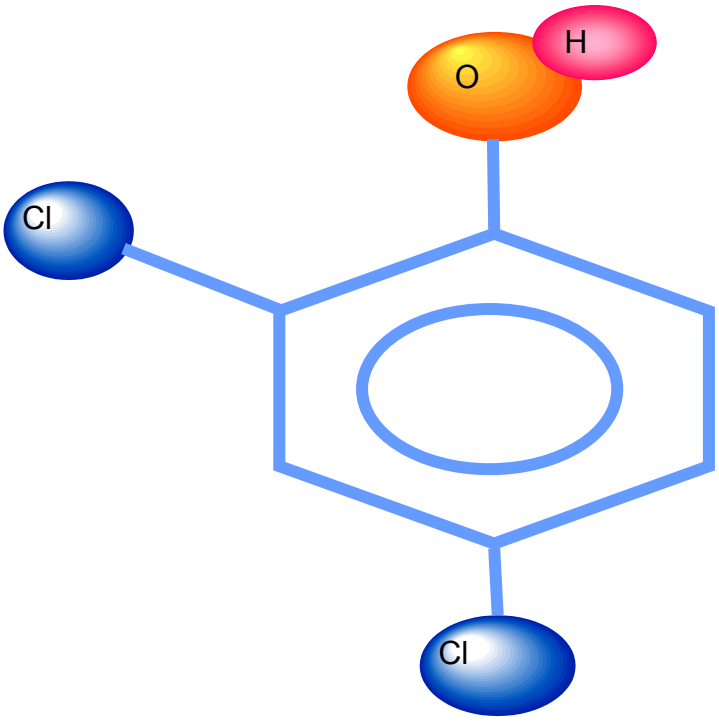

Table 2.3. Chemcial Properties of 2,4-Dichlorophenol.

Chemical Formula:	$C_6H_4Cl_2O$
Molecular Weight:	163
Boiling Point (@1atm):	210°C
Specific Gravity:	1.383

Table 2.4. Summary of Experimental Conditions and Rate Constants for the Photo-Oxidation of 2,4-Dichlorophenol via TiO_2 in Suspension.

Source	Reactor Volume (mL)	UV Light Source	Initial DCP Concentration (ppm)	TiO_2 Loading	O_2 supply	Pseudo-First Order Reaction Rate Constant	Langmuir Hinshelwood Rate Constant	Langmuir-Hinshelwood Equilibrium Adsorption Constant
Serra, F.; Trillas, M.; Garcia, J.; Domenech, X. *J. Environ. Sci. Health*. **1994**, *A29*, 1409-1421.	40	125 W Phillips HPK High-Pressure Mercury Vapor Lamp w/a UV incipient signal at 365 nm	8 - 16	2g/L; Degussa P25		0.0328/min	4.5×10^{-5} M/min	3.2×10^{3}/M
Hugul, M., Ercag, E., Apak, R. *J. Environ. Sci. Health*. **2002**, *A37*(3), 365-383.	750	125 W Phillips HPK Medium-Pressure Mercury Vapor Lamp w/a wavelength range of 240-570nm (max. quantum efficiency @ 254nm)	120	0		0.0066/min	-----	-----
				0.1g/L; anatase from Fluka		0.01488/min	1.88×10^{-5} M/min	1.296×10^{-3}/M
				0.2g/L; anatase from Fluka		0.01698/min	1.09×10^{-5} M/min	4.999×10^{-3}/M
				0.5g/L; anatase from Fluka		0.02178/min	1.06×10^{-5} M/min	6.997×10^{-3}/M
Ku, Y.; Hsieh, C. *Wat. Res*. **1992**, *26*(11), 1451-1456.	100	UVP XX-155 Low-Pressure Mercury Lamp with a radiative flux output of approx 5.8 W near the 254 nm wavelength	-----	1.4 g/L; anatase from CERAC Inc			pH = 3: 4.05×10^{-4}M/min	1.58×10^{3}
							pH = 5: 4.31×10^{-4}M/min	1.32×10^{3}
							pH = 7: 4.26×10^{-4}M/min	1.60×10^{3}
							pH = 9: 4.65×10^{-4}M/min	1.76×10^{3}
							pH = 11: 5.52×10^{-4}M/min	1.37×10^{3}
Jardim, W. F.; Moraes, S. G.; Takiyama, M. M. K. *Wat. Res*. **1997**, *32*, 1728 - 1732.	800	125 W High-Pressure Phillips HPL-n Mercury Lamp w/glass bulb removed	20	0.1g/L; Degussa P25	forced air at 560ml/min		-----	-----

CHAPTER III.

EXPERIMENTAL METHODS AND MATERIALS

At the University of Alabama, William Adams and Dr. Martin G. Bakker adapted a procedure to prepare thin films of mesoporous silica to incorporate titanium dioxide within the film's mesoporous structure. The photoreactivity of titanium dioxide in thin films of mesoprorous silica was established in batch reactions at Alabama: tubes were coated with a thin film of titanium dioxide in mesoporous silica, immersed in eight milliliters of 50 ppm 2,4-dichlorophenol (2,4-DCP), and exposed to UV light (Figure 3.1). Continuing work at Alabama includes determining the effect of both titanium dioxide loading and film thickness on photoreactivity. Work at Mississippi State included the design and evaluation of a continuous, bench-scale, photo-chemical reactor utilizing the thin film technology of titanium dioxide in mesoporous silica established at Alabama to degrade 2,4-dichlorophenol.

Experimental efforts at Mississippi State consisted of two phases of work: (i) batch reactions and (ii) continuous reactions. Batch reactions were conducted to establish a baseline to which the continuous reactions could be compared. The same ultra-violet light source and quartz cooling jacket, both from Ace Glass, were used throughout both phases of this work. The ultra-

violet light source was a 200-watt medium-pressure, mercury-vapor lamp with 47.6% of the total radiated energy in the ultra-violet spectrum. Both reactors were covered entirely with aluminum foil to ensure that the mercury-vapor lamp was the only source of light available to affect photodegradation.

The sources of each chemical compound utilized throughout experimentation and analysis are specified in Table 3.1. Table 3.2 lists the supplies and equipment utilized, as well as their manufacturer. The experimental matrixes for both phases of experimentation are given in Table 3.3. Each experiment within each phase was run a minimum of three times to ensure repeatability; a set of experiments refers to all of the experiments conducted under the same conditions. The results of each set of experiments were statistically analyzed to determine the least significant difference between experimental conditions (reactor type, ultra-violet light, titanium dioxide, and/or hydrogen peroxide) (Appendix A).

The initial concentration of 2,4-dichlorophenol (2,4-DCP) was approximately 190 parts per million (ppm) throughout both phases of experimentation. Both batch and continuous experiments were conducted with and without ultra-violet (UV) light, with and without hydrogen peroxide (H_2O_2), and with and without titanium dioxide (TiO_2). Throughout experimentation a three-percent hydrogen peroxide (H_2O_2) in water solution was employed to provide additional electron acceptors; as specified in Table 3.3, the concentration of H_2O_2 in reacting solutions was 750 milligrams per

liter of solution. All samples were collected in 1.5 milliliter amber vials, capped, and refrigerated in the dark until analysis. All of the samples from a given set of experimental conditions were analyzed at the same time and within one week of generation. The same 2,4-DCP solution was analyzed on three consecutive days; the average value was 194.04 ppm +/- 0.07 (Appendix A).

In batch experiments, titanium dioxide was utilized in aqueous suspensions (slurries), only. In continuous experiments, titanium dioxide was utilized in both aqueous suspensions and thin films of mesoporous silica. The calcinations required to form the mesoporous structure of the thin films permanently bonded the silica to the reactor and was not employed in batch reactions in an effort to preserve the integrity of the reactor vessel. It should be noted that suspensions of TiO_2 and thin films of TiO_2 in mesoporous silica were never utilized simultaneously. In those experiments that included TiO_2 suspensions, TiO_2 was added to the 2,4-DCP solution and stirred thoroughly before the mixture was introduced to the reactor; samples were taken before and after the addition of TiO_2 to the unreacted 2,4-DCP solution, and results were reported with respect to the initial sample after filtration. TiO_2 slurries were filtered via Millipore Millex-HV 0.45 micrometer syringe-driven filters prior to analysis. Eight samples of 2,4-DCP solution (without TiO_2) were analyzed before and after filtration via an Agilent 1100 series high-pressure liquid chromatograph (HPLC); there was an average loss of 2.02 milligrams of

2,4-DCP per liter of water after filtration. The resulting HPLC chromatographs of one sample before and after filtration are illustrated in Figure 3.2. Thirteen samples of the same 2,4-DCP solution with 0.05 weight percent TiO_2 in suspension were analyzed before and after the addition of TiO_2. As appropriate, TiO_2 was filtered from each sample prior to analysis; initial samples, without TiO_2, were not filtered. There was an average loss of 4.15 milligrams of 2,4-DCP per liter of water; subtracting the average loss due to filtration alone, approximately two milligrams of 2,4-DCP were adsorbed onto the titanium dioxide. The resulting chromatographs of one sample before and after the addition of 0.05 weight percent TiO_2 are illustrated in Figure 3.3.

Phase I: Batch Reactions

The batch reactor obtained from Ace Glass is a one-liter standard photochemical reactor with a jacketed quartz immersion well as shown in Figure 3.4. Cooling water was circulated through the immersion well jacket to cool the ultra-violet light, which was housed in the immersion well. The UV light was turned on and allowed to warm-up for at least 15 minutes before the reactor was charged with 2,4-DCP solution. Batch systems were vigorously stirred via a magnetic stir bar and stir plate. Guided by the experimental design in Table 3.3, titanium dioxide and/or hydrogen peroxide were added to the 2,4-DCP solution. Titanium dioxide particles were suspended within the 2,4-DCP solution, then stirred for five minutes prior to its being charged to the

reactor; hydrogen peroxide was added to the 2,4-DCP solution as it was charged to the batch reactor. Samples were taken before UV exposure, after the addition of TiO_2 (as appropriate), and at least every 5 minutes during the 15 minutes of exposure. Samples were withdrawn via Fisher Scientific cotton-plugged borosilicate glass disposable pipettes from the lowest port on the photochemical reactor; samples of TiO_2 slurry reactions were filtered as previously described.

Phase II: Continuous Reactions

A simplified version of the coiled reactor with immobilized titanium dioxide on its inner walls presented by Matthews (1987) was constructed by aligning nine 12-inch long, 6-millimeter inside-diameter, quartz tubes from Ace Glass along the length of the jacketed quartz immersion well used in batch experimentation. The quartz tubes were connected in series via six-inch pieces of Masterflex fuel and lubricant high-performance tubing. The total volume of the continuous reactor exposed to ultra-violet light was 64.6 milliliters. As in batch experiments, the UV light was allowed to warm-up for 15 minutes inside the quartz immersion well while cooling water circulated through the immersion well jacket. The outlets of two one-liter separatory funnels were connected to a three-way valve in such a manner that flow could originate from either of the individual funnels. The same three-way valve was also connected to a peristaltic pump and then to the reactor. The inside of

one set of quartz tubes was coated with a thin film of titanium dioxide in mesoporous silica. The experimental apparatus is shown in Figure 3.5.

In continuous experimentation, 2,4-DCP was charged to a 1-liter separatory funnel, pumped through the reactor at a rate of 244 milliliters per minute via a peristaltic pump, and collected in another 1-liter funnel; the total exposure time after one throughput was 15.9 seconds. Hydrogen peroxide was added to the 2,4-DCP solution after it had been charged to the separatory funnel but before the pump was turned on. Once the 2,4-DCP solution had been completely drained from the inlet funnel, the three-way valve was switched such that the effluent could be re-circulated through the reactor and collected in the now empty, original funnel. The flow through the reactor continued uninterrupted throughout experimentation. Samples were collected from the effluent stream during each reactor cycle and filtered as appropriate. At least four liters of reverse-osmosis water were flushed through the reactor after each experiment.

Thin Film of Titanium Dioxide in Mesoporous Silica

The procedure for preparing well-ordered mesostructured silica thin films was developed by Alberius et al. (2002). At the University of Alabama, William A. Adams and Dr. Martin G. Bakker adapted this procedure to incorporate titanium dioxide within the mesoporous silica structure. By immobilizing titanium dioxide in a thin film, a separation mechanism to

recover the titanium dioxide particles from the reactor effluent is no longer necessary.

All glassware that was used to prepare the silica solution was soaked in a base solution for half an hour, rinsed with reverse osmosis water, dried, soaked in an acid solution for five minutes, then rinsed and dried again. The base solution consisted of 120 grams of sodium hydroxide, 120 milliliters of reverse osmosis water, and 1 liter of 200-proof ethanol. The acid solution consisted of 100 milliliters of concentrated hydrochloric acid and 900 milliliters of reverse osmosis water.

The first step in preparation of mesoporous silica was to hydrolyze silicon alkoxide. This was achieved in a single-phase system at room temperature by combining 75 grams of pH 2 water, 180 grams of ethanol, and 156 grams of tetraethyl orthosilicate (TEOS). Following at least one hour of vigorous stirring, 41.25 grams of Pluronic P123, a triblock copolymer, dissolved in 120 grams of ethanol, and 6.3 grams of TiO_2 was added to the ethanol-TEOS mixture. The ratio between TEOS and Pluronic P123 was chosen such that a hexagonal pore structure would result in the silica.

After stirring the TEOS-P123-TiO_2 mixture for eight hours, the inside of each quartz tube was coated with the resulting solution. To prevent silica formation on the outside of the tubes, the length of each tube was wrapped with in aluminum foil such that only the inside of the tube would be exposed to the TEOS-P123-TiO_2 mixture. Each tube was submerged completely in the

TEOS-P123-TiO_2 solution, allowed to soak for five minutes, and then withdrawn at a rate of one millimeter per second. Dip-coating controlled the rate at which the tubes were extracted from the silica solution, and, by controlling this rate, the thickness of the resulting film was also controlled. To increase the extent of silica cross linkage, the tubes were suspended vertically and allowed to air dry for 12 hours. Next, the tubes were calcined to both remove the P123 and increase the cross-linkage of the inorganic framework. During calcinations the temperature was increased to 400^{o}C at a rate of 1^{o}C per minute, held constant at 400^{o}C for 4 hours, then cooled at a rate of 1^{o}C per minute.

Analysis

Samples were analyzed for 2,4-dichlorphenol by high-pressure liquid chromatography (HPLC) via EPA method 604 for phenols. This method utilized a Symmetry C_8 5-micrometer column 3.9 millimeters in diameter and 150 millimeters in length from Waters Corporation. Two mobile phases were employed at a flow rate of 1.2 milliliters per minute: 1% acetic acid in reverse osmosis water and 1% acetic acid in acetonitrile. The ratio of the acetonitrile solution ramped from 30% to 100% over 20 minutes. The sample injection volume was 40 microliters, and the UV detector was set at 280 nanometers. The Agilent 1100 series HPLC was equipped with an autosampler.

A certified standard of 500 ppm 2,4-DCP was used to prepare secondary standards for calibration and instrument performance checks. The secondary standards were fashioned by sequential dilution of 1.0 milliliter of the 500 ppm 2,4-DCP certified standard with reverse osmosis water; secondary standards ranged from 0 to 250 ppm 2,4-DCP (1 ppm = 1mg/L H_2O). Standards of known 2,4-DCP concentration were analyzed approximately every two weeks to maintain an accurate calibration curve. Each calibration curve had an R-squared value of 0.997 or greater. Five injections of the same sample of 2,4-DCP resulted in an average value of 176.41 ppm +/- 0.64 ppm, an error of 0.4% (Appendix A). A minimum detectable concentration, C_{min}, of 0.09 ppm was determined via equation 43:

$$C_{min} = 3*s_{bl}/m \quad (43)$$

where s_{bl} is the standard deviation of a sample and m is the slope of the calibration curve (Hugul et al., 2002).

Figure 3.6 is a representative chromatograph of 195 ppm of 2,4-dichlorophenol that has not been exposed to UV light. The 2,4-DCP peak eluted between 7.3 and 7.5 minutes throughout experimentation. The peak at approximately 20.9 minutes results from a change in mobile phase concentration and is consistent throughout all of the chromatographs.

Because chlorohydroquinone and 4-chlorophenol had been identified as byproducts of the photo-oxidation of 2,4-dichlorophenol (Serra et al., 1994), concentrated solutions of both species were analyzed via the HPLC

method for 2,4-DCP. As illustrated in Figure 3.7, chlorohydroquinone and 4-chlorophenol eluted at approximately 2.17 minutes and 5.22 minutes, respectively.

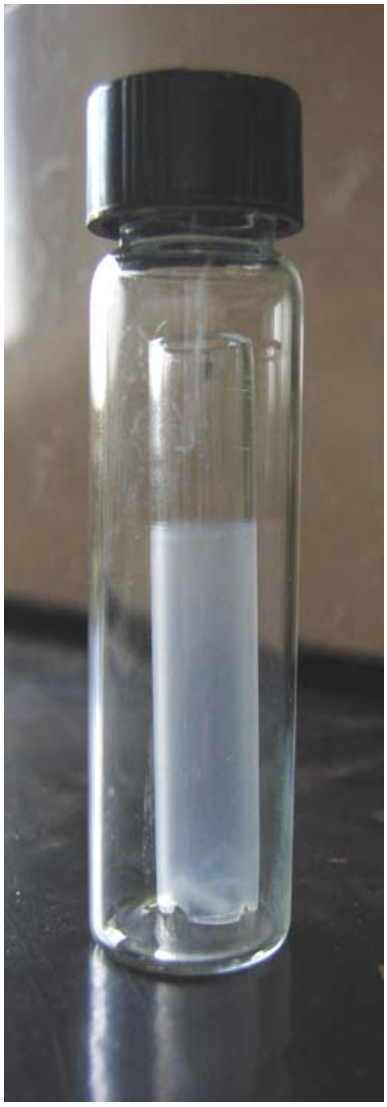

Figure 3.1. The University of Alabama's 8mL Batch Reactor Utilized to Establish the Photo-Reactivity of the Thin Film of Titanium Dioxide in Mesoporous Silica.

Table 3.1. Chemical Compounds Utilized During Experimentation and/or Analysis and Their Sources.

Manufacturer	**Chemical**
Aldrich 800-558-9160	200 proof Ethyl Alcohol, reagent grade
	Tetraethyl orthosilicate (TEOS)
	97% Sodium Hydroxide Flakes
	4-chlorophenol
	chlorohydroquinone
	2, 4 - dichlorophenol (DCP)
BASF 800-443-6460	Pluronic P123
Degussa 732-981-5274	Titanium Dioxide (P25)
Fisher Scientific 800-766-7000	Hydrochloric Acid
	HPLC grade Acetonitrile
	HPLC grade Acetic Acid, glacial
	3% Hydrogen Peroxide (H_2O_2)
Supelco 800-325-3010	1mL, 500 ppm DCP standard

Table 3.2. List of Equipment and Manufacturers.

Manufacturer	**Equipment or Material**
Agilent 800-227-9770	1100 Series High-Pressure Liquid Chromatograph with Autosampler
Ace Glass 800-223-4524	6mm I.D. Quartz Tubing
	Jacketed Quartz Immersion Well
	1L Standard Photochemical Reactor
	200W Medium-Pressure Mercury-Vapor Lamp
Cole-Palmer 800-323-4340	Masterflex Fuel and Lubricant Tubing L/S 35
Fisher Scientific 800-766-7000	Cotton-Plugged Borosilicate Glass Disposable Pipettes
	Millipore Millex-HV 0.45 Micrometer Syringe-Driven Filters
Waters Corporation 800-252-4752	Symmetry C8 Column 5μm 3.9x150mm

Table 3.3. Experimental Matrixes for the Photocatalytic Oxidation of 2,4-Dichlorophenol via TiO_2.

Reactor	UV-Light	H_2O_2	TiO_2 (Slurry)	TiO_2 (silica)	"Experiment"
BATCH	OFF				**Dark Blank**
	OFF	750 ppm			**Dark H_2O_2 Only (300mL)**
	OFF		0.05 wt%		**Dark TiO_2 (slurry) Only**
	OFF	750 ppm	0.05 wt%		**Dark TiO_2 (slurry) w/H_2O_2**
	ON				**UV Blank**
	ON	750 ppm			**UV H_2O_2 Only**
	ON		0.05 wt%		**UV TiO_2 (slurry) Only**
	ON	750 ppm	0.05 wt%		**UV TiO_2 (slurry) w/H_2O_2**
PFR	OFF				**Dark Blank**
	OFF	750 ppm			**Dark H_2O_2**
	OFF		0.05 wt%		**Dark TiO_2 (slurry) Only**
	OFF	750 ppm			**Dark TiO_2 (slurry) w/H_2O_2**
	ON				**UV Blank**
	ON	750 ppm			**UV H_2O_2 Only**
	ON		0.05 wt%		**UV TiO_2 (slurry) Only**
	ON	750 ppm	0.05 wt%		**UV TiO_2 (slurry) w/H_2O_2**
	OFF			12.5 wt% of Silica	**Dark TiO_2 (film) Only**
	ON			12.5 wt% of Silica	**UV TiO_2 (film) Only**
	OFF	750 ppm		12.5 wt% of Silica	**Dark TiO_2 (film) w/H_2O_2**
	ON	750 ppm		12.5 wt% of Silica	**UV TiO_2 (film) w/H_2O_2**

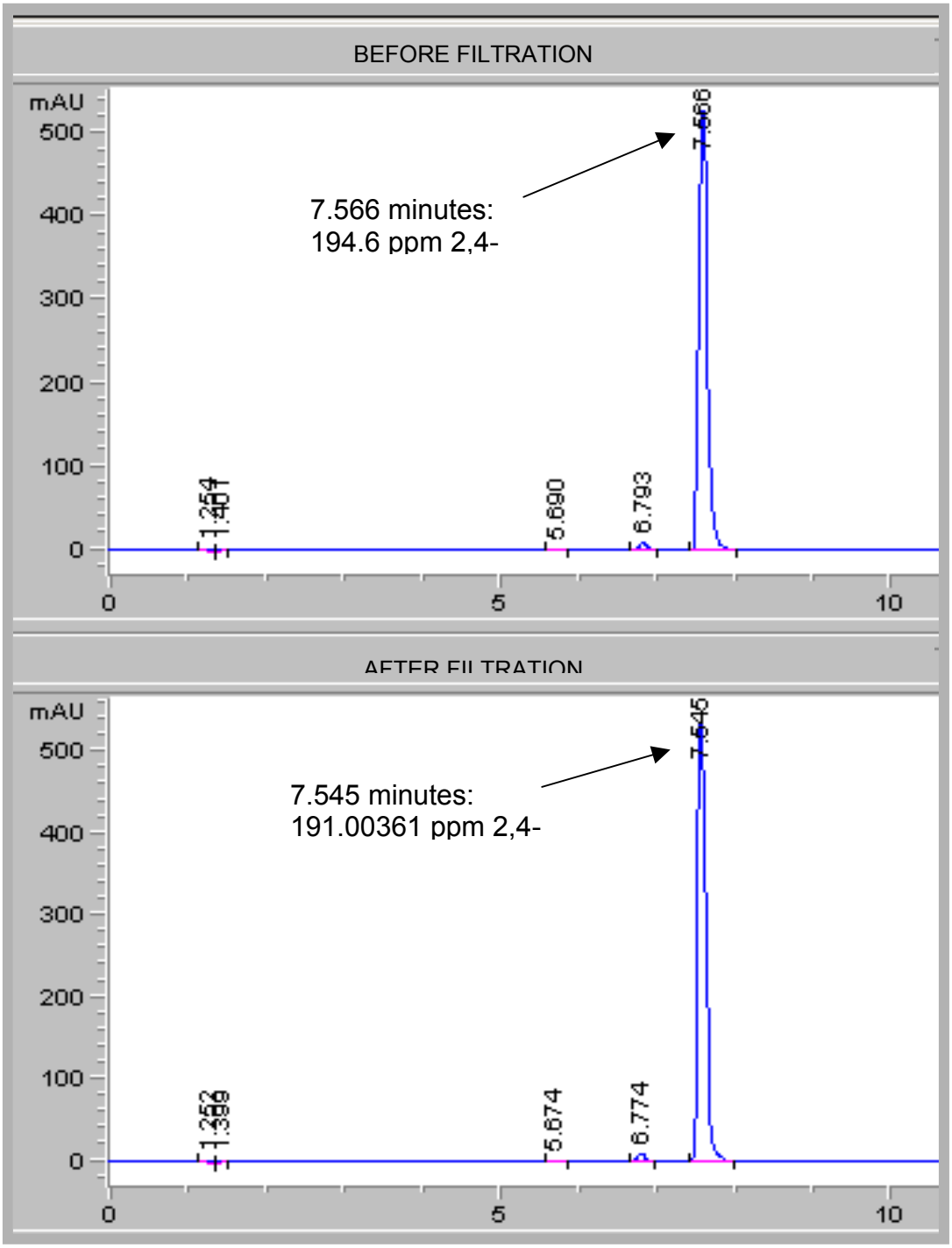

Figure 3.2. HPLC Chromatographs of the same 2,4-DCP sample (no TiO_2) before and after filtration.

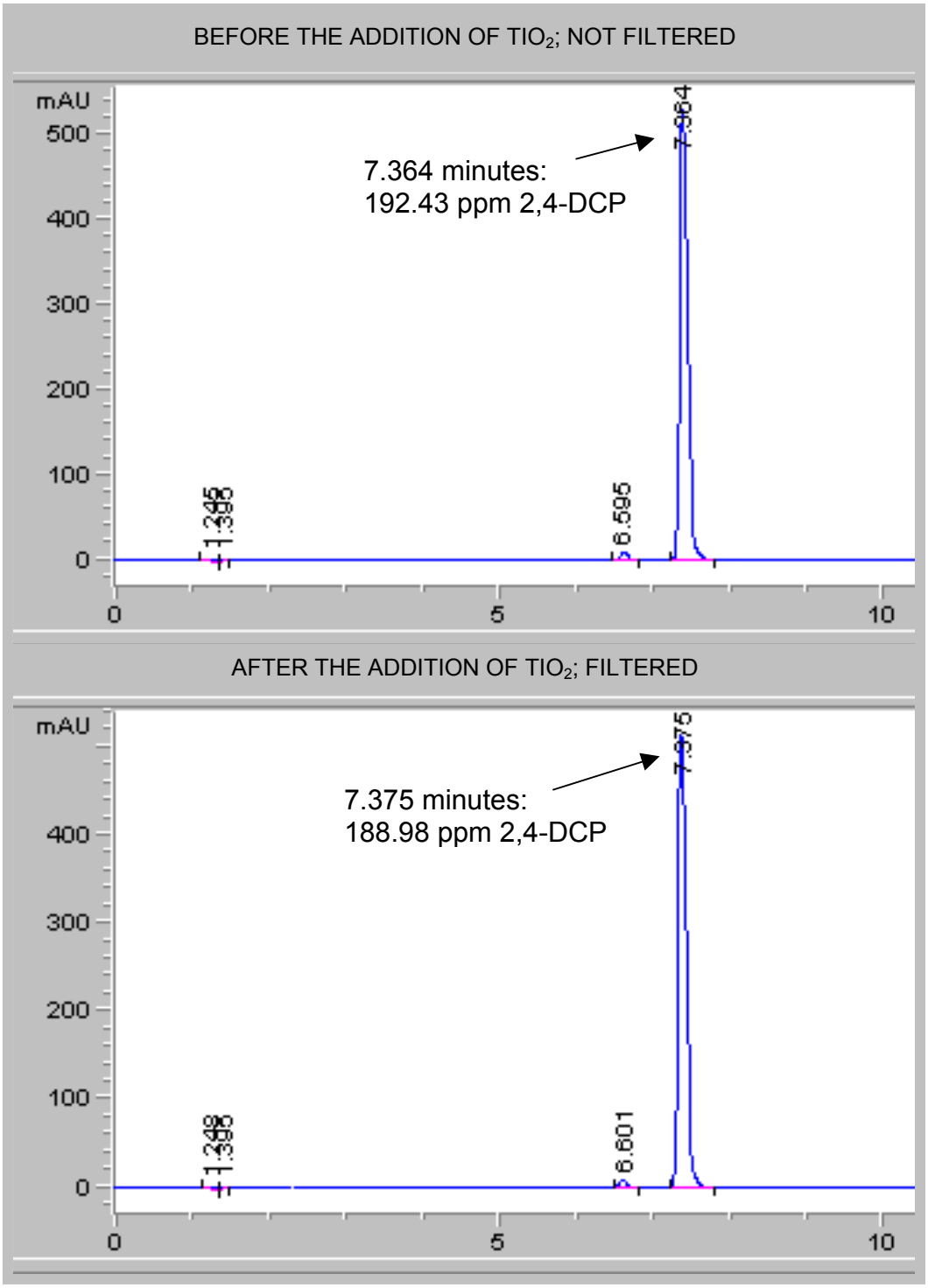

Figure 3.3. HPLC chromatographs of the same 2,4-DCP solution before the addition of TiO_2 (not filtered) and after the addition of TiO_2 (filtered).

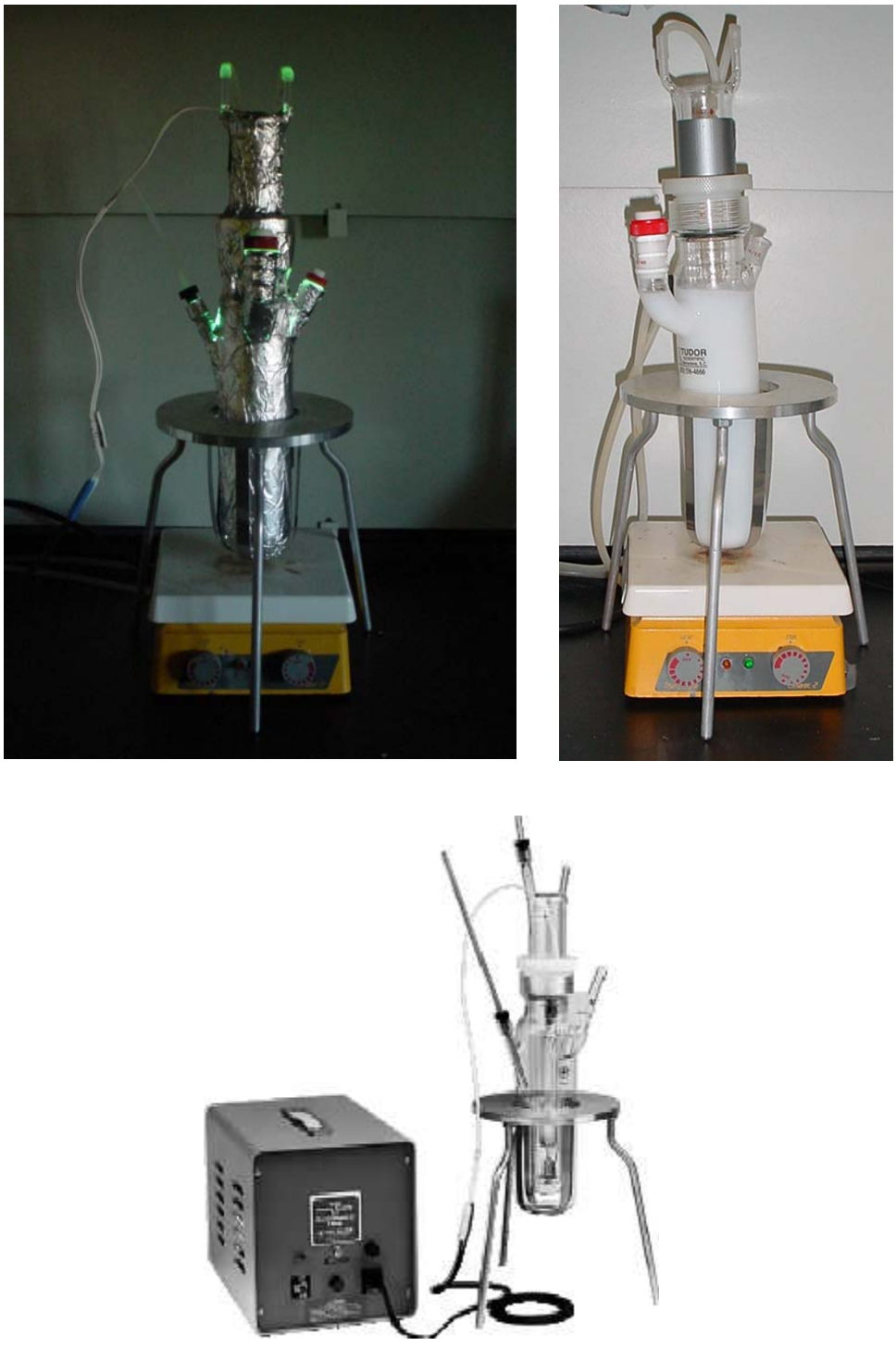

Figure 3.4. Batch Reactor Configuration.

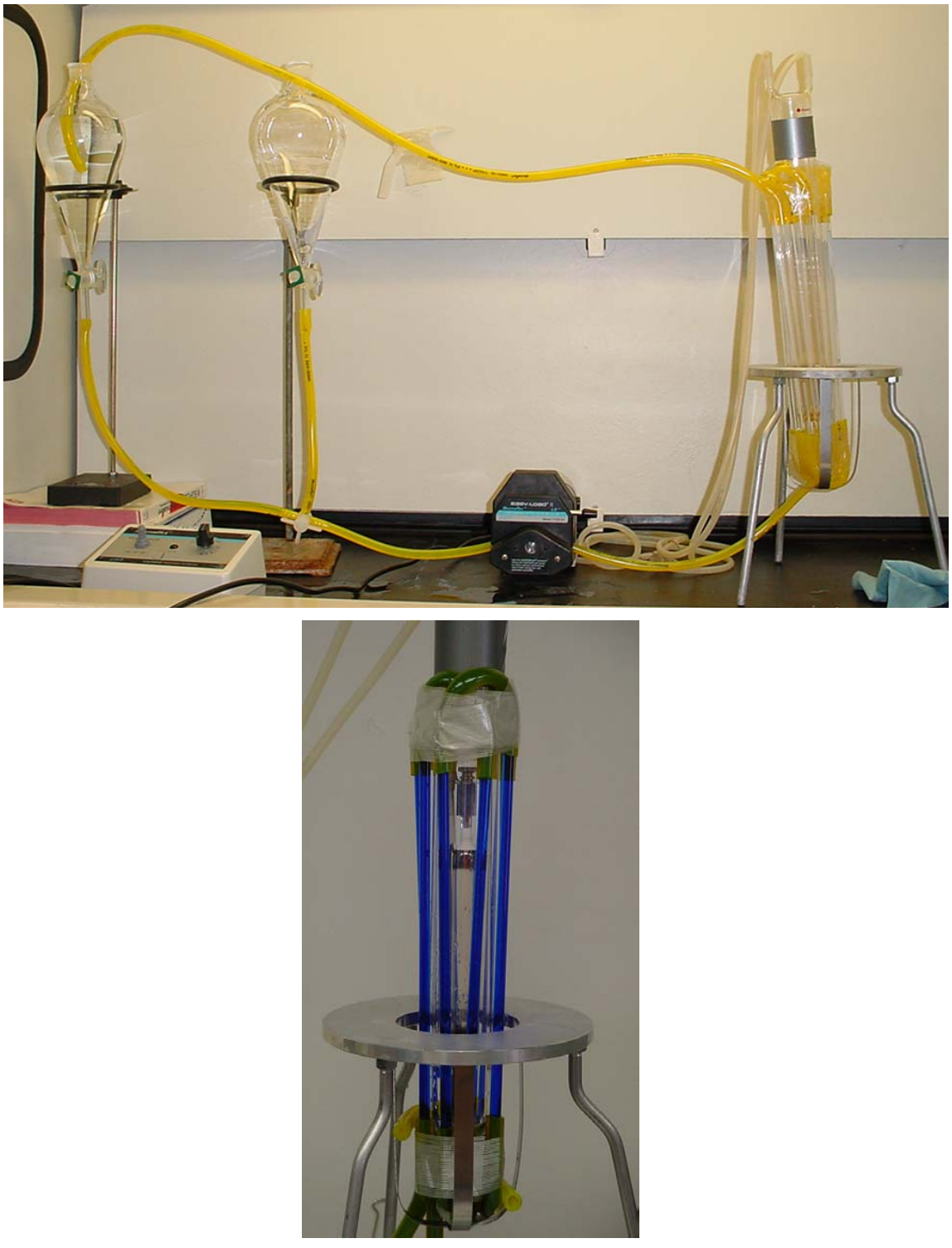

Figure 3.5. Continuous Reactor Configuration.

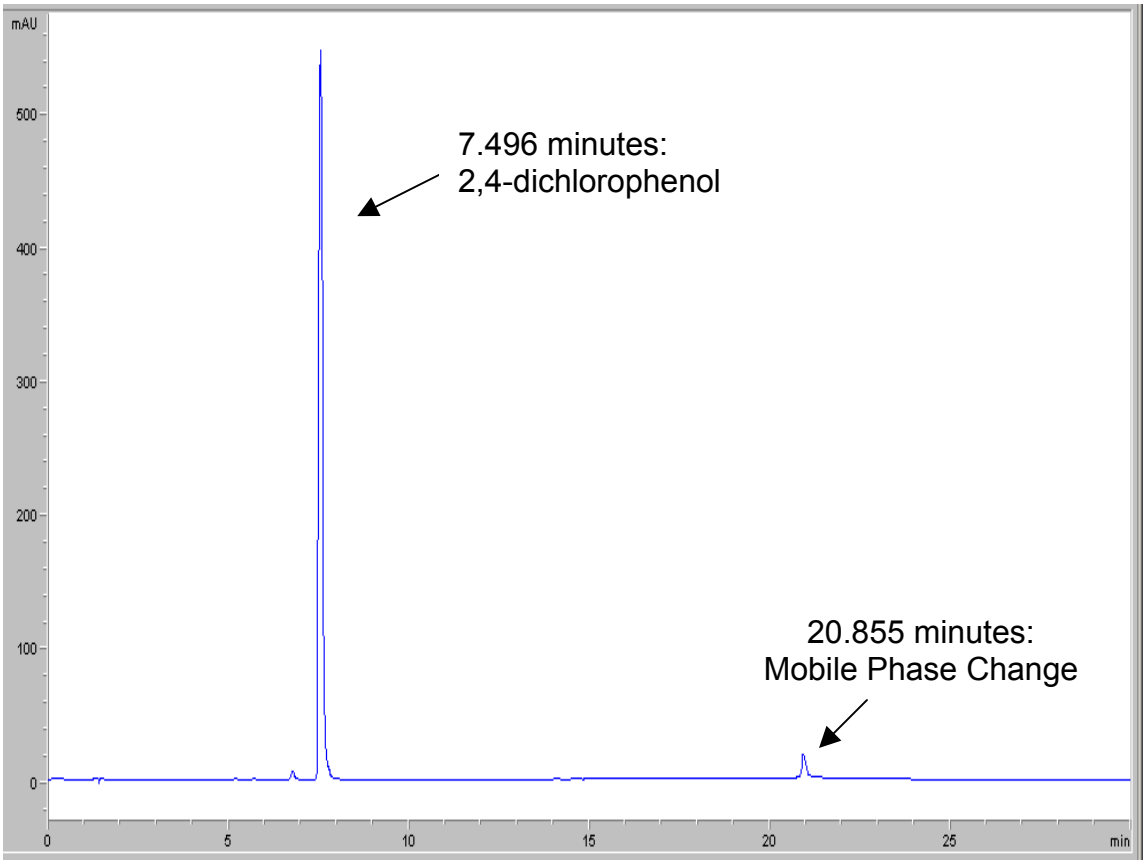

Figure 3.6. A Representative Chromatograph of 195 ppm 2,4-Dichlorophenol.

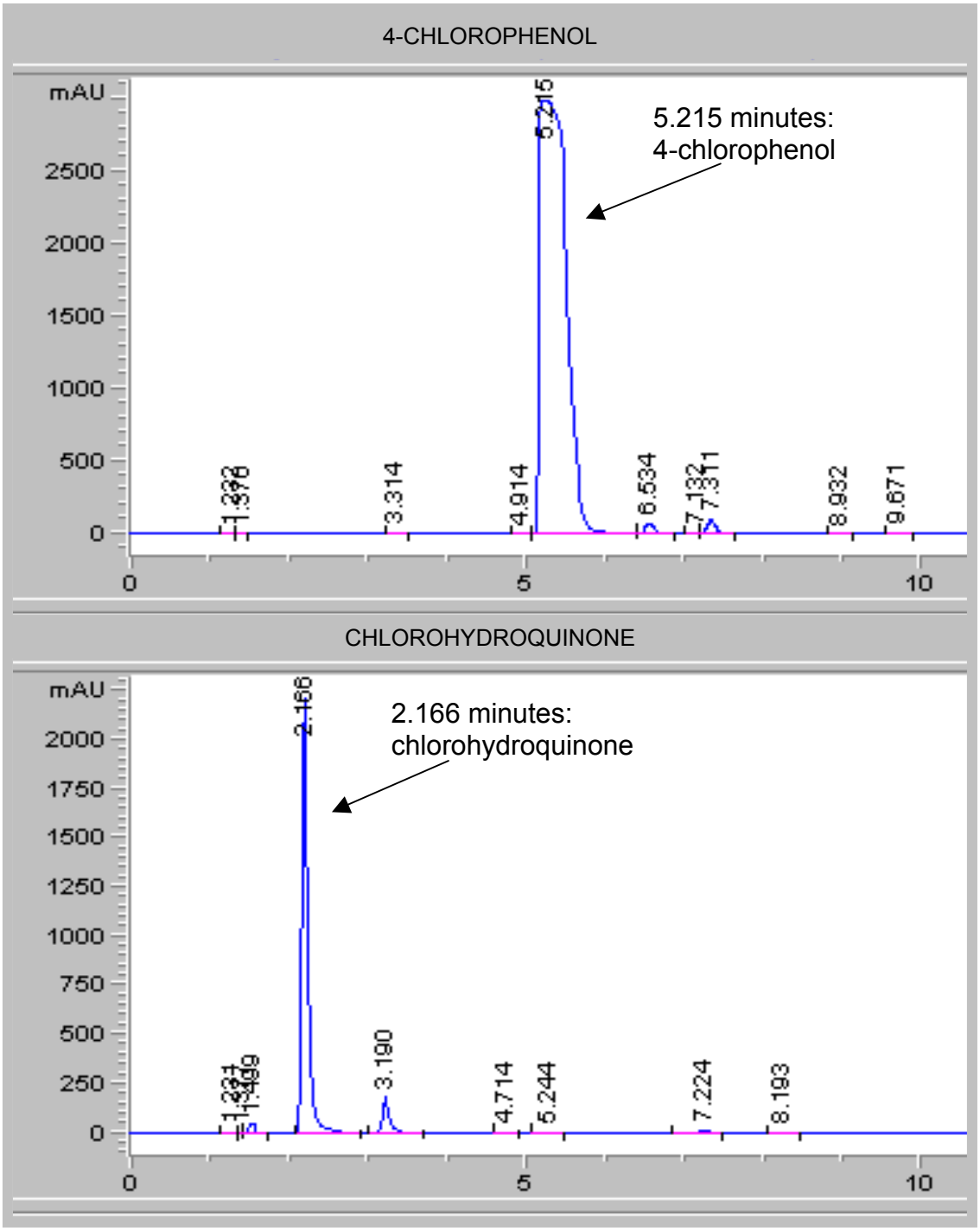

Figure 3.7. HPLC Chromatographs of 4-Chlorophenol and Chlorohydroquinone Analyzed via the Same Method as 2,4-Dichlorophenol.

CHAPTER IV.

RESULTS AND DISCUSSION

Preliminary batch-wise experiments were conducted to establish a procedure, perfect laboratory technique, and determine suitable operating conditions. The resulting batch procedure and laboratory techniques are described in the chapter of this report entitled Experimental Methods and Materials. Operating conditions that were evaluated in preliminary experimentation include initial 2,4-DCP concentration, TiO_2 loading, and reactor volume. Batch experiments utilizing only UV light were conducted at an initial 2,4-DCP concentration of 50, 100, and 200 milligrams per liter of water (50, 100, and 200 ppm) (Figure 4.1). Because the combined effect of UV light, TiO_2, and/or H_2O_2 was sought, an initial concentration of 200 ppm was chosen as it retained the most 2,4-DCP (46%) and thereby provided the best basis for comparison. Preliminary experiments conducted at 0.1 weight percent (0.1 wt%) titanium dioxide in suspension resulted in an average loss of 22% of the initial 2,4-DCP concentration (Figure 4.2). This was attributed to both the opacity of the 0.1 wt% solution and a lack of electron acceptors. To reduce the opacity of the solution, the titanium dioxide suspension was

reduced to 0.05 wt%; this change in titanium dioxide loading produced an average loss of 30% of the initial 2,4-DCP concentration (Figure 4.2). To increase the availability of irreversible electron acceptors, hydrogen peroxide was added to the UV/TiO_2 matrix (Figure 4.3). Further, the batch reactor volume was reduced from 400mL to 300mL in an effort to both improve mixing and minimize waste production.

Phase I: Batch Reactions

After 15 minutes, the average loss of 2,4-dichlorophenol in batch reactions follows the order: UV/TiO_2(slurry)/H_2O_2 = UV/H_2O_2 > UV only > UV/TiO_2(slurry) > Dark (Figure 4.4). Figure 4.5 is a plot of the normalized 2,4-DCP concentration (final concentration/initial concentration) versus elapsed time for each set of experiments; the standard deviation for each data point is presented graphically in Appendix B.

Dark batch experiments include all of the experiments conducted batch-wise without the use of ultra-violet light. The results of all four dark batch experiments with and without titanium dioxide in suspension and/or hydrogen peroxide are statistically the same throughout experimentation (Appendix A). After 15 minutes of stirring in the batch reactor, the average loss of 2,4-DCP in dark experiments was 1.46% of the initial concentration, which is greater than the analytical error associated with the HPLC (0.4%). The loss of 2,4-DCP in dark TiO_2(slurry) systems can be attributed to the

adsorption of 2,4-DCP onto titanium dioxide particles in solution. The loss of 2,4-DCP in dark H_2O_2 systems may be attributed to the degradation of 2,4-DCP via hydroxyl radicals resulting from dissociated H_2O_2. Of all of the dark batch experiments, the greatest loss of 2,4-DCP, 3.42%, occurred in the dark TiO_2/H_2O_2 system; this loss may be attributed to both the production of hydroxyl radicals via H_2O_2 dissociation and the adsorption of 2,4-DCP onto titanium dioxide. The dark system with neither TiO_2 nor H_2O_2 resulted in a 0.77% increase in 2,4-DCP, which is greater than the error associated with analysis, but, assuming 2,4-DCP was not created in a dark, stirred, batch reactor, this increase must be attributed to a combination of analytical and human error.

The loss of 49.3% of the initial concentration of 2,4-DCP in batch reactions after 15 minutes of exposure to UV light without TiO_2 or H_2O_2 can be attributed to photolysis, the physical destruction of a compound via the adsorption of light. The enhanced disappearance of 2,4-DCP in batch UV/H_2O_2 systems may be attributed to the simultaneous photolysis of H_2O_2, resulting in hydroxyl radical formation via reaction 17, and photolysis of 2,4-DCP directly.

$$H_2O_2 + h\nu \rightarrow 2OH^* \qquad (17)$$

After 15 minutes of exposure, batch UV/TiO_2(slurry) systems degraded less 2,4-DCP than systems utilizing UV light alone. However, batch UV/TiO_2(slurry)$/H_2O_2$ systems degrade more than 99% of the initial 2,4-DCP

concentration after 15 minutes of exposure. The success of the UV/TiO_2(slurry)/H_2O_2 system suggests that the failure of the UV/TiO_2(slurry) system can be attributed, at least in part, to recombination of the electron-hole pair in the absence of electron acceptors.

After three minutes of exposure to UV light, the UV/H_2O_2 batch system degraded more 2,4-dichlorophenol than did the UV/TiO_2(slurry)/H_2O_2 batch system; however, after 15 minutes of exposure, the UV/H_2O_2 and UV/TiO_2(slurry)/H_2O_2 systems were not statistically different with respect to the disappearance of 2,4-DCP (Appendix A and Figure 4.5). This discrepancy may be the result of a change in the rate of reaction in both systems, as evidenced by irregular curves in the plot of normalized concentration versus time between 60 and 240 seconds (Figure 4.5). Because reaction rate is strongly dependent upon the concentration of species present in a system (equation 21), the rate at which a reaction takes place will vary as the concentration of a species increases or decreases.

$$-r_A = k_A C_A^{\alpha} C_B^{\beta} \qquad (21)$$

After only 1 minute, the concentration of 2,4-DCP decreased by more than 50% in both the UV/H_2O_2 and UV/TiO_2(slurry)/H_2O_2 batch systems, which very likely contributed to the apparent rate changes in both of these systems. Further, it is possible that the hydrogen peroxide concentration was significantly reduced or depleted during the course of both reactions, essentially resulting in the less efficient UV only and UV/TiO_2(slurry) systems.

The advantage of UV/TiO_2 technology is the eventual destruction of contaminant species via mineralization to carbon dioxide, water, and inorganic salts. However, the disappearance of 2,4-DCP is not necessarily an indication of its mineralization but merely its oxidation. By following the appearance and disappearance of byproducts in each system, some sense of the mineralization achieved in each system may be attained.

As illustrated by the appearance of significant peaks before 2,4-DCP in the HPLC chromatographs of solutions exposed to UV light for 15 minutes (Appendix B), the disappearance of 2,4-DCP is complemented by the appearance of several byproducts. As expected, dark chromatographs do not indicate the formation of byproducts (Appendix B). Although 4-chlorophenol and chlorohydroquinone were identified as byproducts by Serra et al. (1994) and both were identified via HPLC analysis at 2.17 and 5.22 minutes, respectively, neither species consistently produced a significant peak area in the chromatographs of exposed solution. Conversely, an unidentified byproduct that eluted between 3.7 and 3.8 minutes was present in the chromatographs of each batch system exposed to UV light throughout exposure. However, because this byproduct was not identified, its concentration could not be quantified. Assuming that concentration is proportional to peak area, the peak area of the 3.7-minute eluter was plotted with the peak area of 2,4-DCP over the course of one reaction from each set of system conditions with UV light in Figures 4.6 through 4.9.

As 2,4-dichlorophenol disappeared in UV only batch experiments, the peak area of the 3.7-minute eluter appeared at a constant rate, as indicated in Figure 4.6. In contrast to the UV only system, the 3.7-minute eluter plateaued after the first minute of UV exposure in the UV/H_2O_2 system (Figure 4.7), and the rate of disappearance of 2,4-DCP slowed dramatically after 240 seconds, both of which may be the result of the depletion of hydrogen peroxide, and thus hydroxyl radicals, and the predominance of the photolysis of 2,4-DCP as in UV only systems. The 3.7-minute eluter did not appear in the UV/TiO_2(slurry) system until the fourth minute of exposure (Figure 4.8). As previously stated, the recombination of the electron-hole pair seems to prevail over the formation of hydroxyl radicals in the UV/TiO_2(slurry) system due to a lack of electron acceptors, and the slow formation of the 3.7-minute eluter is consistent with the inefficient production of hydroxyl radicals. In the UV/TiO_2(slurry)/H_2O_2 system, the 3.7- minute eluter had a maximum peak area at 120 seconds of exposure and disappeared after 900 seconds of exposure, which is indicative of the simultaneous degradation of 2,4-DCP and at least one of its byproducts (Figure 4.9). The maximum peak area of the 3.7-minute eluter coincides with the rate change in the UV/TiO_2(slurry)/H_2O_2 system between 60 and 240 seconds, an indication that the 3.7-minute eluter is likely adsorbed on the surface of the titanium dioxide and may be competing with 2,4-DCP for hydroxyl radicals. As evidenced by the HPLC chromatographs of batch systems employing UV light (Figure B.9), the

$UV/TiO_2(slurry)/H_2O_2$ system had both the lowest final concentration of 2,4-DCP and the fewest byproduct peaks after 15 minutes of exposure, further supporting the simultaneous degradation of byproducts and 2,4-DCP in this particular batch system.

With respect to the oxidation of 2,4-DCP, the UV/H_2O_2 and $UV/TiO_2(slurry)/H_2O_2$ systems are the most advantageous of the batch systems. By gauging the mineralization of 2,4-DCP by the appearance and disappearance of the 3.7-minute eluter, the $UV/TiO_2(slurry)/H_2O_2$ system is superior to all of the batch systems.

Phase II: Continuous Reactions

After 190.8 seconds, the average loss of 2,4-dichlorophenol in continuous reactions follows the order: $UV/TiO_2(slurry)/H_2O_2 = UV/H_2O_2 > UV/TiO_2(film)/H_2O_2 = UV/TiO_2(slurry)$; $UV/TiO_2(slurry) = UV\ only = UV/TiO_2(film) = dark$ (Figure 4.10). Figure 4.11 is a plot of the normalized 2,4-DCP concentration versus elapsed time for each set of experiments; the standard deviation for each data point is presented graphically in Appendix C.

Dark continuous experiments include all of the continuous experiments conducted without the use of UV light. The results of all of the dark batch experiments were statistically the same (Appendix A). An average of 30% of the initial 2,4-DCP concentration disappeared after 8 cycles through the tubular reactor in dark experiments. While some fraction of this loss may be

accounted for by the adsorption of 2,4-DCP onto TiO_2 or degradation as a result of hydroxyl radical formation via dissociation of H_2O_2, the vast majority is attributed to an interaction between 2,4-DCP and the Masterflex tubing and must be taken into account when considering all of the Phase II results. This is supported by both the loss of approximately 30% of the initial 2,4-DCP concentration in dark continuous experiments after without TiO_2 or H_2O_2 and dark batch TiO_2(slurry)/H_2O_2 experiments that resulted in an average loss of only 3.6% of the initial 2,4-DCP concentration. The interaction between 2,4-DCP and the Masteflex tubing could be an adsorption or dissolution mechanism. The repeatability of continuous experiments, as signified by low standard deviation among data points of different experiments within the same system (Appendix C), suggests that the effect of the Masteflex/2,4-DCP interaction is consistent throughout experimentation. To ensure that 2,4-DCP did not desorb from the Masterflex tubing during the course of a reaction, one-inch pieces of tubing were submerged in amber jars of 2,4-DCP solution at various initial concentrations. The loss of 2,4-DCP over a period of one hour followed linear trendlines for each set of data (Appendix C) insinuating that the interaction effect is consistent over the course of a continuous experiment. It should be obvious that a pilot-plant or industrial scale reactor would be constructed of a rigid, less adsorbent material.

The UV only (blank) and UV/TiO_2(film) continuous systems are not statistically different from the dark continuous experiments with respect to the

loss of 2,4-DCP. The loss of 2,4-DCP in UV only and UV/TiO_2(slurry) continuous systems are not statistically different after 190.8 seconds of exposure, which is in good agreement with the batch results whereby the UV only system was not statistically different from the UV/TiO_2(slurry) system after 180 seconds of exposure (Figures 4.5 and 4.11 and Appendix A). The retention of 2,4-DCP in UV/H_2O_2 systems was approximately 47% less than that of dark systems. As in batch UV/H_2O_2 systems, the enhanced disappearance of 2,4-DCP in continuous UV/H_2O_2 systems is most likely a result of both the photolysis of H_2O_2, resulting in hydroxyl radical formation, as well as the direct photolysis of 2,4-DCP. The loss of 2,4-DCP in the UV/TiO_2(slurry)/H_2O_2 continuous system was greater than that of the UV/TiO_2(slurry) continuous system but not statistically different than the UV/H_2O_2 continuous system, further mimicking batch results.

Although the results of the UV/TiO_2(film) system were statistically the same as the continuous dark experiments, the UV/TiO_2(film)/H_2O_2 system was more successful than the UV only system with respect to the disappearance of 2,4-DCP. This is an indication that the thin film of titanium dioxide in mesoporous silica did not completely inhibit the penetration of UV light. The loss of 2,4-DCP in the UV/TiO_2(film)/H_2O_2 system could be a result of hydroxyl radical production via photolysis of H_2O_2, hydroxyl radical production via photo-excitation of TiO_2, and/or the direct photolysis of 2,4-dichlorophenol. Of the possible mechanisms responsible for the

disappearance of 2,4-DCP in continuous UV/TiO_2(film)/H_2O_2 systems, the improved performance over the UV only system makes it very probable that the direct photolysis of 2,4-DCP was enhanced by the photo-excitation of TiO_2 and/or the photolysis of H_2O_2.

As in batch experimentation, the appearance of byproducts was apparent only in those experiments that employed UV light (Appendix C), and by following the appearance and/or disappearance of the 3.7-minute eluter, a rough gauge of mineralization can be deduced. The production of byproducts in continuous systems utilizing UV light also provides a means to qualitatively differentiate the light and dark experiments that are not statistically different with respect to the disappearance of 2,4-dichlorophenol. The 3.7-minute eluter was not present in any of the chromatographs from the continuous dark experiments, further supporting the loss of 2,4-DCP due to interaction with the Masterflex tubing.

As in the UV only batch experiments (Figure 4.6), the disappearance of 2,4-DCP and the appearance of the 3.7-minute eluter steadily increased throughout the course of the continuous UV only experiments (Figure 4.12). The appearance of the 3.7-minute eluter is an indication that at least some of the loss of 2,4-DCP in continuous UV only experiments can be attributed to the photolysis of 2,4-DCP. The appearance of the 3.7-minute eluter in the continuous UV/H_2O_2 system seems much slower than that of the continuous UV only system (Figure 4.13), but it is also possible that the 3.7-minute eluter

is being simultaneously degraded by hydroxyl radicals and/or interacting with the Masterflex tubing. Although ambiguous in Figure 4.14, the 3.7-minute eluter very gradually appears after 127 seconds of exposure in the UV/TiO_2(slurry) system, and its peak area fluctuates throughout the remainder of the UV/TiO_2(slurry) experiment, which could be a result of simultaneous degradation, interaction with the Masterflex tubing, and/or adsorption onto the suspended titanium dioxide particles. The 3.7-minute eluter appears at a constant rate in the UV/TiO_2(film) system signifying that the loss of 2,4-DCP is not solely a function of the Masterflex/2,4-DCP interaction and distinguishing the UV/TiO_2(film) system from the dark continuous experiments in which the 3.7-minute eltuer did not appear (Figure 4.15). The 3.7-minute eluter seems to appear at a slower rate in the UV/TiO_2(film)/H_2O_2 system than in the UV/TiO_2(film) system (Figure 4.16), which may be an indication of the degradation of the 3.7-minute eluter during the course of the experiment. As illustrated in Figure 4.17, the peak area of the 3.7-minute eluter in continuous UV/TiO_2(slurry)/H_2O_2 systems did not trend upward, as in the continuous UV/H_2O_2 system, but rather fluxuated at low peak areas (Figure 4.13); as in batch UV/TiO_2(slurry)/H_2O_2 experiments, it is likely that the 3.7-minute eluter is adsorbed on the surface of the titanium dioxide, competing for and being degraded by hydroxyl radicals.

With respect to the disappearance of 2,4-dichlorophenol only, the continuous UV/H_2O_2 and UV/TiO_2(slurry)/H_2O_2 system are the most

advantageous. Further, the appearance and disappearance of the 3.7-minute eluter indicates more complete mineralization in the continuous UV/TiO_2(slurry)/H_2O_2 system than any of the other continuous systems. These results are in agreement with the batch results.

Pseudo-First Order Reaction Rate Constants

Pseudo-first order reaction rate constants, k_{p-1}, were determined for those experiments including ultra-violet light via the following equation:

$$-r_{DCP} = \ln\left(\frac{[DCP]}{[DCP]_o}\right) = k_{p-1}\, t \qquad (42)$$

where $-r_{DCP}$ denotes the rate of disappearance of 2,4-dichlorophenol, [DCP] is the concentration of 2,4-dichlorophenol at time t, $[DCP]_o$ is the initial concentration of 2,4-dichlorophenol, and t is the exposure time. Results have been reported in Tables 4.1 and 4.2 based on 3 and 15 minutes of exposure, respectively. Plots from both phases of experimentation are included in Appendix C.

The conditions of the batch UV/TiO_2(slurry) system in Phase I of this work mimic the experimental conditions employed by Hugul et al. (2002): medium-pressure UV light and 0.05 wt% TiO_2 in suspension (Table 2.4 and 3.2). Further, the pseudo-first order reaction rate constant calculated for the batch UV/TiO_2(slurry) system over 15 minutes of exposure via equation 42 is in good agreement with the pseudo-first order reaction rate constant reported

by Hugul et al., 0.018 and 0.0217 per minute, respectively (Table 4.2 and 2.4).

The pseudo-first order reaction rate constants for continuous systems are misleading as they include the loss of 2,4-DCP due to a reaction with the Masterflex tubing and prevent comparison between batch and continuous systems directly. However, the relative effect of ultra-violet light, titanium dioxide, and hydrogen peroxide on reaction rates in both phases of work as well as reaction rates within the same phase can be compared. The pseudo-first order reaction rate for UV only and UV/TiO_2(slurry) systems are the same for continuous experiments but differ by 0.0005 in batch experiments. Also, the fastest pseudo-first order reaction rate for the continuous system is the UV/TiO_2(slurry)/H_2O_2 system, but the UV/H_2O_2 system is the fastest of the batch reactions. The improved rate of reaction in the continuous UV/TiO_2(slurry) system with respect to the continuous UV only system, as well as the rate of the relative rate of reaction of the continuous UV/TiO_2(slurry)/H_2O_2 system may be attributed to the most obvious difference between systems: reactor configuration. The distance from the quartz immersion well to the wall of the batch reactor is approximately 10.7 millimeters, but the diameter of the quartz tubes in the continuous reactor is only 6 millimeters, thereby shortening the distance the UV light must traverse by 4.7 millimeters and improving performance of the UV/TiO_2(slurry)/H_2O_2 system in the continuous reactor. This is an indication that performance of

the batch UV/TiO_2(slurry) may be a result of the inadequate penetration of UV light as well as the aforementioned recombination of the electron-hole pair.

Langmuir-Hinshelwood Kinetics

Langmuir-Hinshelwood kinetics are intended to compensate for the adsorption of a species onto the surface of a catalyst within a reacting system, and as such experiments in this work that did not utilize ultra-violet light and titanium dioxide were not expected to conform to a Langmuir-Hinshelwood kinetic plot owing to the fact that either no reaction took place and/or no catalyst was present in those systems. The Langmuir-Hinshelwood specific reaction rate constant, k, and adsorption equilibrium constant, K, calculated from the plots in Appendix E and equation 30 are listed in Table 4.3.

$$\frac{1}{R_i} = \frac{1}{kKC_i} + \frac{1}{k} \tag{30}$$

Because each set of batch experiments in a given system employed the same initial stock solution of 2,4-DCP, nearly identical initial concentrations of 2,4-DCP resulted, thus preventing the calculation of Langmuir-Hinshelwood rate constants. Of all of the continuous experiments utilizing ultra-violet light, continuous UV/H_2O_2, UV/TiO_2(slurry), UV/TiO_2(slurry)/H_2O_2 and UV/TiO_2(film) systems fit a Langmuir-Hinshelwood kinetic plot of $1/R_i$ versus $1/C_i$, the inverse of the initial reaction rate and the initial concentration, respectively,

with an R-squared value greater than 0.8 (Table 4.3 and Appendix E). Treating the interaction of 2,4-DCP and the Masterflex tubing as a reaction, results from continuous dark experiments were similarly plotted and fit with linear trendlines that resulted in R-squared values greater than 0.7 for continuous dark/H_2O_2, dark TiO_2(slurry), and dark/TiO_2(film)/H_2O_2 systems (Table 4.3 and Appendix E).

All of the Langmuir-Hinshelwood kinetic plots in the literature have both a positive slope and a positive intercept (Serra et al., 1994; Hugul et al., 2002; Ku and Hsieh, 1992; Jardim et al., 1997). However, of the meaningful results calculated from continuous data (R-squared > 0.7), the slope and/or intercept were negative. As such, none of the calculated Langmuir-Hinshelwood constants have any significance. This may be attributed to the interaction between 2,4-DCP and the Masteflex tubing.

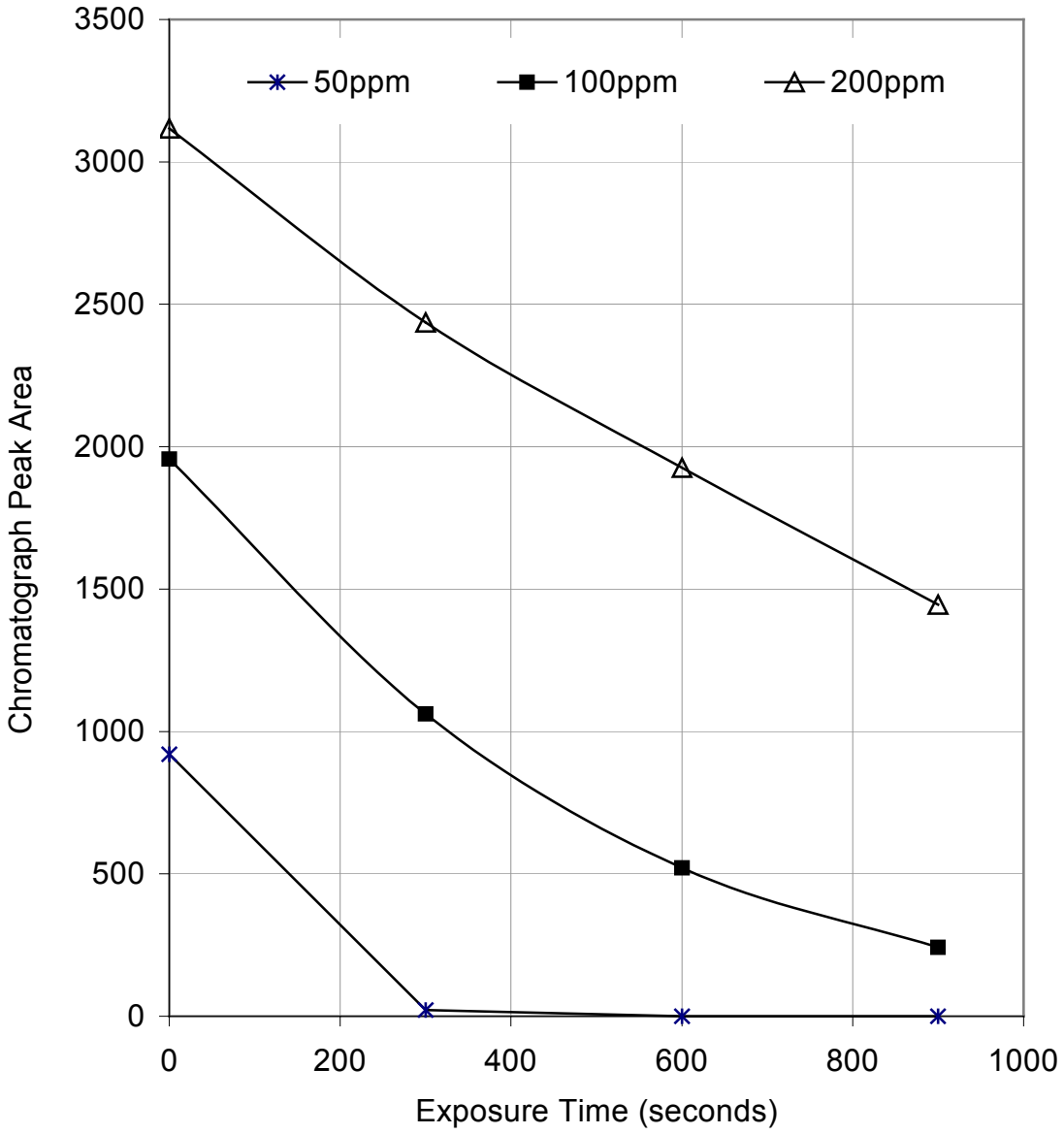

Figure 4.1. The Degradation of 2,4-Dichlorophenol at Initial Concentrations of 50, 100, and 200 ppm in a 400mL Batch Reactor Utilizing UV Light Only.

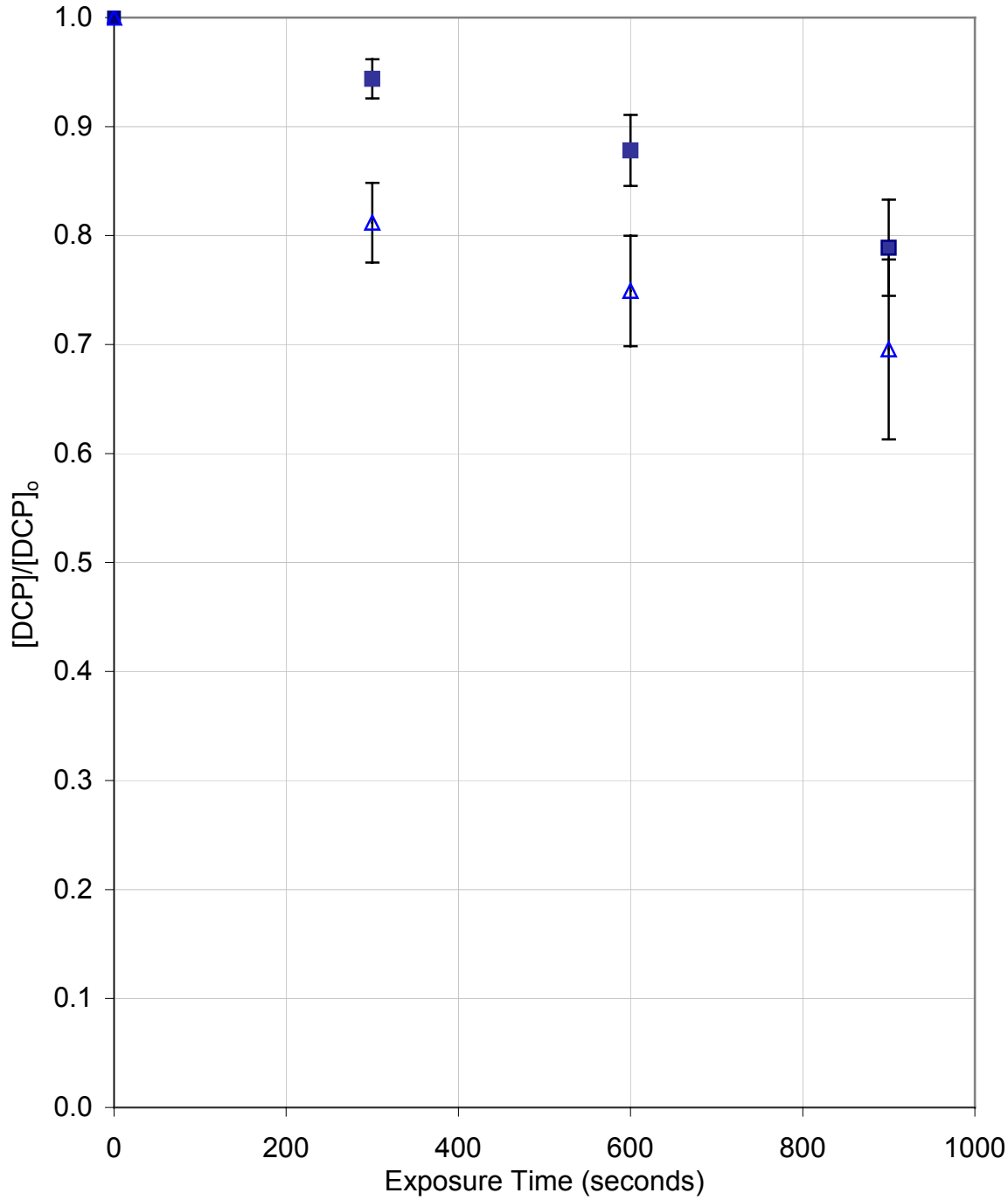

Figure 4.2. The Degradation of 200 ppm 2,4-Dichlorophenol in a 400mL Batch Reactor Utilizing UV Light with either 0.1 wt% TiO_2 in Suspension (■) or 0.05 wt% TiO_2 in Suspension (△).

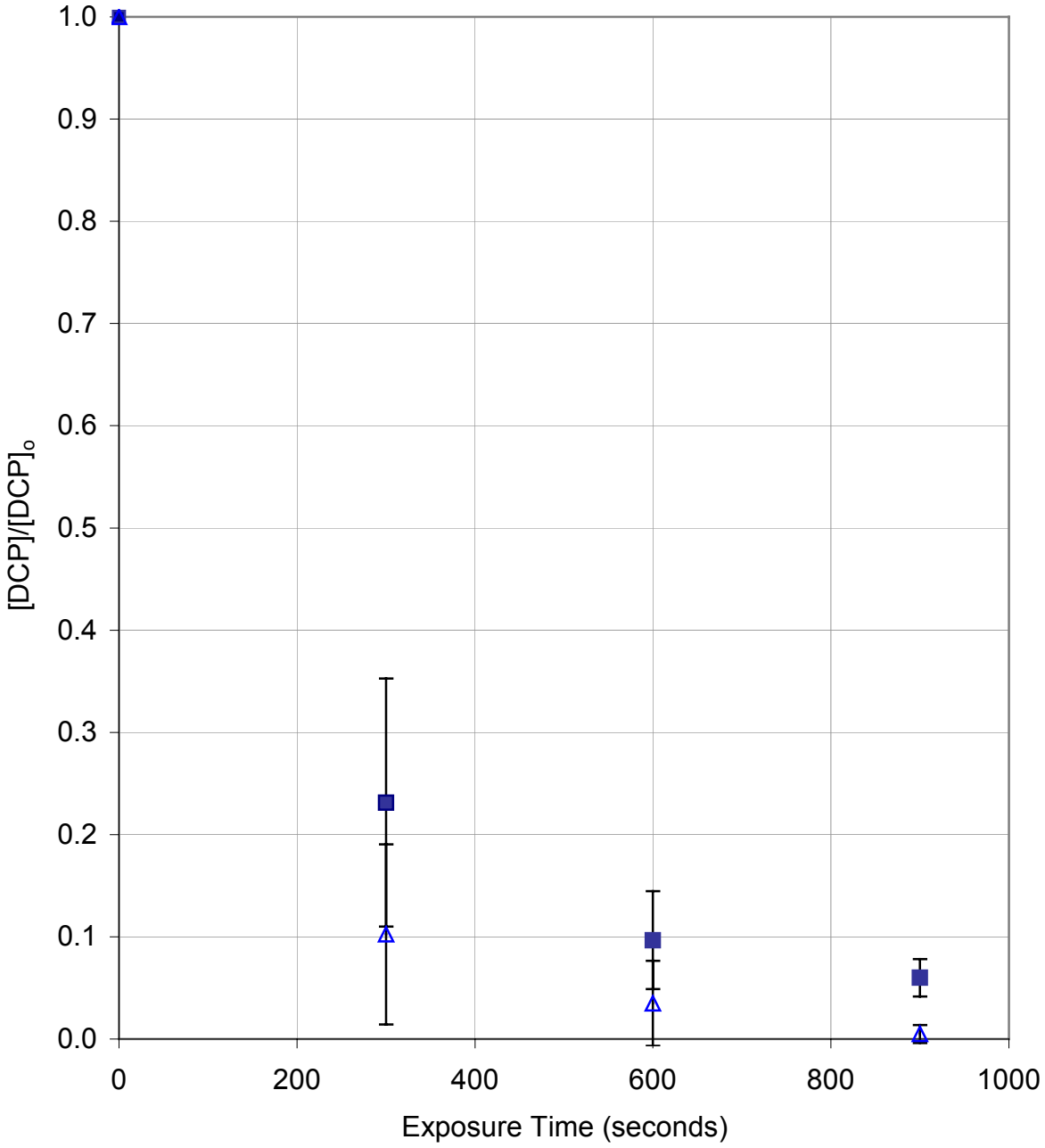

Figure 4.3. The Degradation of 200 ppm 2,4-DCP in a 400mL Batch Reactor Utilizing either UV Light with 0.1 wt% TiO_2 in Suspension and 560 ppm H_2O_2 (△) or UV Light with 560 ppm H_2O_2 (no TiO_2) (■).

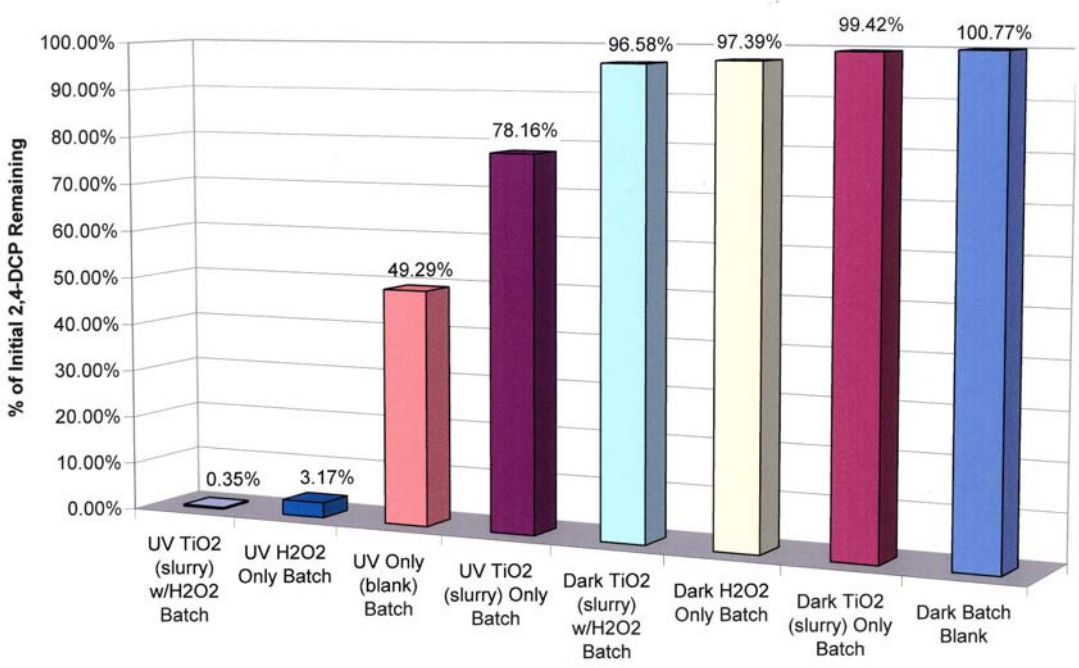

Figure 4.4. The Retention of 2,4-DCP after 15 minutes in Batch Experiments.

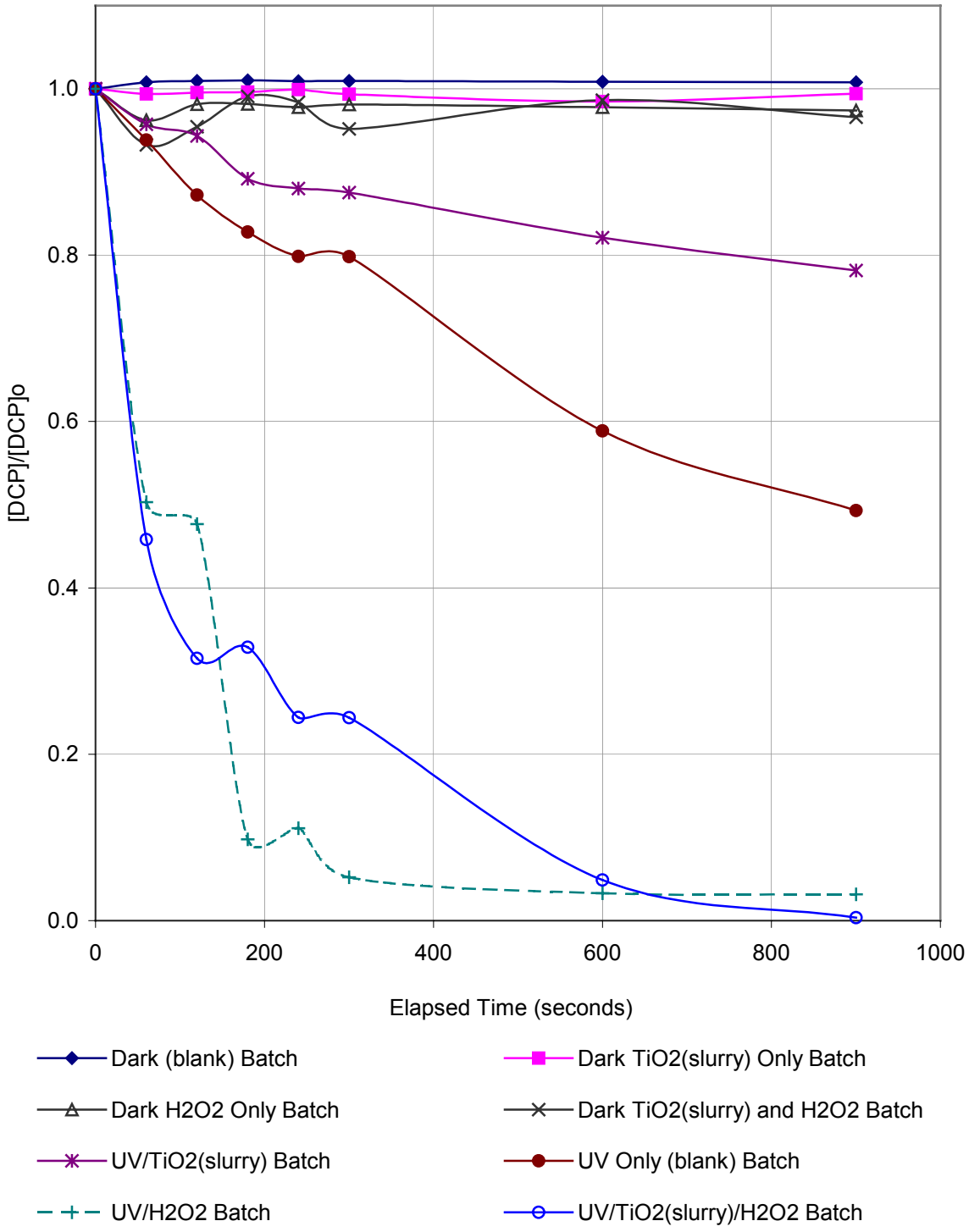

Figure 4.5. Average Rate of Removal of 2,4-DCP in 300mL Batch Photochemical Studies.

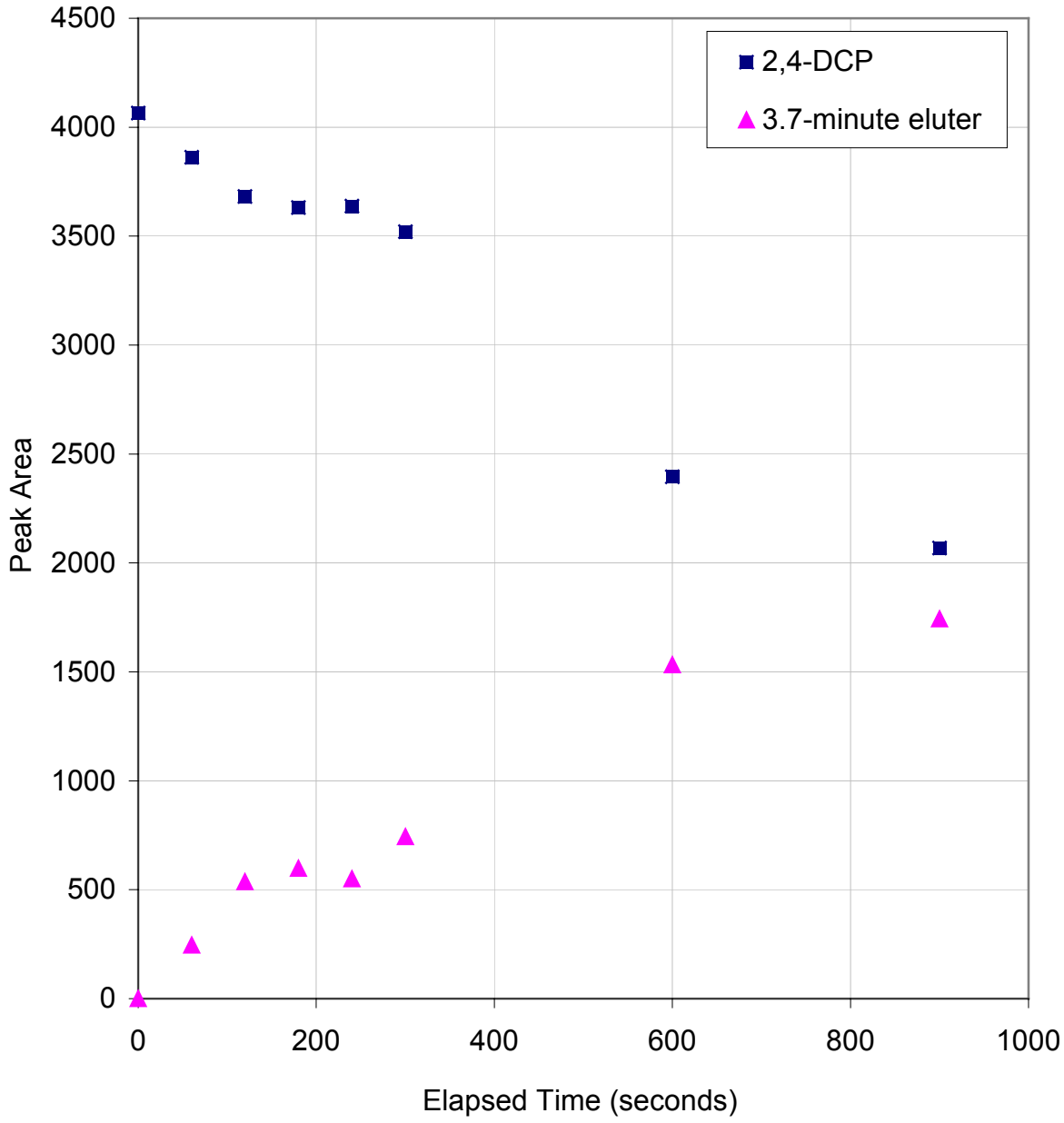

Figure 4.6. The Peak Areas of 2,4-DCP and the 3.7-Minute Eluter in UV Only Batch Systems.

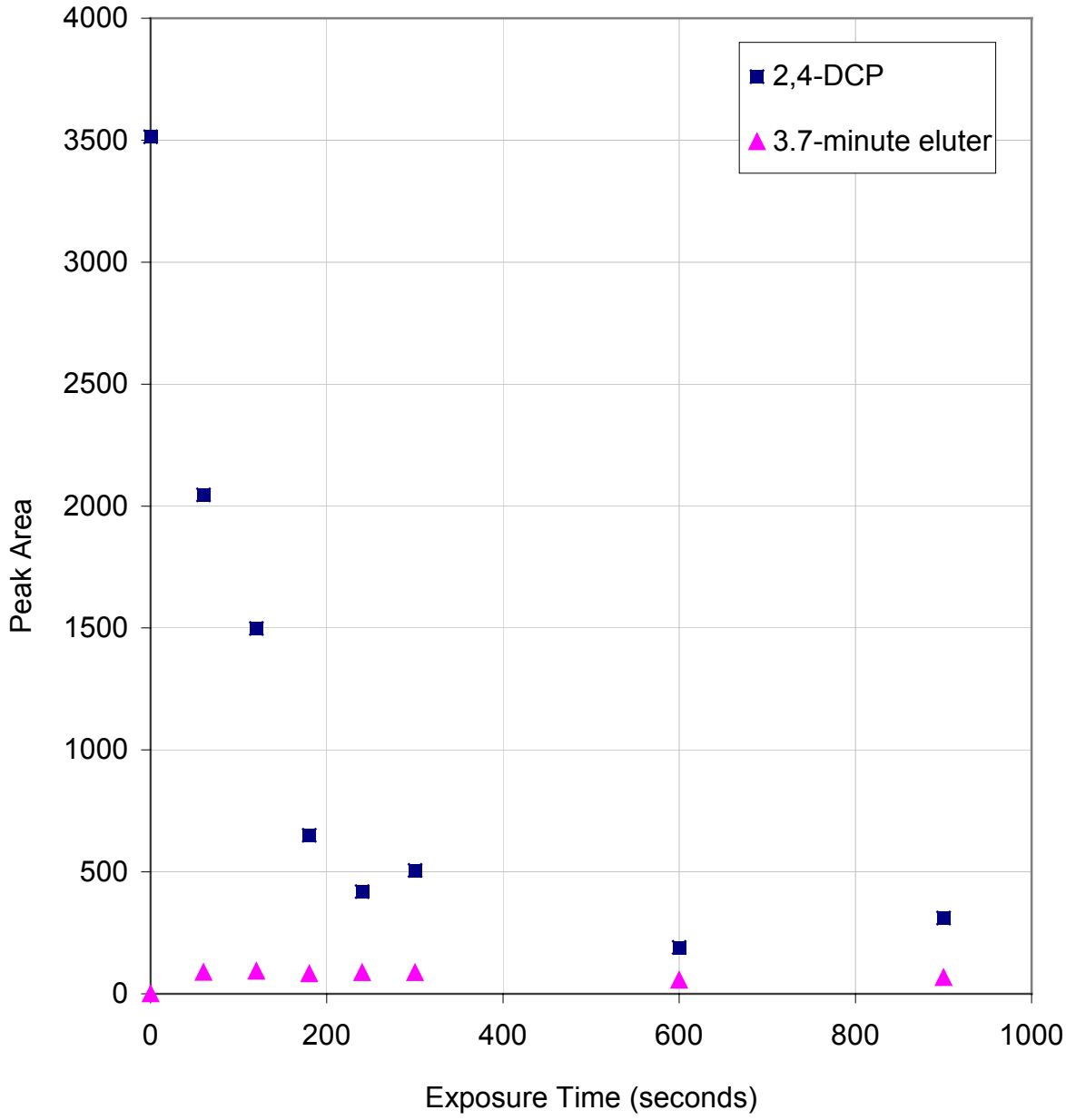

Figure 4.7. The Peak Areas of 2,4-DCP and the 3.7-Minute Eluter in UV/H_2O_2 Batch Systems.

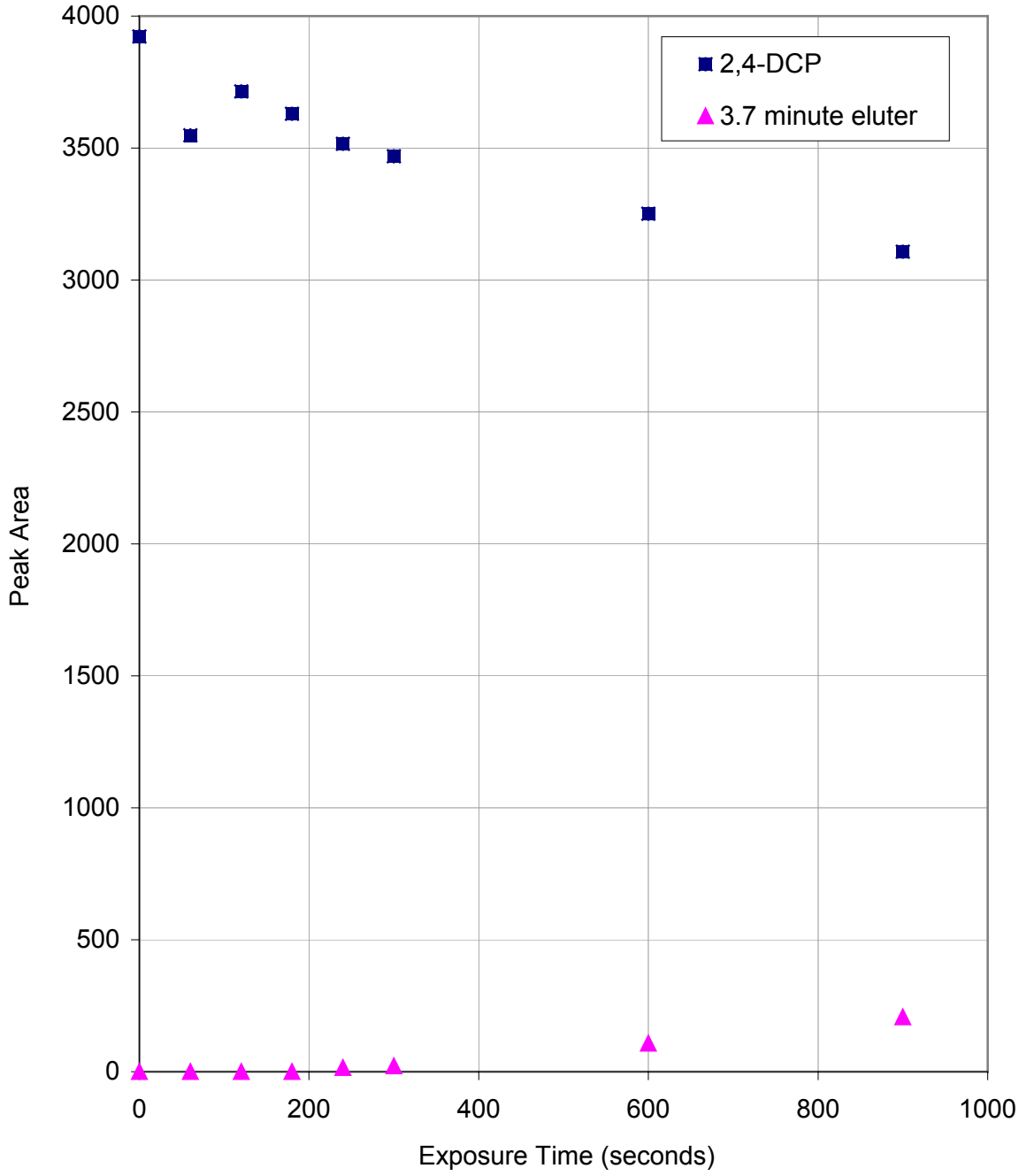

Figure 4.8. The Peak Areas of 2,4-DCP and the 3.7-Minute Eluter in UV/TiO_2(slurry) Batch Systems.

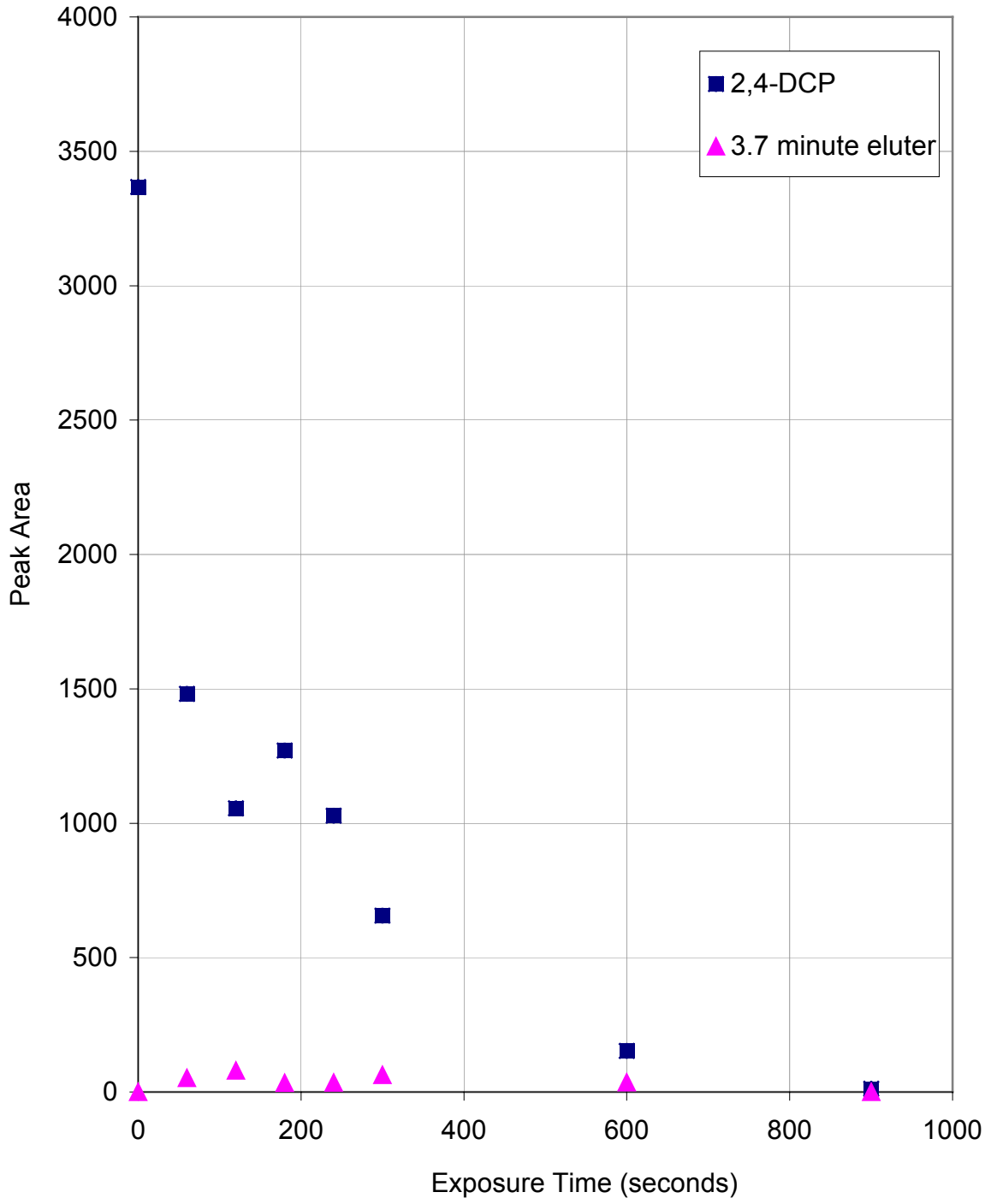

Figure 4.9. The Peak Areas of 2,4-DCP and the 3.7-Minute Eluter in UV/TiO_2(slurry)/H_2O_2 Batch Systems.

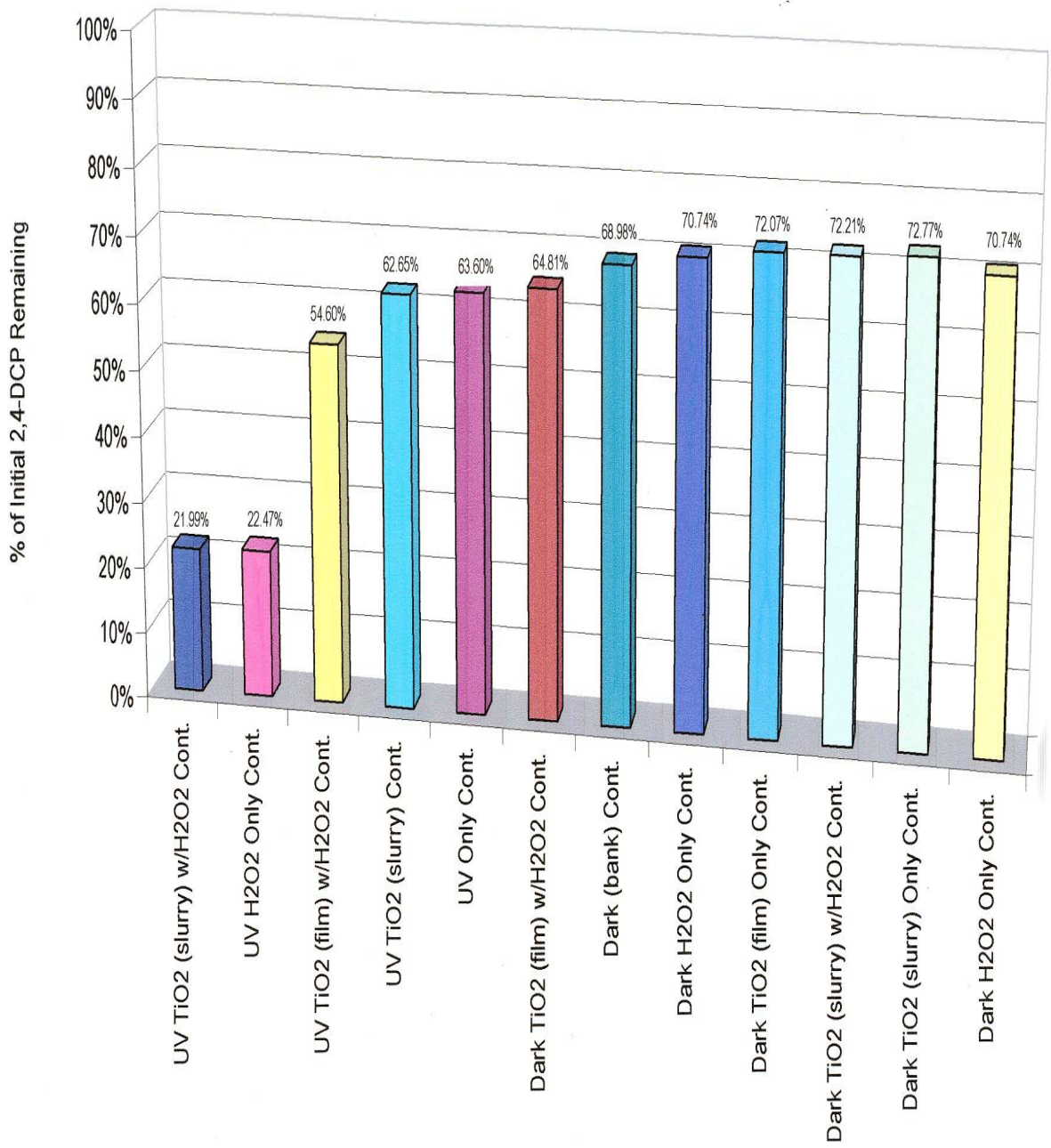

Figure 4.10. The retention of 2,4-DCP After 190 Seconds in the Continuous Reactor.

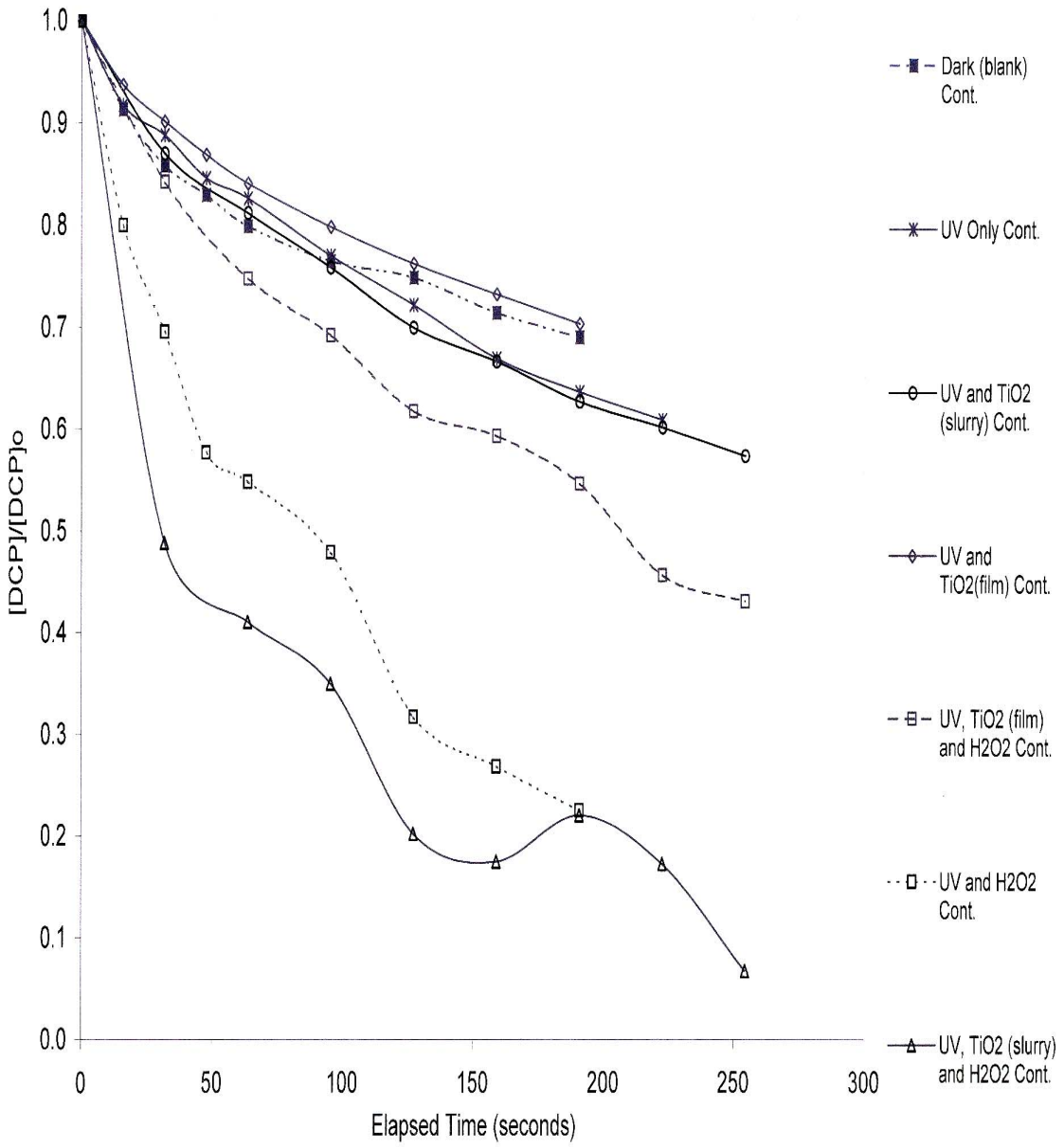

Figure 4.11. Average Rate of Removal of 2,4-DCP in Continuous Photochemical Studies.

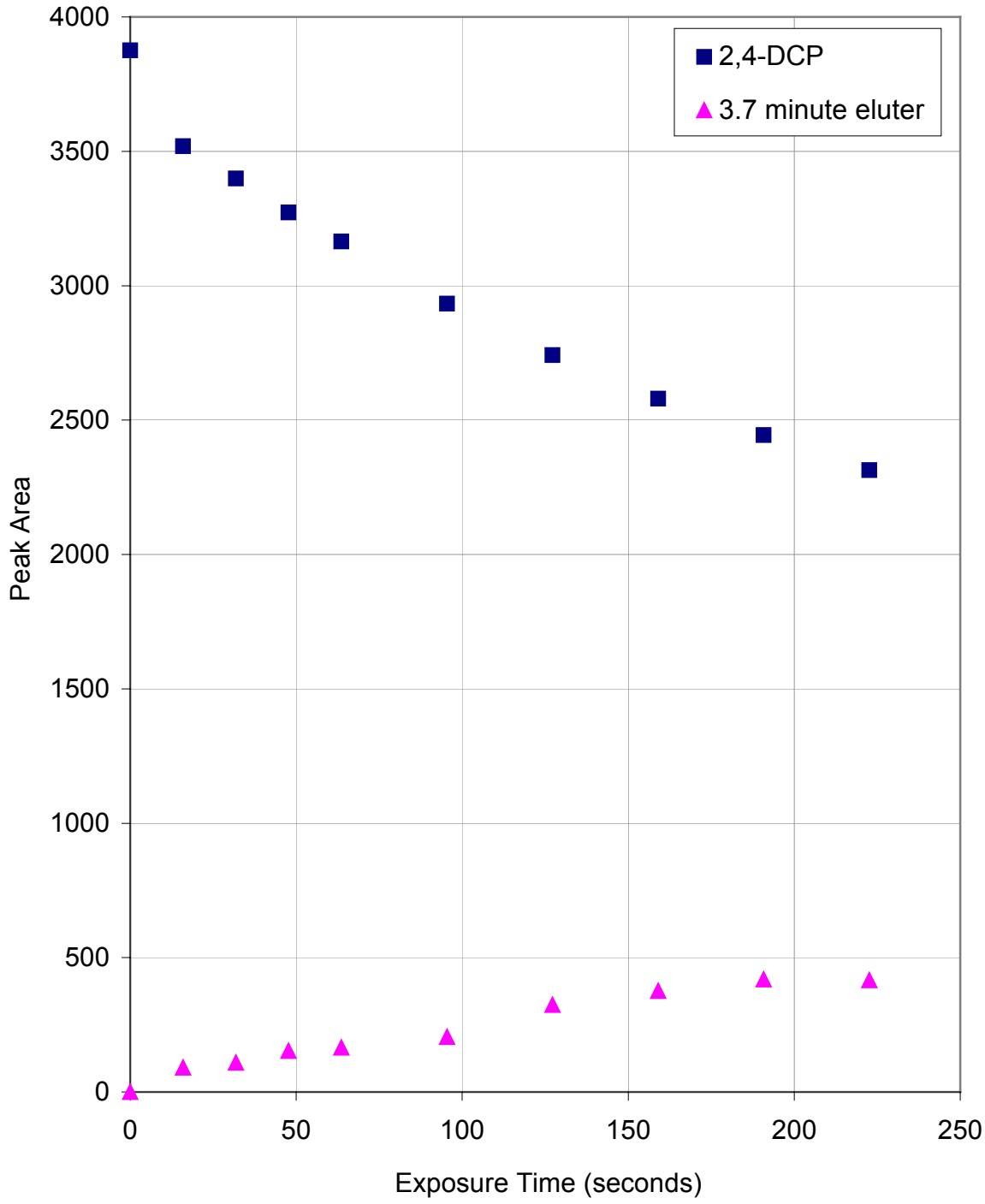

Figure 4.12. The Peak Areas of 2,4-DCP and the 3.7-Minute Eluter in UV Only (blank) Continuous Systems.

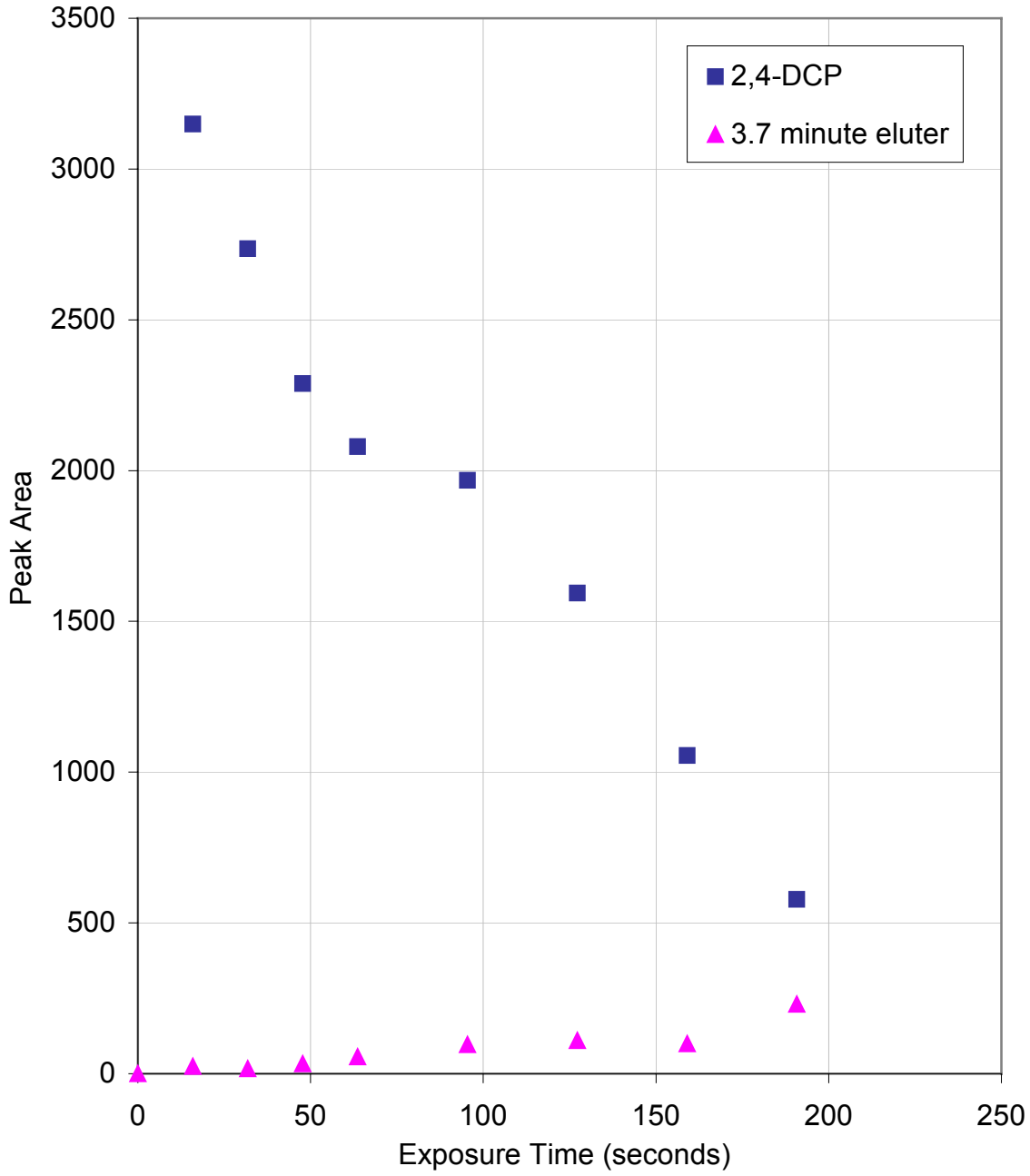

Figure 4.13. The Peak Areas of 2,4-DCP and the 3.7-Minute Eluter in UV/H2O2 Continuous Systems.

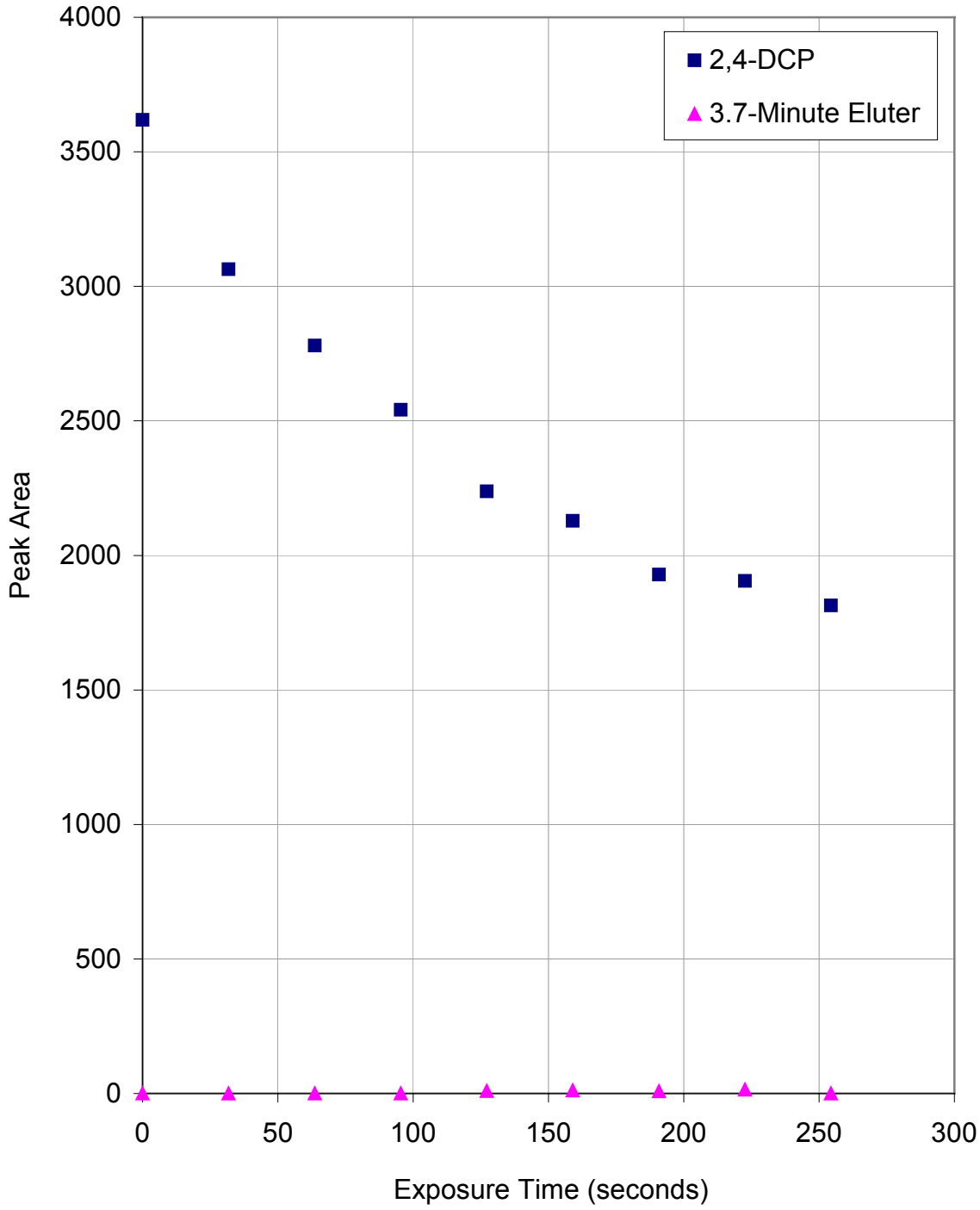

Figure 4.14. The Peak Areas of 2,4-DCP and the 3.7-Minute Eluter in UV/TiO_2(slurry) Continuous Systems.

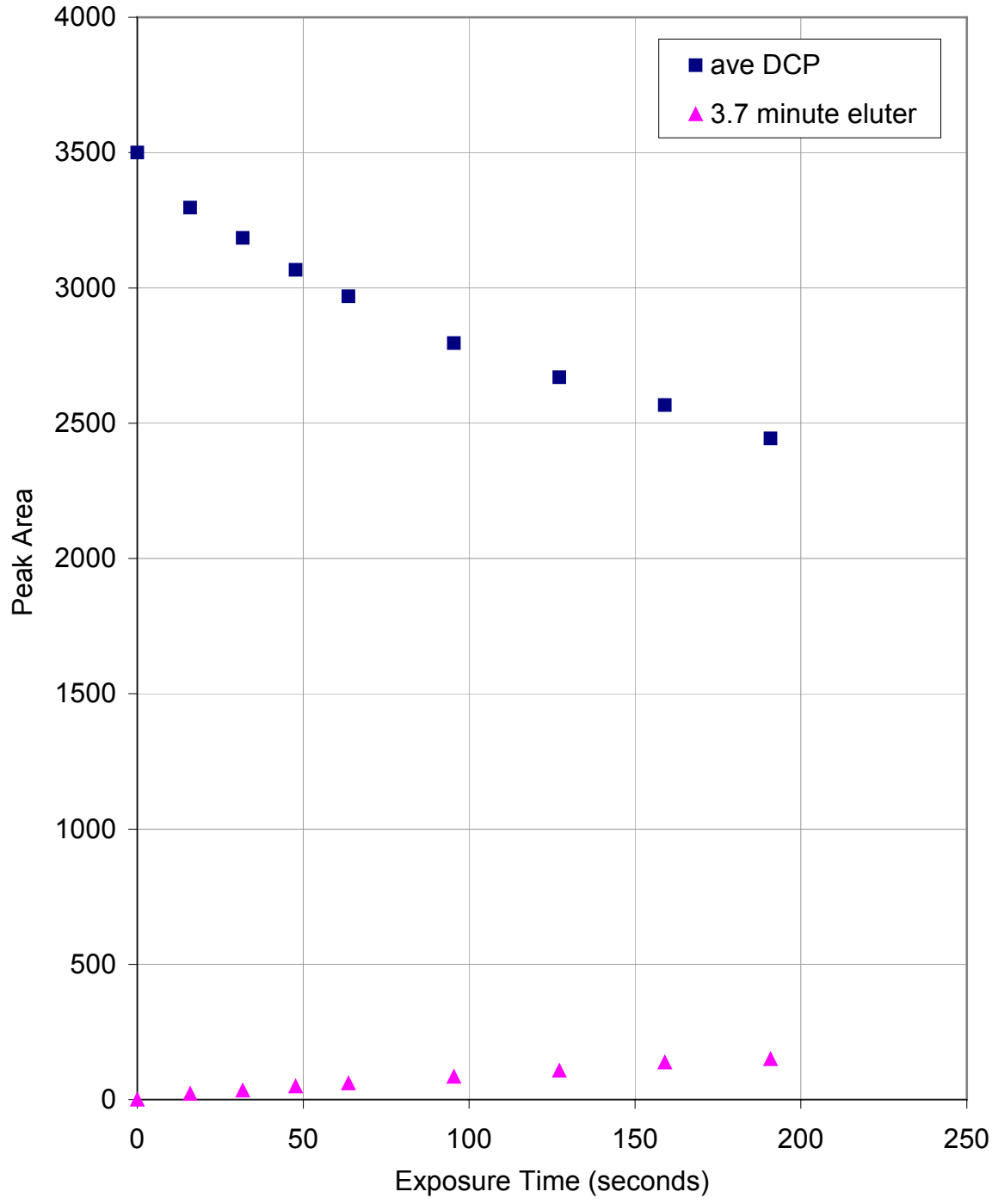

Figure 4.15. The Peak Areas of 2,4-DCP and the 3.7-Minute Eluter in Continuous UV/TiO_2(film) Systems.

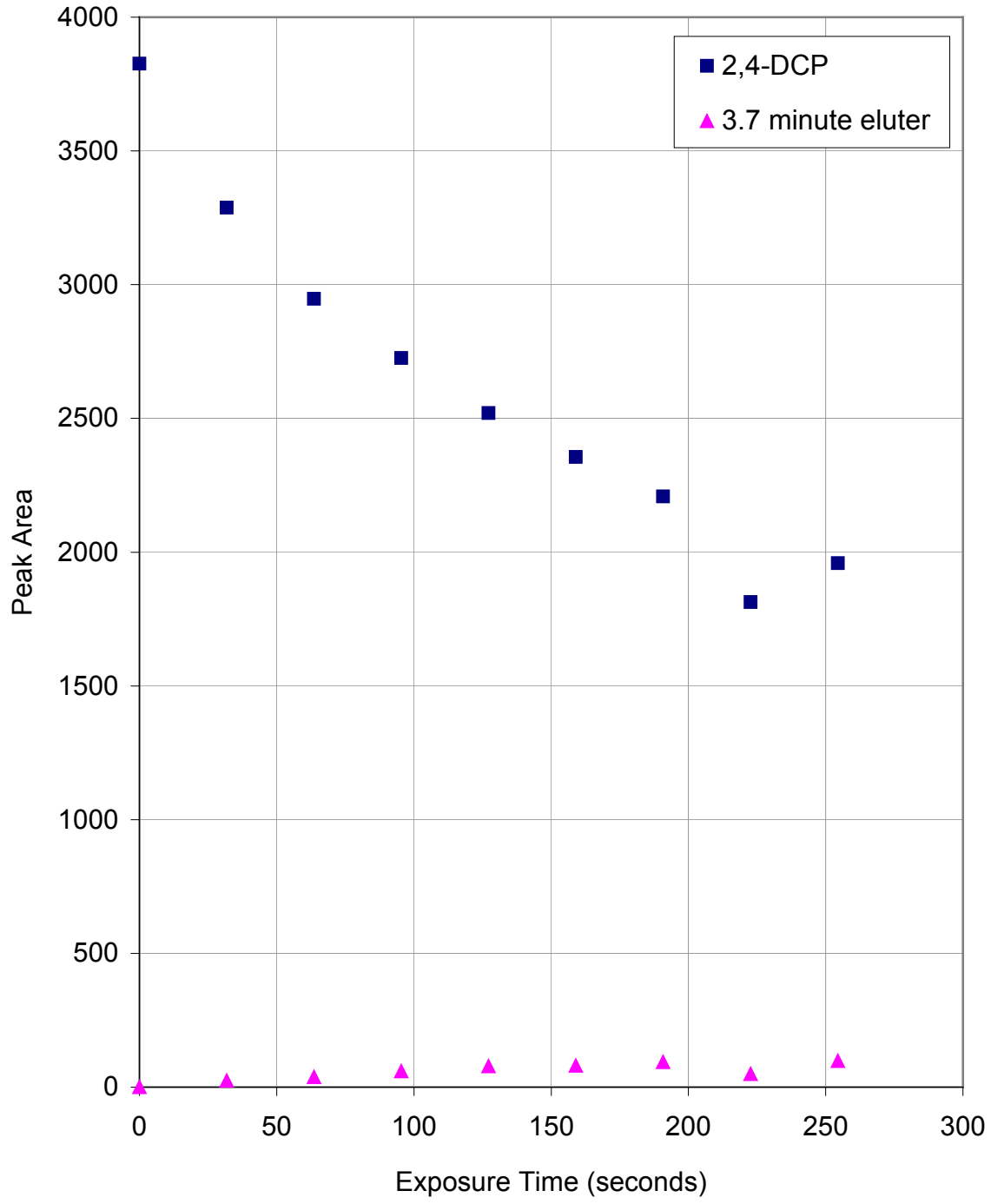

Figure 4.16. The Peak Areas of 2,4-DCP and the 3.7-Minute Eluter in UV/TiO_2(film)/H_2O_2 Continuous Systems.

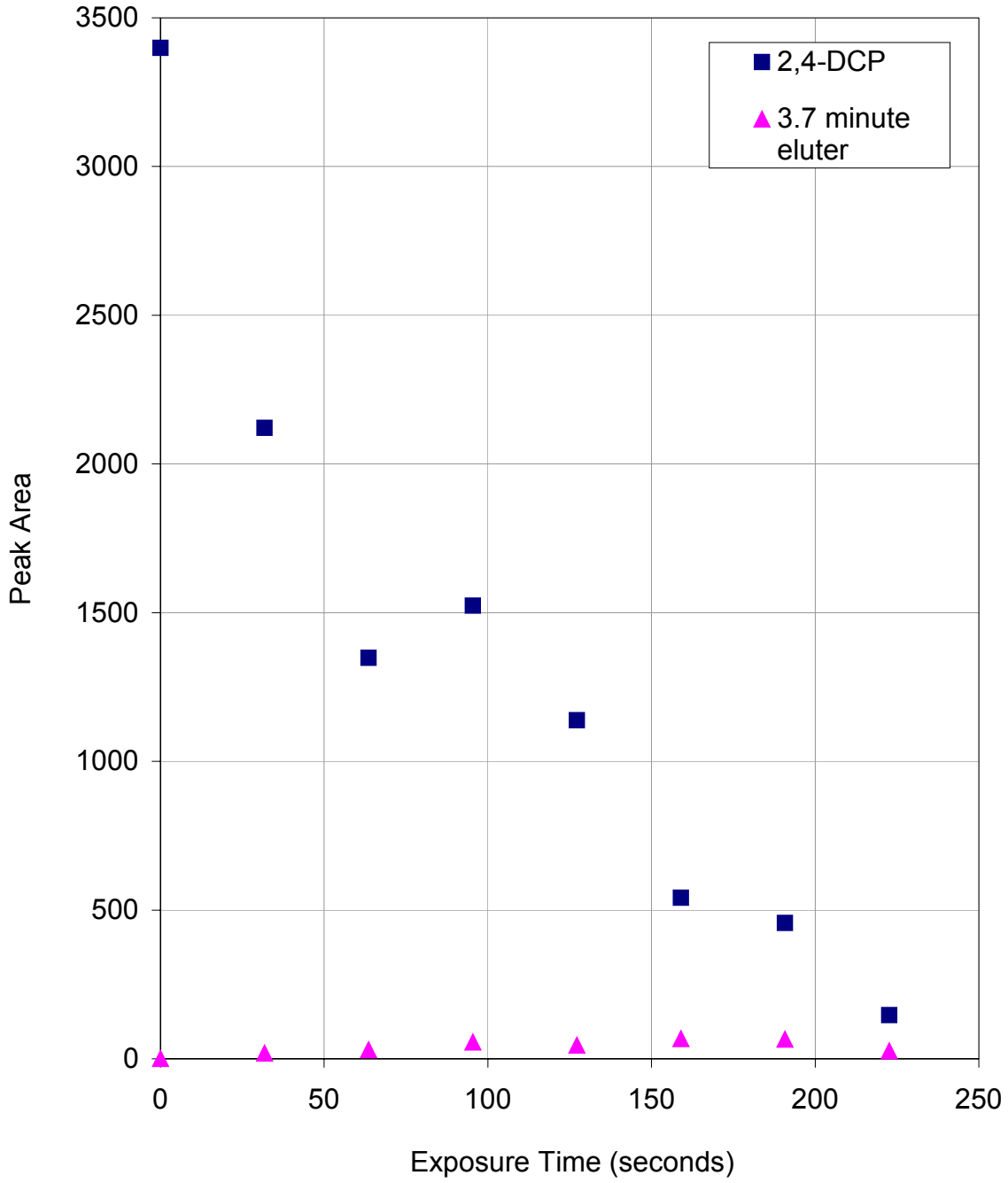

Figure 4.17. The Peak Areas of 2,4-DCP and the 3.7-Minute Eluter in UV/TiO_2(slurry)/H_2O_2 Continuous Systems.

Table 4.1. Pseudo-First Order Reaction Rate Constants Calculated via 3 Minutes of Data (Plots in Appendix D).

Conditions	**Pseudo-First Order Rate Constant**		**R^2**
	(sec-1)	**(min-1)**	
Batch UV Only	0.0011	0.066	0.9961
Batch UV H_2O_2 Only	0.0109	0.654	0.8432
Batch UV TiO_2 (slurry) Only	0.0006	0.036	0.957
Batch UV TiO_2 (slurry) w/H_2O_2	0.0077	0.462	0.733
Cont.UV Only	0.0024	0.144	0.9541
Cont. UV H_2O_2 Only	0.0084	0.504	0.9675
Cont. UV TiO_2 (slurry)	0.0024	0.144	0.9397
Cont. UV TiO_2 (slurry) w/H_2O_2	0.0098	0.588	0.8412
Cont. UV TiO_2 (film) Only	0.0021	0.126	0.9193
Cont. UV TiO_2 (film) w/H_2O_2	0.0034	0.204	0.9715

Table 4.2. Pseudo-First Order Reaction Rate Constants Calculated from 15 Minutes of Data (Plots in Appendix E).

Conditions	**Pseudo-First Order Rate Constant**		**R^2**
	(sec-1)	**(min-1)**	
UV Only Batch	0.0008	0.048	0.9828
H2O2 Only Batch	0.0099	0.594	0.9206
TiO2 (slurry) w/H2O2 Batch	0.0053	0.318	0.8824
TiO2 (slurry) Only Batch	0.0003	0.018	0.7844

Table 4.3. Langmuir-Hinshelwood Rate Constants.

System	slope	intercept	R^2	Langmuir-Hinshelwood Reaction Rate Constant (Molar/second)	Langmuir-Hinshelwood Adsorption Equilibrium Constant ($Molar^{-1}$)
Dark (blank) Cont.	-6.80E-03	3.117	0.245	meaningless	
Dark H2O2 Cont.	-4.98E-02	42.358	0.996	2.361E-02	-8.506E+02
Dark TiO2(slurry) Cont.	-3.26E-02	26.282	0.999	3.805E-02	-8.062E+02
Dark TiO2(slurry) H2O2 Cont.	5.90E-03	-8.608	0.403	meaningless	
Dark TiO2(film) Cont.	2.00E-03	-4.290	0.007	meaningless	
Dark TiO2(film) H2O2 Cont.	6.30E-03	-7.683	0.739	-1.302E-01	-1.220E+03
UV Only (blank) Cont.	6.80E-03	-8.160	0.181	meaningless	
UV H2O2 Cont.	3.20E-03	-3.540	0.912	-2.825E-01	-1.106E+03
UV TiO2(slurry) Cont.	-4.02E-02	36.188	0.999	2.763E-02	-9.002E+02
UV TiO2(slurry) H2O2 Cont.	-3.00E-04	0.065	0.808	1.529E+01	-2.180E+02
UV TiO2(film) Cont.	3.10E-03	-5.770	0.900	-1.733E-01	-1.861E+03
UV TiO2(film) H2O2 Cont.	1.60E-03	-2.690	0.043	meaningless	

CHAPTER V.

CONCLUSIONS

The following conclusions may be drawn based on the experimental evidence obtained:

1. As evidenced by its disappearance, the following batch systems will oxidize 2,4-dichlorophenol: UV only, UV/H_2O_2, UV/TiO_2(slurry), and UV/TiO_2(slurry)/H_2O_2.
2. As evidenced by its disappearance, the following continuous systems will oxidize 2,4-dichlorophenol: UV/H_2O_2, UV/TiO_2(slurry), and UV/TiO_2(slurry)/H_2O_2.
3. As evidenced by both the disappearance of 2,4-dichlorophenol and the appearance of the 3.7-minute eluter, the continuous UV only, UV/TiO_2(film) and UV/TiO_2(film)/H_2O_2 systems are capable of oxidizing 2,4-dichlorophenol.
4. In both phases of work, the UV/H_2O_2 and UV/TiO_2(slurry)/H_2O_2 systems were the most advantageous with respect to the disappearance of 2,4-dichlorophenol.
5. The UV/TiO_2(slurry)/H_2O_2 system was superior to the all of the other systems with respect to the disappearance of both 2,4-dichlorophenol and the 3.7-minute eltuer in both phases of work.

6. The batch configuration is a good predictor of the performance of the continuous reactor.
7. The shorter path length of the ultra-violet light in the continuous reactor results in a faster reaction, as evidenced by the relative pseudo-first order reaction rate constants for both reactor configurations.
8. The addition of hydrogen peroxide significantly enhanced the performance of titanium dioxide systems in both phases of work.
9. The psuedo-first order reaction rate constant for the batch UV/TiO_2 system agrees with those reported in the literature for similar systems.
10. The experimental data do not fit the Langmuir-Hinshelwood model, which is most likely due to the interaction between the Masterflex tubing and 2,4-dichlorophenol.
11. The continuous UV/TiO_2(film) system behaves similarly to the continuous UV/TiO_2(slurry) system with respect to the behavior of the 3.7-minute eluter, and both systems are significantly enhanced by the addition of hydrogen peroxide. However, the continuous UV only and UV/TiO_2(film) systems were not statistically different, and there is no evidence to distinguish the reaction mechanism in the continuous UV/TiO_2(film)/H_2O_2 system from the continuous UV/H_2O_2 system. The performance of the UV/TiO2(film) system could be due to the photolysis of 2,4-DCP and/or the production of hydroxyl radicals via the photo-excitation of titanium dioxide. The performance of the

UV/TiO_2(film)/H_2O_2 system could be accounted for by the photolysis of H_2O_2 hindered by the penetration of light through the thin film of mesoporous silica and/or the photo-excitation of titanium dioxide enhanced by the addition of electron acceptors. The titanium dioxide loading in the UV/TiO_2(film) system is not comparable to the 0.05 wt% in suspension in the UV/TiO_2(slurry) or UV/TiO_2(slurry)/H_2O_2 systems and may also be responsible for the difference in system performance.

CHAPTER VI.

SUGGESTIONS FOR FUTURE WORK

Several opportunities exist for further research:

1. The coated quartz tubes could be analyzed for titanium dioxide via metals analysis to determine the titanium dioxide available to the contaminant species. This had previously been included within the scope of this thesis but was not completed due to equipment malfunction.
2. The tubes at Alabama could be coated on only one side to determine the effect of reactor configuration. The established photo-reactivity of the thin films of titanium dioxide in mesoporous silica could be a result of the excitation of the titanium dioxide on the outside of the coated tubes only, which would insinuate that a different continuous reactor configuration would better utilize the thin film of titanium dioxide.
3. The species eluted at 3.7 minutes throughout this work could be identified.
4. The photo-reactivity of the thin-films of titanium dioxide could be harnessed in a different reactor configuration; a falling film reactor

surrounding a UV light source and utilizing a thin film of titanium dioxide immobilized on its walls might prove to be successful.

5. The source and quantity of oxidant could be optimized. The advantages and disadvantages of air, ozone, and hydrogen peroxide in photochemical systems with and without titanium dioxide could be identified.
6. With an established continuous reactor design, the most advantageous research employing ultra-violet light/titanium dioxide technology would investigate mixtures of different contaminant species and real samples of industrial wastewater.

WORKS CITED

Acros Organics. "Material Safety Data Sheet for 2,4-Dichlorophenol." Fairlawn, 2002.

Alberius, P. C. A.; Frindell, K. L.; Hayward, R. C.; Kramer, E. J.; Stucky, G. D.; Bhmelka, B. F. *Chem. Mater*. **2002**, *14*, 3284-3294.

Almquist, C. B.; Sahle-Demessie, E.; Enriques, J.; Biswas, P. *Environ Prog*. **2003**, *22*(1), 14-23.

Bahnemann, D. In *Environmental Photo-chemistry*; Hutzinger, O., Ed.; Photocatalytic Detoxification of Polluted Waters; Springer: New York, 1999; Chapter 11.

Environmental Protection Agency. *Advanced Photochemical Oxidation Processes Handbook*, U.S. Office of Research and Development. U.S. Government Printing Office: Washington, DC, 1998; EPA/625/R-98/004.

Chang, H. T.; Wu, N,; Zhu, F. *Wat. Res*. **2000**, *34*(2), 407-416.

Fogler, H. S. *Elements of Chemical Reaction Engineering*; Prentice: Upper Saddle River, 1999.

Hill, C. G. *An Introduction to Chemical Engineering Kinetics and Reactor Design*; Wiley: New York, 1977.

Hoffman, M. R.; Martin, S. T.; Choi, W.; Bahnemann, D. W. *Chem. Rev.* **1995**, *95*, 69-96.

Hugul, M., Ercag, E., Apak, R. *J. Environ. Sci. Health*. **2002**, *A37*(3), 365-383.

Jardim, W. F.; Moraes, S. G.; Takiyama, M. M. K. *Water Res.* **1997**, *32*, 1728 - 1732.

Kotz, J. C.; Treichel, P. *Chemistry and Chemical Reactivity*; Harcourt Brace: New York, 1996; pp 188-198.

Ku, Y.; Hsieh, C. *Wat. Res.* **1992**, *26*(11), 1451-1456.

Legrini, O.; Oliveros, E.; Braun, A. M. *Chem. Rev*. **1993**, *93*, 671-698.

Matthews, R. W. *Sol. Energy*. **1987**, *38*(6), 405-413.

Matthews, R. *Water Res*. **1990**, *24*(5), 653-660.

Munter, R.; Preis, S.; Kallas, J.; Trapido, M.; Veressiniina, Y. *J. Chem. Technol. Biotechnol*. **2001**, *76*(3), 312-320.

Ohno, T.; Sarukawa, K.; Tokieda, K.; Matsumura, M. *J. Catal*. **2001**, *203*, 82-86

Ollis, D. F.; Turchi, C. *Environ. Prog*. **1990**, *9*(4), 229-324.

Rupert, J.; Bauer, R. *Chemosphere*. **1994**, *28*, 1447-1454.

Serra, F.; Trillas, M.; Garcia, J.; Domenech, X. *J. Environ. Sci. Health*. **1994**, *A29*, 1409-1421.

Sigma-Aldrich. "Material Safety Data Sheet for 2,4-Dichlorophenol." St. Louis, 2002.

Smith, J. M. *Chemical Engineering Kinetics*; McGraw-Hill: New York, 1970.

Supelco, Inc. "Material Safety Data Sheet for 2,4-Dichlorophenol." Bellefonte, 2002.

Suri, R. P. S.; Liu, J.; Hand, D. W.; Criienden, J. C.; Perram, D. L.; Mullins, M. E. *Wat. Environ. Res*. **1993**, *65*(5), 665-673.

Trapido, M.; Veressinina, Y.; Munter, R. *J. Environ. Eng.* **1998**, *124*(8), 690-694.

Turchi, C. S.; Ollis, D. F. *J. Catal*. **1990**, *122*, 178-192.

.

APPENDIX A: STATISTICS

Table A.1. Statistical Analysis of Results from the Same Sample Analyzed on Three Consecutive Days via HPLC.

Date	Peak Area	2,4-DCP Concentration (ppm)
24-Feb-03	4115.8442	194.0768
25-Feb-03	4113.4180	193.9627
26-Feb-03	4116.1157	194.0896

Descriptive Statistics

Mean	194.0430
Standard Error	0.0403
Median	194.0768
Standard Deviation	0.0699
Sample Variance	0.0049
Range	0.1269
Minimum	193.9627
Maximum	194.0896
Sum	582.1291
Count	3
Confidence Level(95.0%)	0.1736

Table A.2. Statistical Analysis of Results from the Same Sample Analyzed Five Consecutive Times via HPLC.

Injection	Peak Area	2,4-DCP Concentration (ppm)
1	3755.1895	177.1078
2	3749.9356	176.8606
3	3742.5435	176.5128
4	3732.0230	176.0178
5	3721.8245	175.5379

Descriptive Statistics

Mean	176.4074
Standard Error	0.2841
Median	176.5128
Standard Deviation	0.6354
Sample Variance	0.4037
Range	1.5699
Minimum	175.5379
Maximum	177.1078
Sum	882.0369
Count	5
Confidence Level(95.0%)	0.7889

Table A.3. Statistics for Batch Experiments after 3 minutes of UV Exposure.

Run	dark blank batch	dark h2o2 batch	dark tio2 slurry batch	dark tio2 slurry h2o2 batch	uv only batch	uv h2o2 batch	uv tio2 slurry batch	uv tio2 slurry h2o2 batch	Total	
1	0.9960	0.9676	0.9974	1.0060	0.8932	0.1850	0.9252	0.3442		
2	0.9981	1.0069	0.9968	0.9762	0.8366	0.0312	0.8892	0.2646		
3	1.0364	0.9711	0.9940	0.9910	0.7537	0.0764	0.8609	0.3772		
sum	3.0305	2.9456	2.9882	2.9732	2.4835	0.2926	2.6753	0.9860	18.3749	total
mean	1.0102	0.9819	0.9961	0.9911	0.8278	0.0975	0.8918	0.3287	2.2969	average
SS_i	0.0010	0.0009	0.0000	0.0004	0.0098	0.0125	0.0021	0.0067	0.0336	SSE
S_i^2	0.0005	0.0005	0.0000	0.0002	0.0049	0.0062	0.0010	0.0034	0.0021	MSE
								$t^{16}_{0.025}$=	2.1200	
								LSD(0.05) =	0.0793	

	Exp.	dark blank batch	dark tio2 slurry batch	dark tio2 slurry h2o2 batch	dark h2o2 batch	uv tio2 slurry batch	uv only batch	uv tio2 slurry h2o2 batch	uv h2o2 batch
	mean	1.0102	0.9961	0.9911	0.9819	0.8918	0.8278	0.3287	0.0975
uv h2o2 batch	0.0975	0.9126 SIG	0.8985 SIG	0.8935 SIG	0.8843 SIG	0.7942 SIG	0.7303 SIG	0.2311 SIG	
uv tio2 slurry h2o2 batch	0.3287	0.6815 SIG	0.6674 SIG	0.6624 SIG	0.6532 SIG	0.5631 SIG	0.4992 SIG		
uv only batch	0.8278	0.1823 SIG	0.1682 SIG	0.1632 SIG	0.1540 SIG	0.0639			
uv tio2 slurry batch	0.8918	0.1184 SIG	0.1043 SIG	0.0993 SIG	0.0901 SIG				
dark h2o2 batch	0.9819	0.0283	0.0142	0.0092					
dark tio2 slurry h2o2	0.9911	0.0191	0.0050						
dark tio2 slurry batch	0.9961	0.0141							
dark blank batch	1.0102								

Table A.4. Statistics for Batch Experiments after 15 minutes of exposure.

Exp.	dark blank batch	dark h2o2 batch	dark tio2 slurry batch	dark tio2 slurry h2o2 batch	uv only batch	uv h2o2 batch	uv tio2 slurry batch	uv tio2 slurry h2o2 batch	Total	
1	0.9930	0.9660	0.9967	0.9682	0.5088	0.0885	0.7921	0.0000		
2	0.9932	0.9938	0.9884	0.9635	0.5575	0.0067	0.7914	0.0069		
3	1.0369	0.9618	0.9975	0.9659	0.4125	0.0000	0.7615	0.0037		
sum	3.0231	2.9216	2.9826	2.8976	1.4788	0.0952	2.3450	0.0106	15.7545	total
mean	1.0077	0.9739	0.9942	0.9659	0.4929	0.0317	0.7817	0.0035	1.9693	average
SS_i	0.0013	0.0006	0.0001	0.0000	0.0109	0.0049	0.0006	0.0000	0.0183	SSE
S_i^2	0.0006	0.0003	0.0000	0.0000	0.0054	0.0024	0.0003	0.0000	0.0011	MSE
							$t^{16}_{0.025}$=		2.1200	
							LSD(0.05) =		0.0586	

	Exp	dark blank batch	dark tio2 slurry batch	dark h2o2 batch	dark tio2 slurry h2o2 batch	uv tio2 slurry batch	uv only batch	uv h2o2 batch	uv tio2 slurry h2o2 batch
Exp	mean	1.0077	0.9942	0.9739	0.9659	0.7817	0.4929	0.0317	0.0035
uv tio2 slurry h2o2 batch	0.0035	1.0042	0.9907	0.9703	0.9623	0.7781	0.4894	0.0282	
		SIG!	SIG!	SIG!	SIG!	SIG!	SIG!		
uv only batch	0.0317	0.9760	0.9625	0.9421	0.9341	0.7499	0.4612		
		SIG!	SIG!	SIG!	SIG!	SIG!	SIG!		
uv tio2 slurry batch	0.4929	0.5148	0.5013	0.4809	0.4729	0.2887			
		SIG!	SIG!	SIG!	SIG!	SIG!			
uv h2o2 batch	0.7817	0.2260	0.2125	0.1922	0.1842				
		SIG!	SIG!	SIG!	SIG!				
dark tio2 slurry h2o2 batch	0.9659	0.0419	0.0284	0.0080					
dark tio2 slurry batch	0.9739	0.0338	0.0203						
dark h2o2 batch	0.9942	0.0135							
dark blank batch	1.0077								

Table A.5. Statistics for Continuous Experiments (part 1 of 2).

Run	dark blank cont	dark h2o2 cont	dark tio2 slurry cont	dark tio2 slurry h2o2	dark tio2 film cont.	dark tio2 film h2o2 cont.	uv only cont	uv h2o2 cont	uv tio2 slurry cont	uv tio2 slurry h2o2 cont	uv tio2 film cont.	uv tio2 film h2o2 cont.	Total	
1	0.6390	0.6570	0.6660	0.7430	0.6930	0.6060	0.6310	0.1480	0.5330	0.1340	0.6980	0.5770		
2	0.7090	0.7140	0.7570	0.6530	0.7240	0.6480	0.6140	0.2810	0.6670	0.2820	0.6950	0.5310		
3	0.7220	0.7510	0.7600	0.7710	0.7460	0.6900	0.6640	0.2450	0.6790	0.2440	0.7160	0.5300		
sum	2.0700	2.1220	2.1830	2.1670	2.1630	1.9440	1.9090	0.6740	1.8790	0.6600	2.1090	1.6380	21.5180	total
mean	0.6900	0.7073	0.7277	0.7223	0.7210	0.6480	0.6363	0.2247	0.6263	0.2200	0.7030	0.5460	1.7932	average
SS_i	0.0040	0.0045	0.0057	0.0076	0.0014	0.0035	0.0013	0.0095	0.0131	0.0118	0.0003	0.0014	0.0641	SSE
S_i^2	0.0020	0.0022	0.0029	0.0038	0.0007	0.0018	0.0006	0.0047	0.0066	0.0059	0.0001	0.0007	0.0027	MSE
													$t^{24}_{0.025}$=	2.0640
													LSD(0.05) =	0.0871

Table A.5 (continued). Statistics for Continuous Experiments (part 2 of 2).

Exp.		dark tio2 slurry h2o2	uv tio2 film cont.	dark tio2 film cont.	dark blank cont	dark tio2 slurry cont	dark h2o2 cont	dark tio2 film h2o2 cont.	uv only cont	uv tio2 slurry cont	uv tio2 film h2o2 cont.	uv h2o2 cont	uv tio2 slurry h2o2 cont
mean		0.7223	0.7030	0.6930	0.6900	0.6660	0.6570	0.6480	0.6363	0.6263	0.5460	0.2247	0.2200
uv tio2 slurry h2o2 cont	0.2200	0.5023 SIG!!	0.4830 SIG!!	0.4730 SIG!!	0.4700 SIG!!	0.4460 SIG!!	0.4370 SIG!!	0.4280 SIG!!	0.4163 SIG!!	0.4063 SIG!!	0.3260 SIG!!	0.0047	
uv h2o2 cont	0.2247	0.4977 SIG!!	0.4783 SIG!!	0.4683 SIG!!	0.4653 SIG!!	0.4413 SIG!!	0.4323 SIG!!	0.4233 SIG!!	0.4117 SIG!!	0.4017 SIG!!	0.3213 SIG!!		
uv tio2 film h2o2 cont.	0.5460	0.1763 SIG!!	0.1570 SIG!!	0.1470 SIG!!	0.1440 SIG!!	0.1200 SIG!!	0.1110 SIG!!	0.1020 SIG!!	0.0903 SIG!!	0.0803			
uv tio2 slurry cont	0.6263	0.0960 SIG!!	0.0767	0.0667	0.0637	0.0397	0.0307	0.0217	0.0100				
uv only cont	0.6363	0.0860	0.0667	0.0567	0.0537	0.0297	0.0207	0.0117					
dark tio2 film h2o2 cont.	0.6480	0.0743	0.0550	0.0450	0.0420	0.0180	0.0090						
dark blank cont	0.6570	0.0653	0.0460	0.0360	0.0330	0.0090							
uv tio2 film cont.	0.6660	0.0563	0.0370	0.0270	0.0240								
dark h2o2 cont	0.6900	0.0323	0.0130	0.0030									
dark tio2 slurry cont	0.6930	0.0293	0.0100										
dark tio2 film cont.	0.7030	0.0193											
dark tio2 slurry h2o2	0.7223												

APPENDIX B: 300 ML BATCH RESULTS

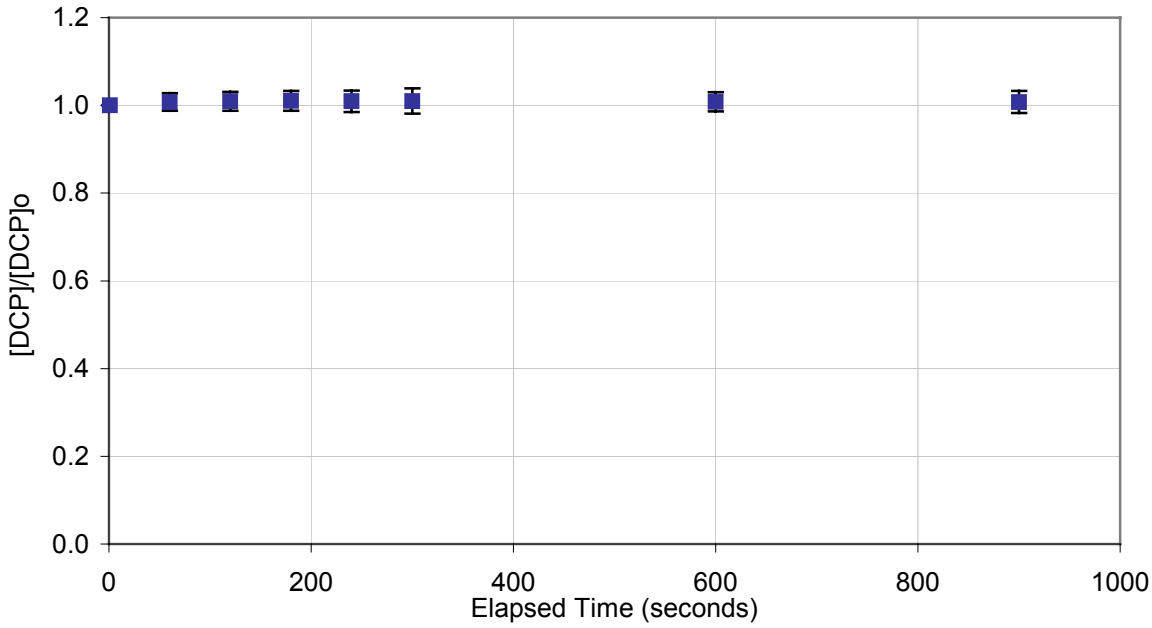

Figure B.1. Average Dark (blank) Batch Results.

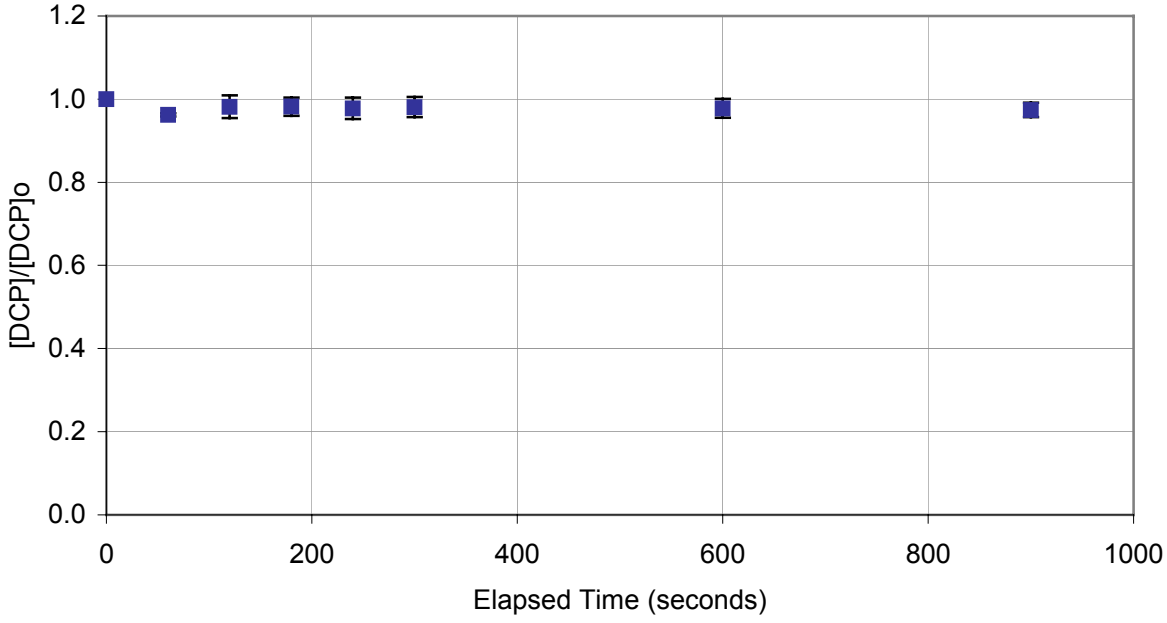

Figure B.2. Average Dark 750 ppm H2O2 Batch Results.

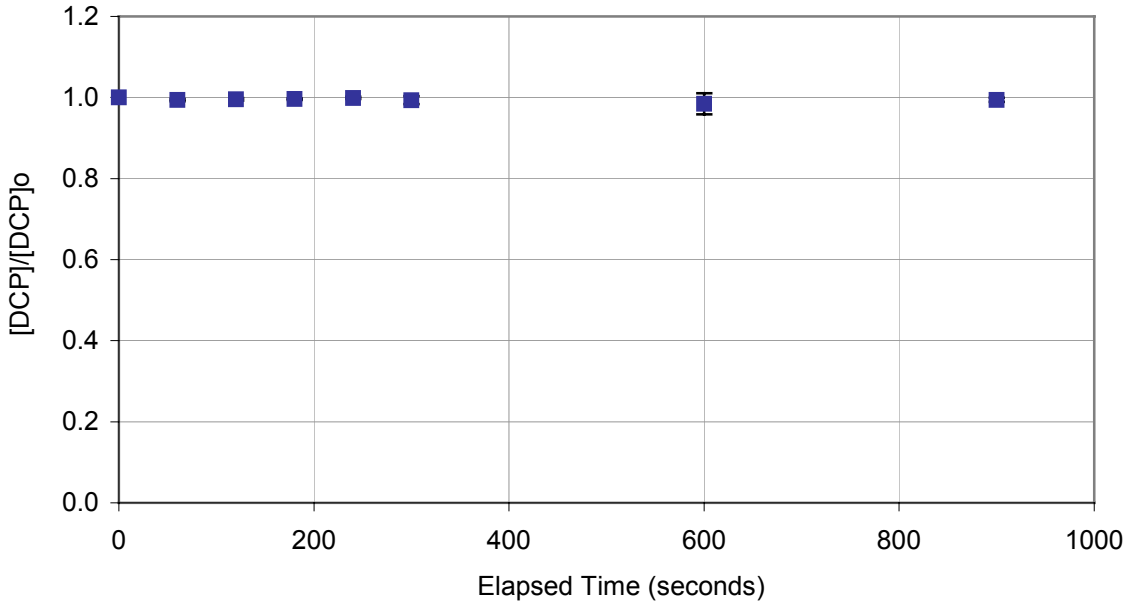

Figure B.3 Average Dark 0.05 wt% TiO2 (slurry) Batch Results.

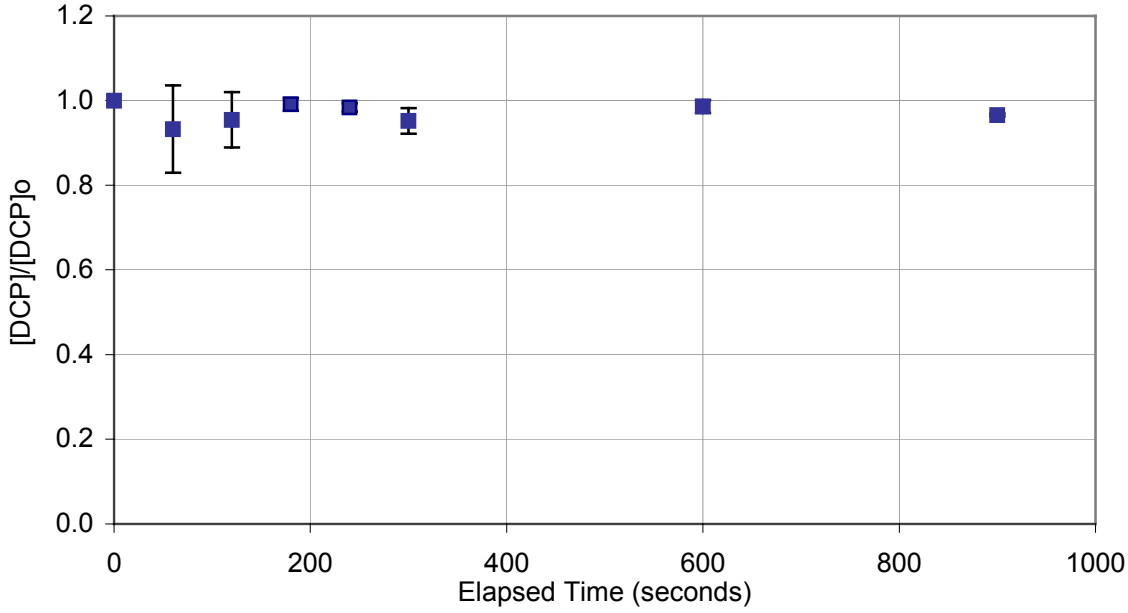

Figure B.4. Average Dark 0.05 wt% TiO2 (slurry) with 750 ppm H2O2 300mL Batch Results.

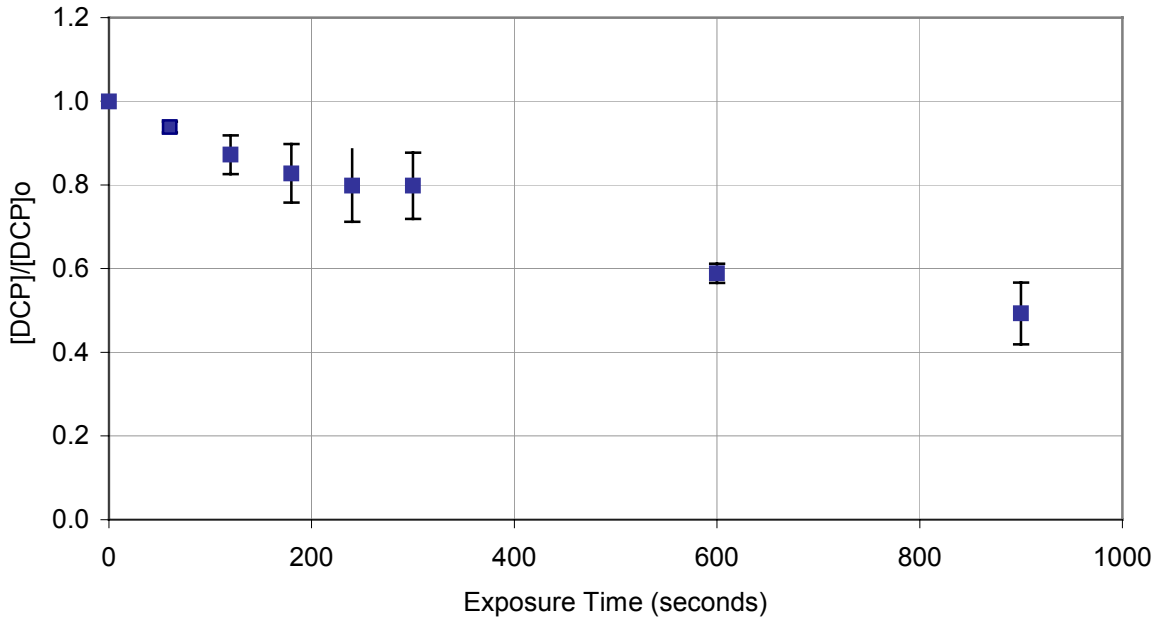

Figure B.5. Average UV Only (blank) Batch 300mL Results.

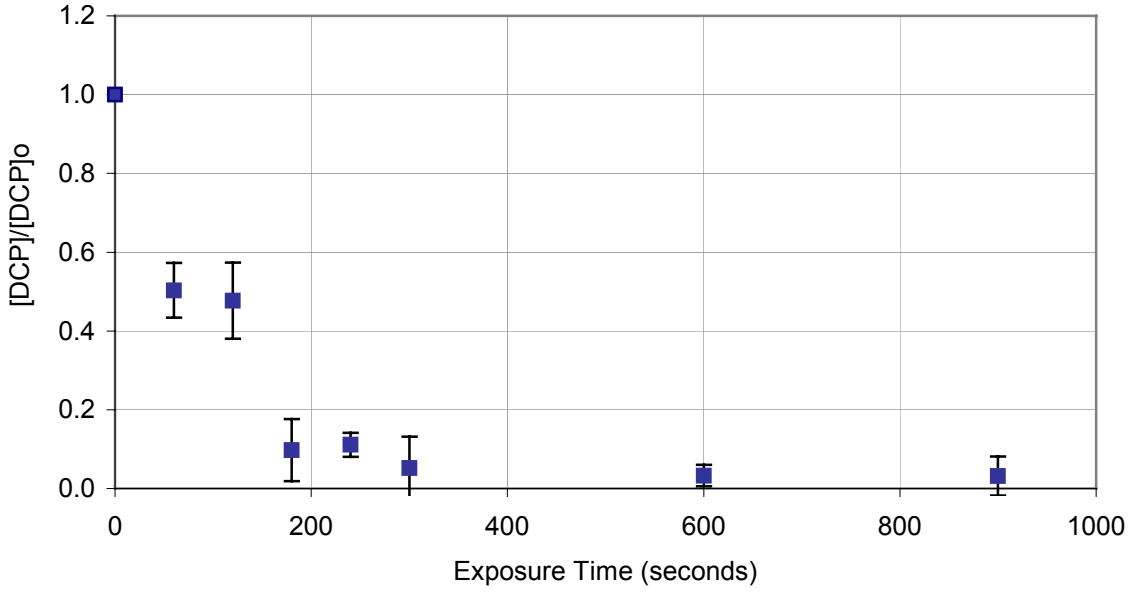

Figure B.6. Average UV/750 ppm H_2O_2 Batch 300mL Results.

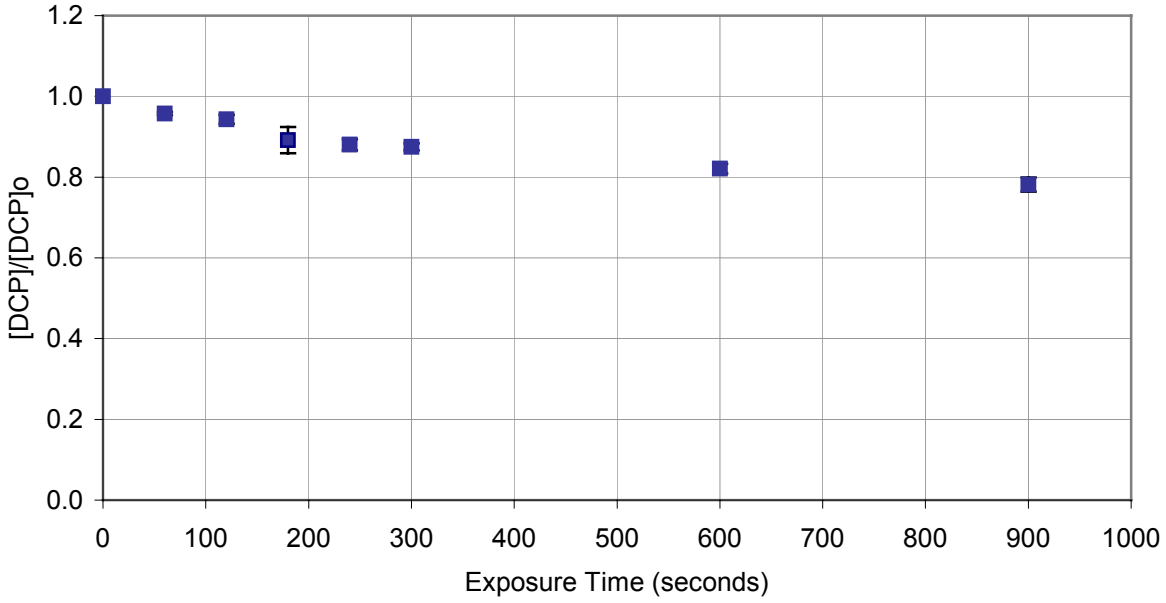

Figure B.7. Average UV/0.05 wt% TiO_2 in Slurry Batch 300mL Results.

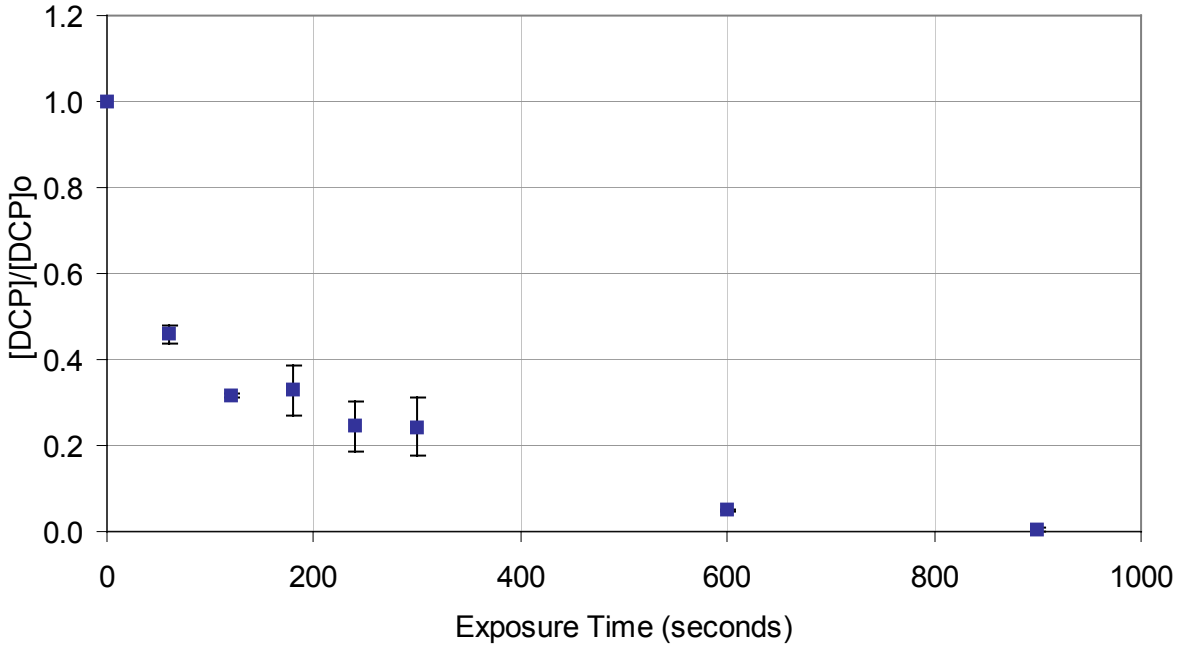

Figure B.8. Average UV/0.05 wt% TiO_2 in Slurry/750 ppm H_2O_2 300mL Batch Results.

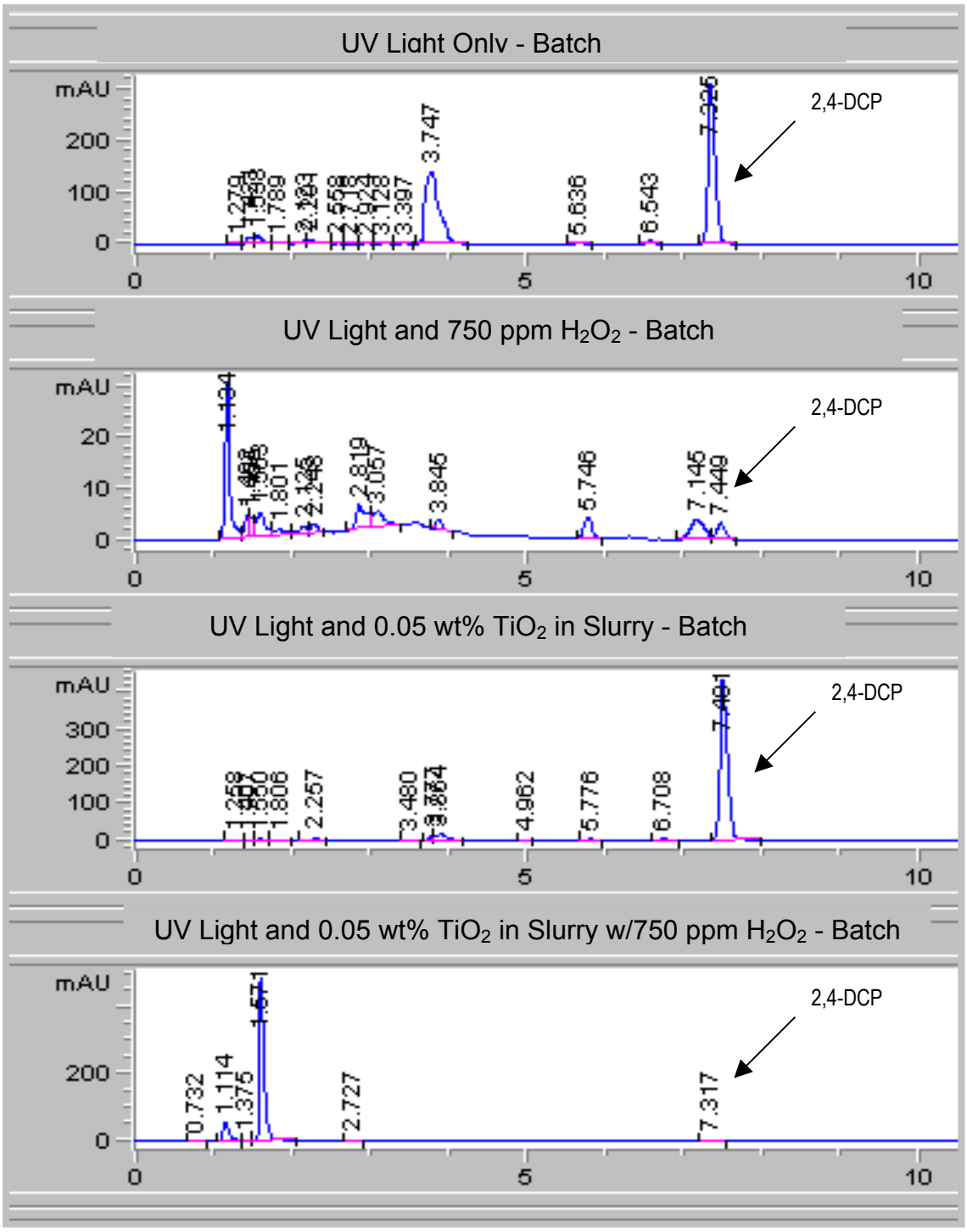

Figure B.9. Chromatographs After 15 Minutes of Exposure to UV Light in the Batch System.

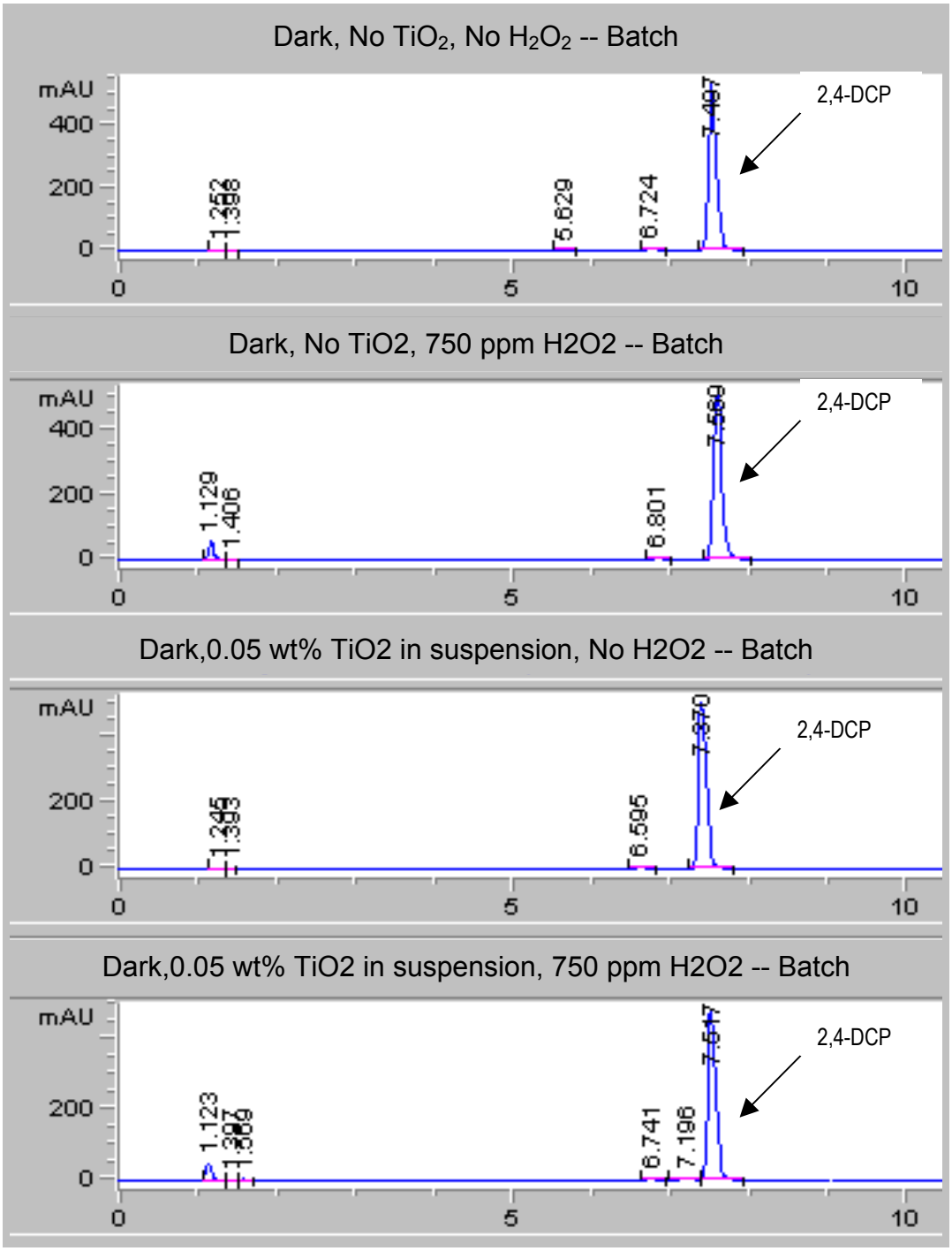

Figure B.10. HPLC Chromatographs After 15 Minutes of Elapsed Time in the Batch Reactor (no UV Exposure).

APPENDIX C: CONTINUOUS RESULTS

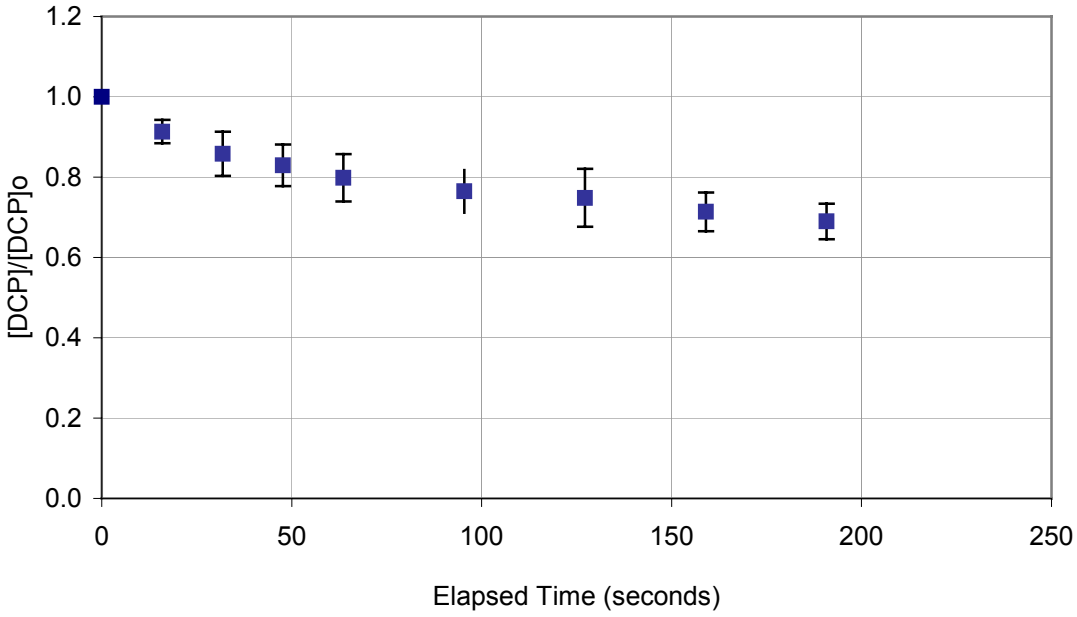

Figure C.1. Average Dark (blank) Continuous Results.

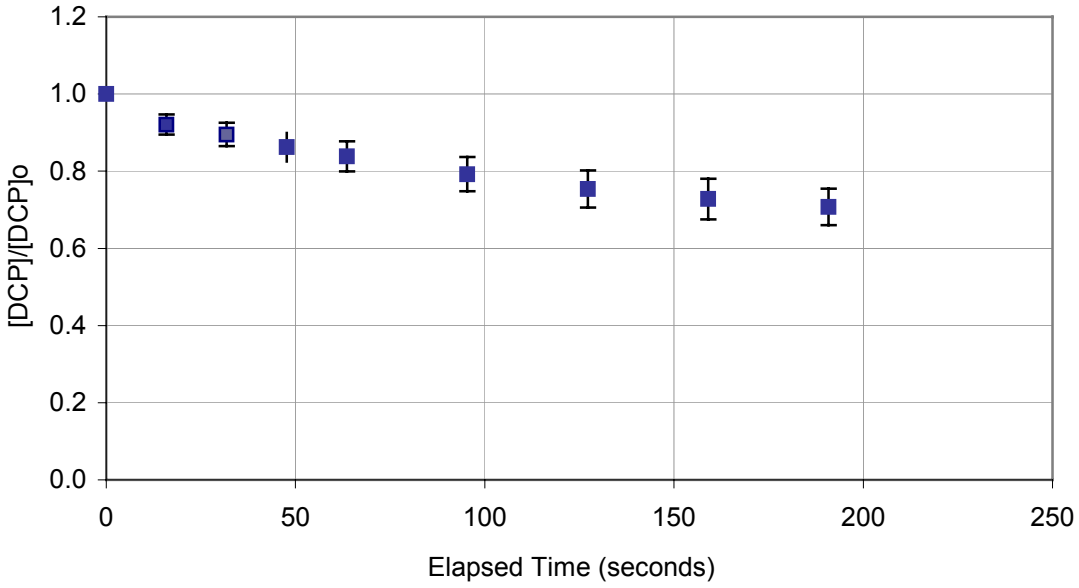

Figure C.2. Average Dark 750 ppm H_2O_2 Continuous Results.

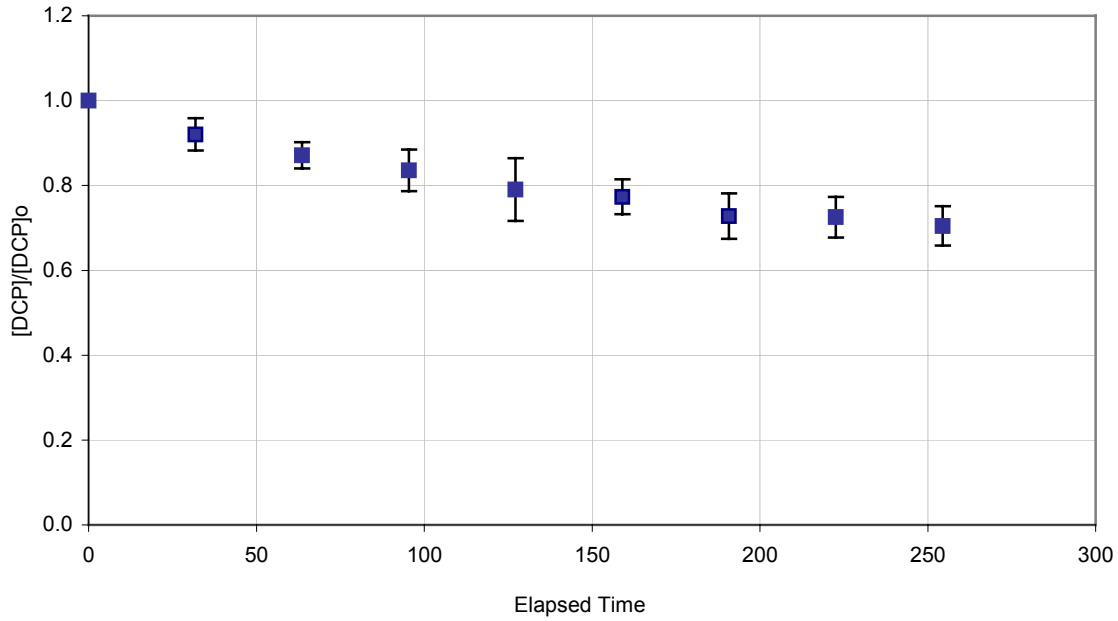

Figure C.3. Average Dark 0.05 wt% TiO_2 in Slurry Continuous Results.

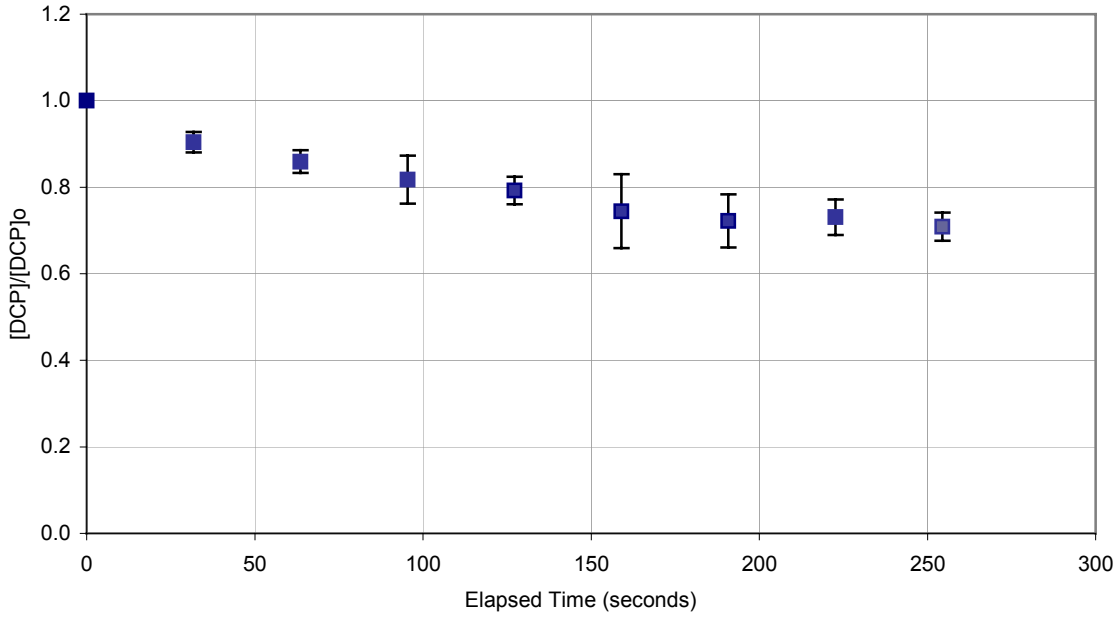

Figure C.4. Average Dark 0.05 wt% TiO_2 in Slurry/750 ppm H_2O_2 Continuous Results.

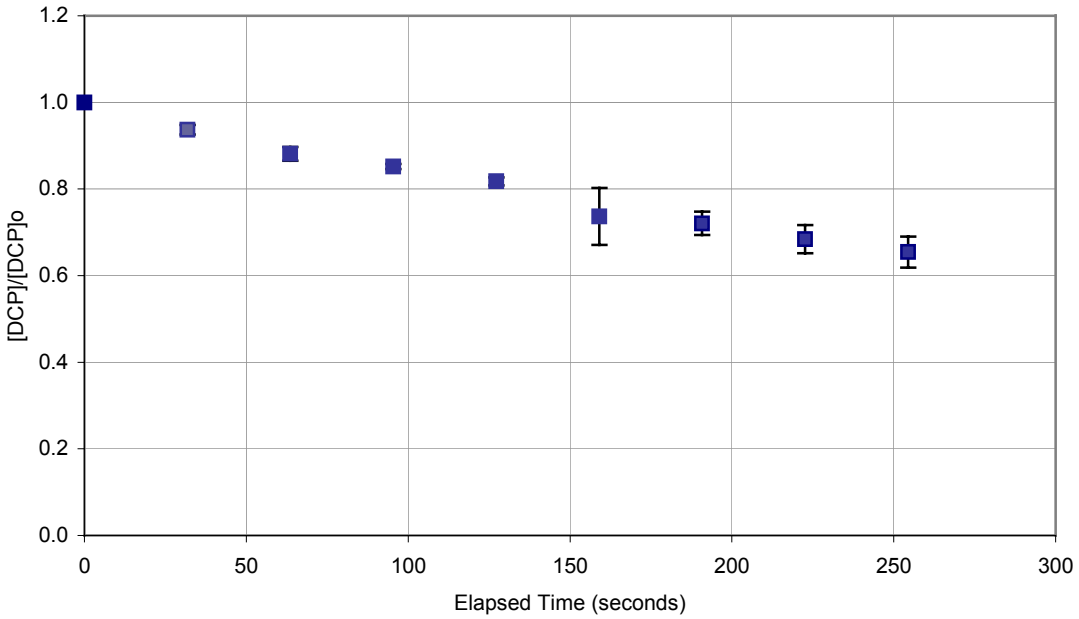

Figure C.5. Average Dark TiO_2 in Film Continuous Results.

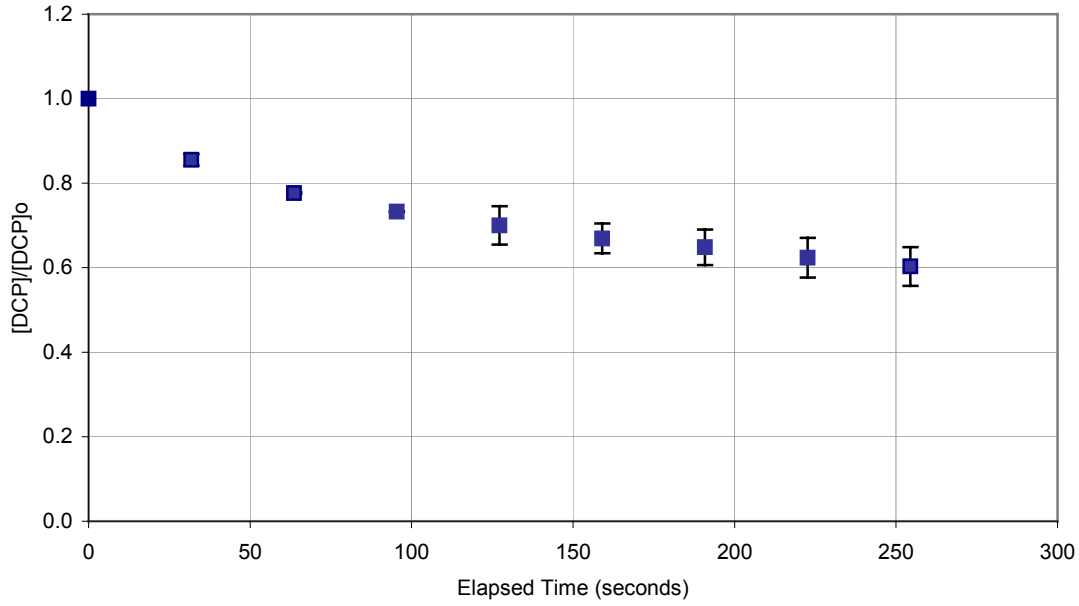

Figure C.6. Average Dark TiO_2 in Film/750 ppm H_2O_2 Continuous Results.

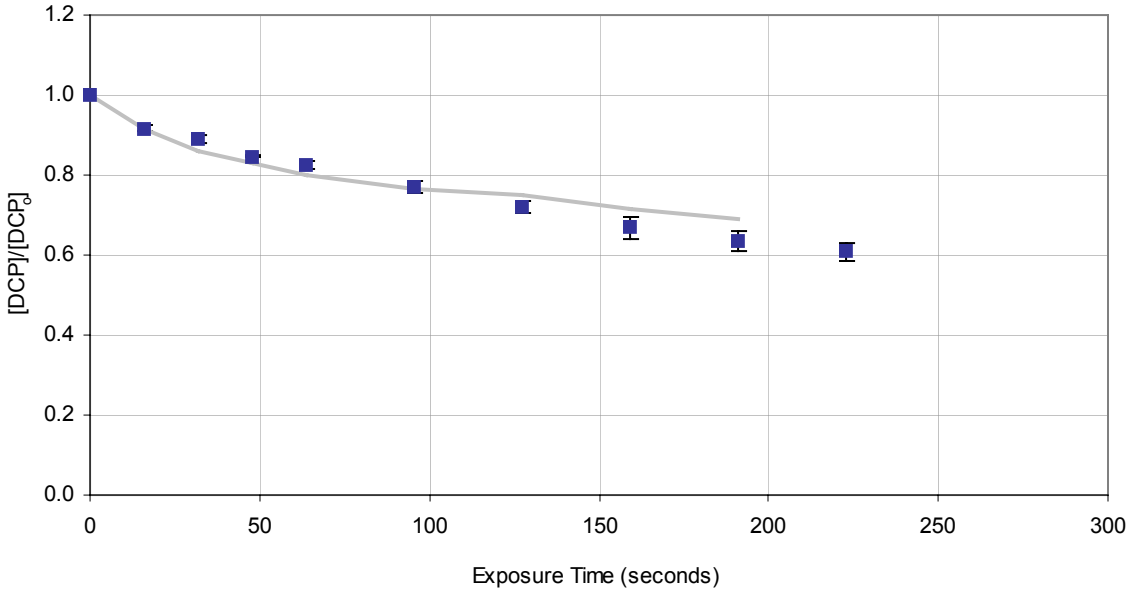

Figure C.7. Average UV (blank) Continuous Results (square data points). The gray line is the average loss of 2,4-DCP in dark blank continuous experiments.

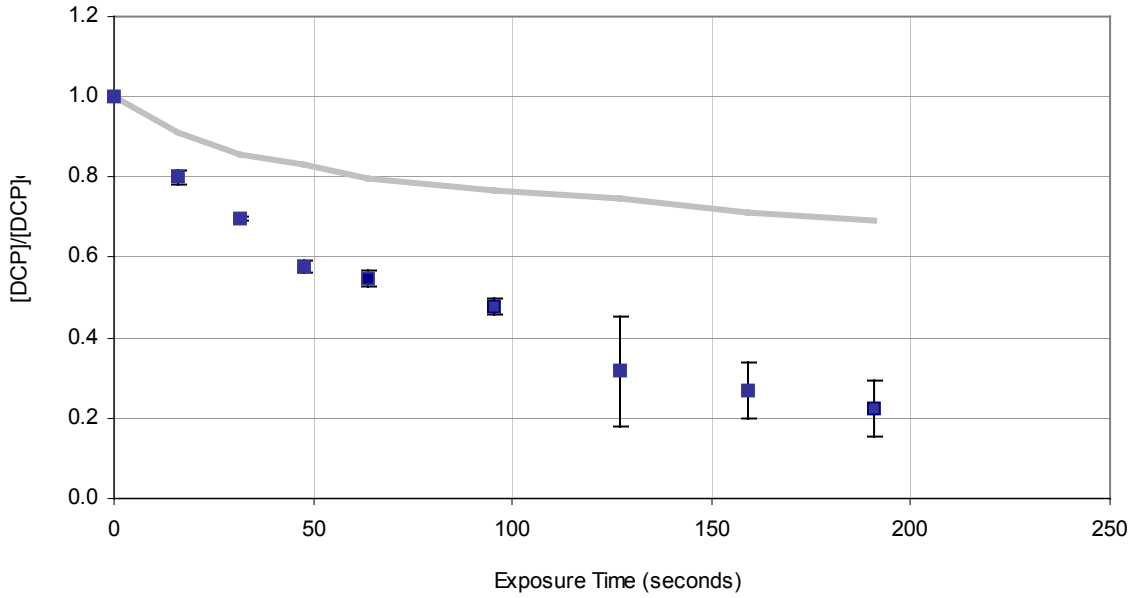

Figure C.8. Average UV 750 ppm H_2O_2 Continuous Results (square data points). The gray line is the average loss of 2,4-DCP in dark blank continuous experiments.

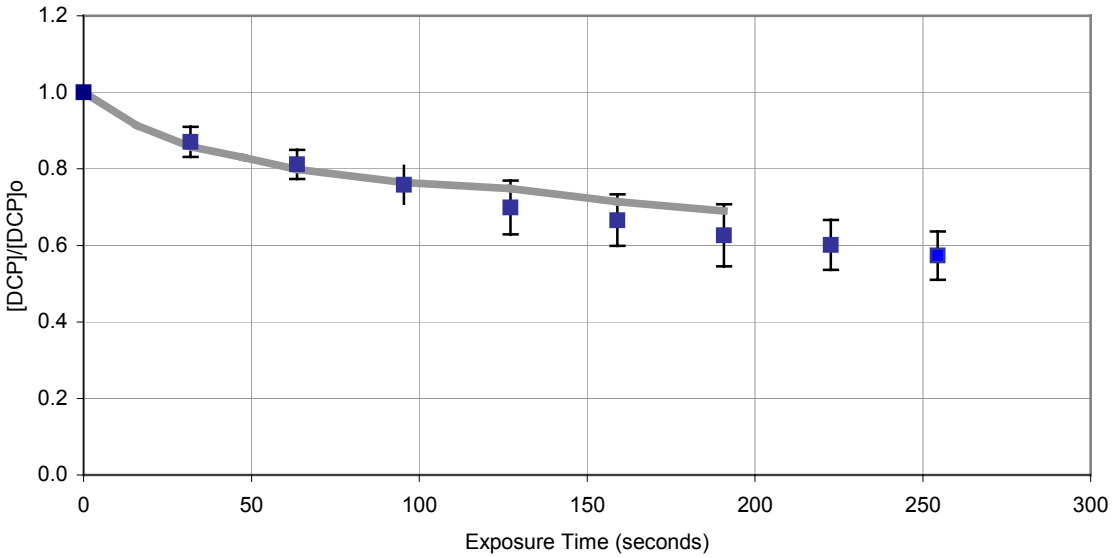

Figure C.9. Average UV 0.05 wt% TiO_2 in Slurry Continuous Results (square data points). The gray line is the average loss of 2,4-DCP in dark blank continuous experiments.

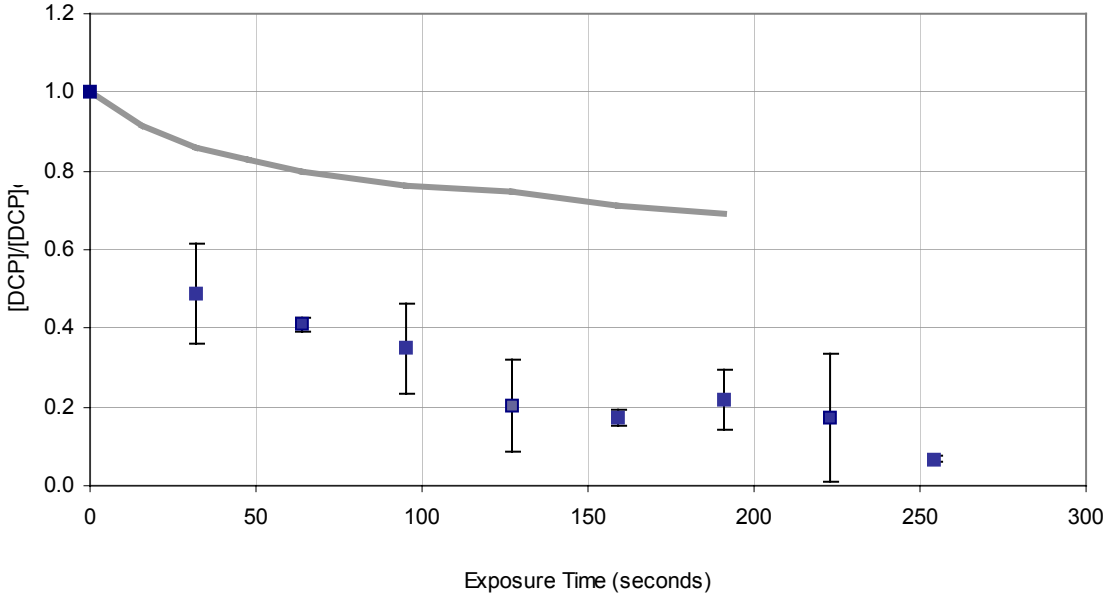

Figure C.10. Average UV 0.05 wt% TiO_2 in Slurry/750 ppm H_2O_2 Continuous Results (square data points). The gray line is the average loss of 2,4-DCP in dark blank continuous experiments.

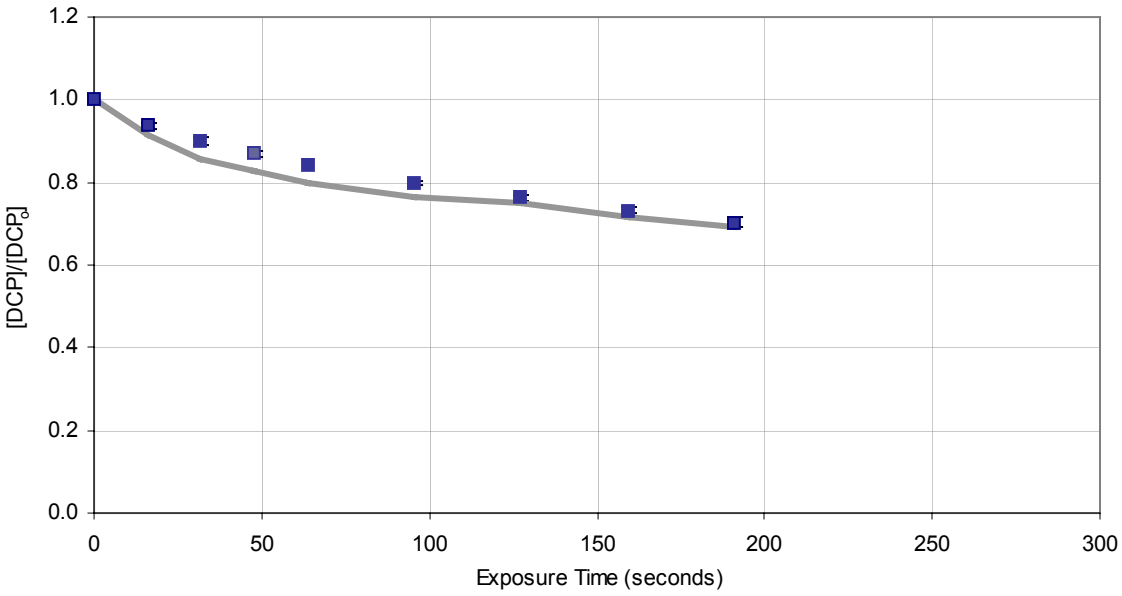

Figure C.11. Average UV TiO_2 in Film Continuous Results (square data points). The gray line is the average loss of 2,4-DCP in dark blank continuous experiments.

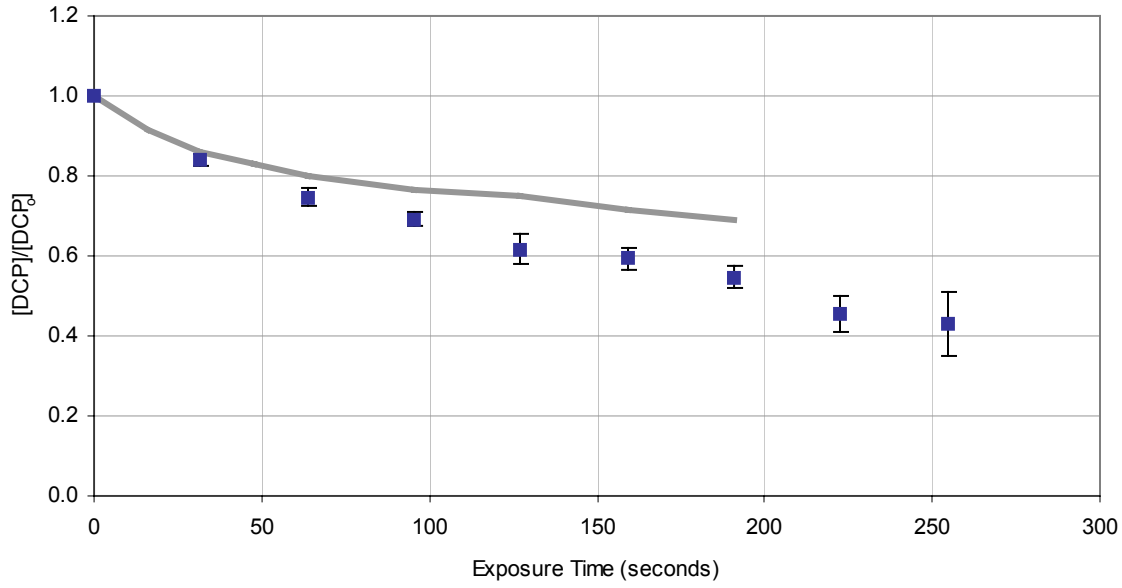

Figure C.12. Average UV TiO_2 in Film/750 ppm H_2O_2 Continuous Results (square data points). The gray line is the average loss of 2,4-DCP in dark blank continuous experiments.

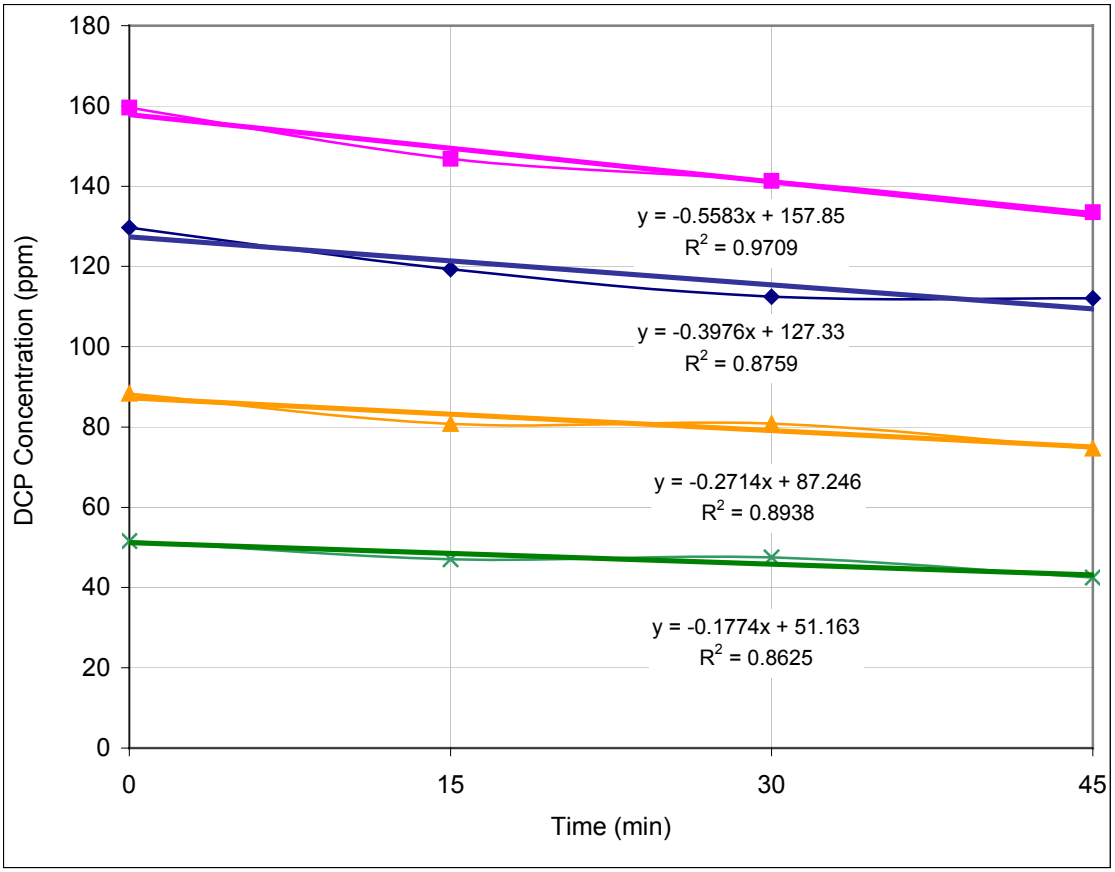

Figure C.13. The Disappearance of 2,4-Dichlorophenol in Closed Amber Jars with One-Inch Pieces of Masterflex Tubing at Four Unique Initial Concentrations.

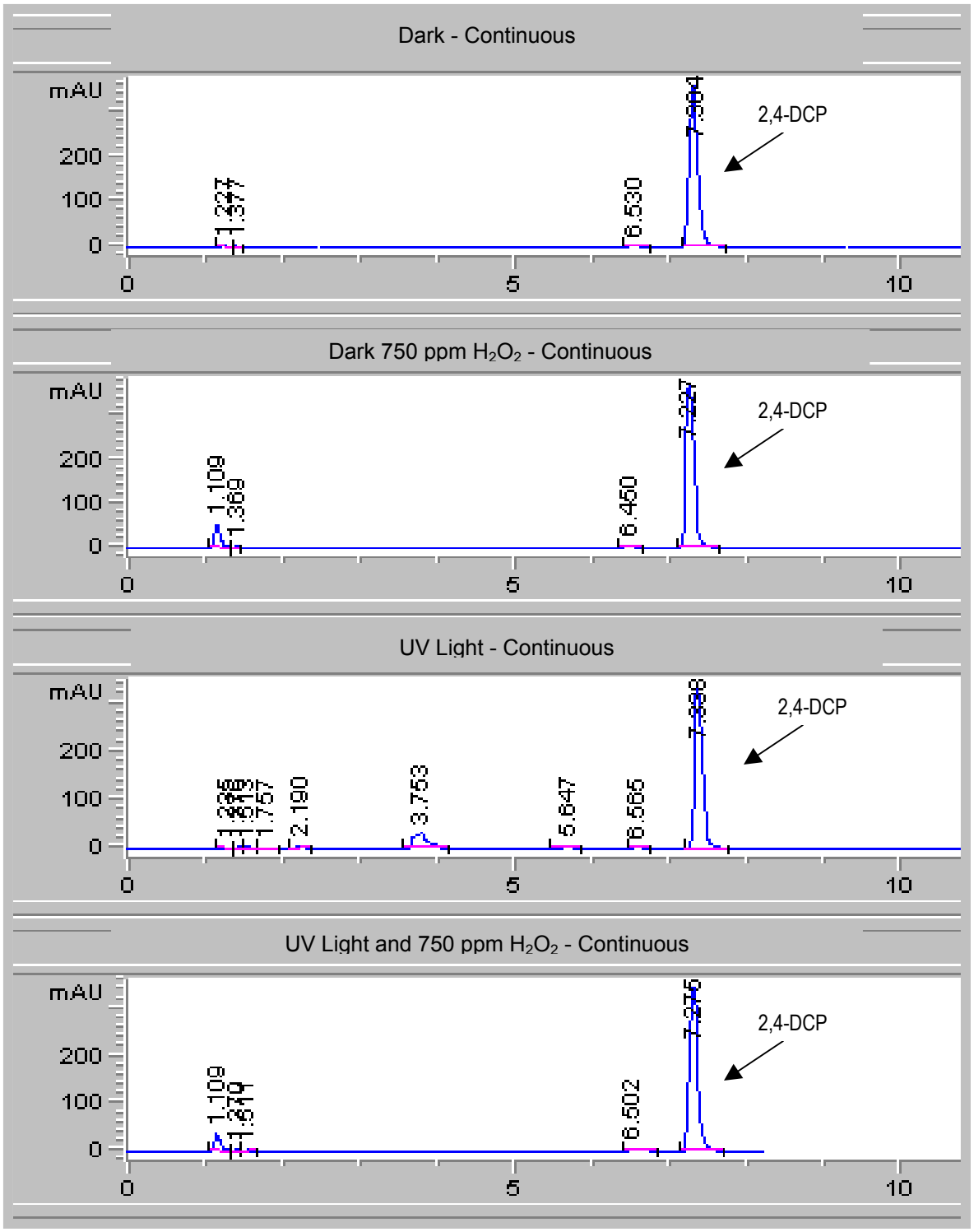

Figure C.14. The Appearance of Byproducts in Continuous UV only and UV/H_2O_2 Systems.

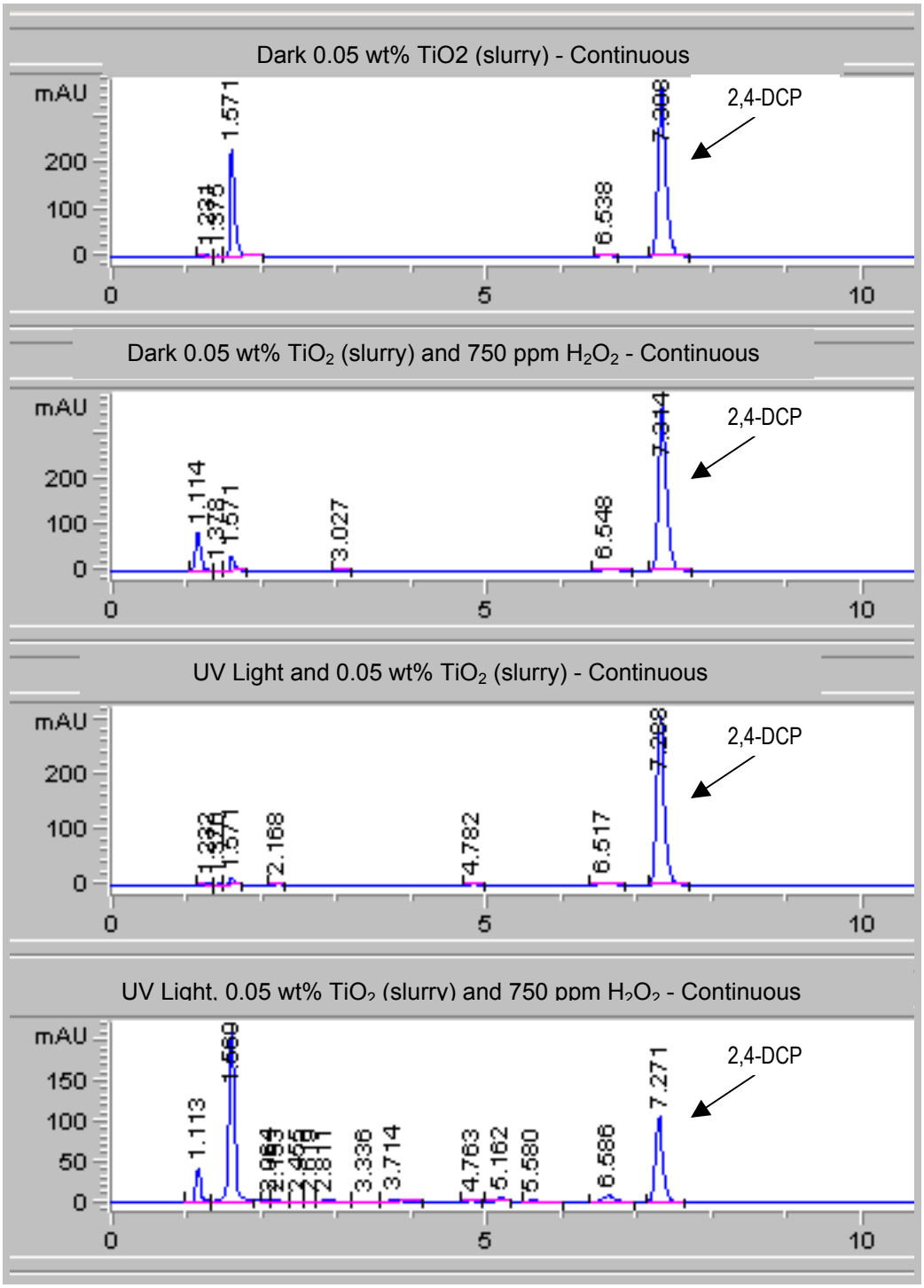

Figure C.15. The Appearance of Byproducts in Continuous Systems Utilizing TiO_2 in suspensions.

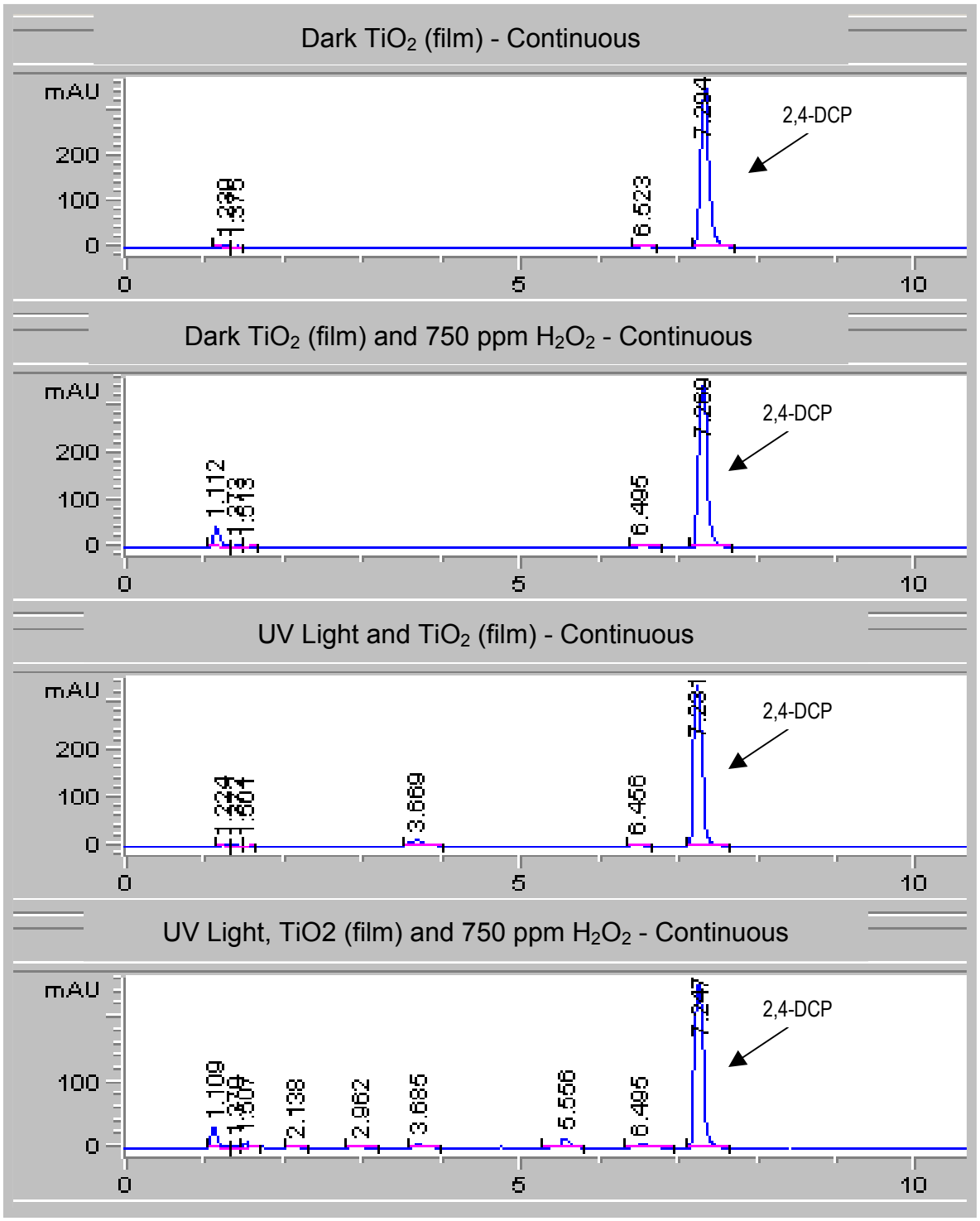

Figure C.16. The Appearance of Byproducts in Continuous Systems Utilizing TiO_2 in Thin Films of Mesoporous Silica.

12:37 PM

APPENDIX D: PSEUDO-FIRST ORDER REACTION RATE CONTSTANTS

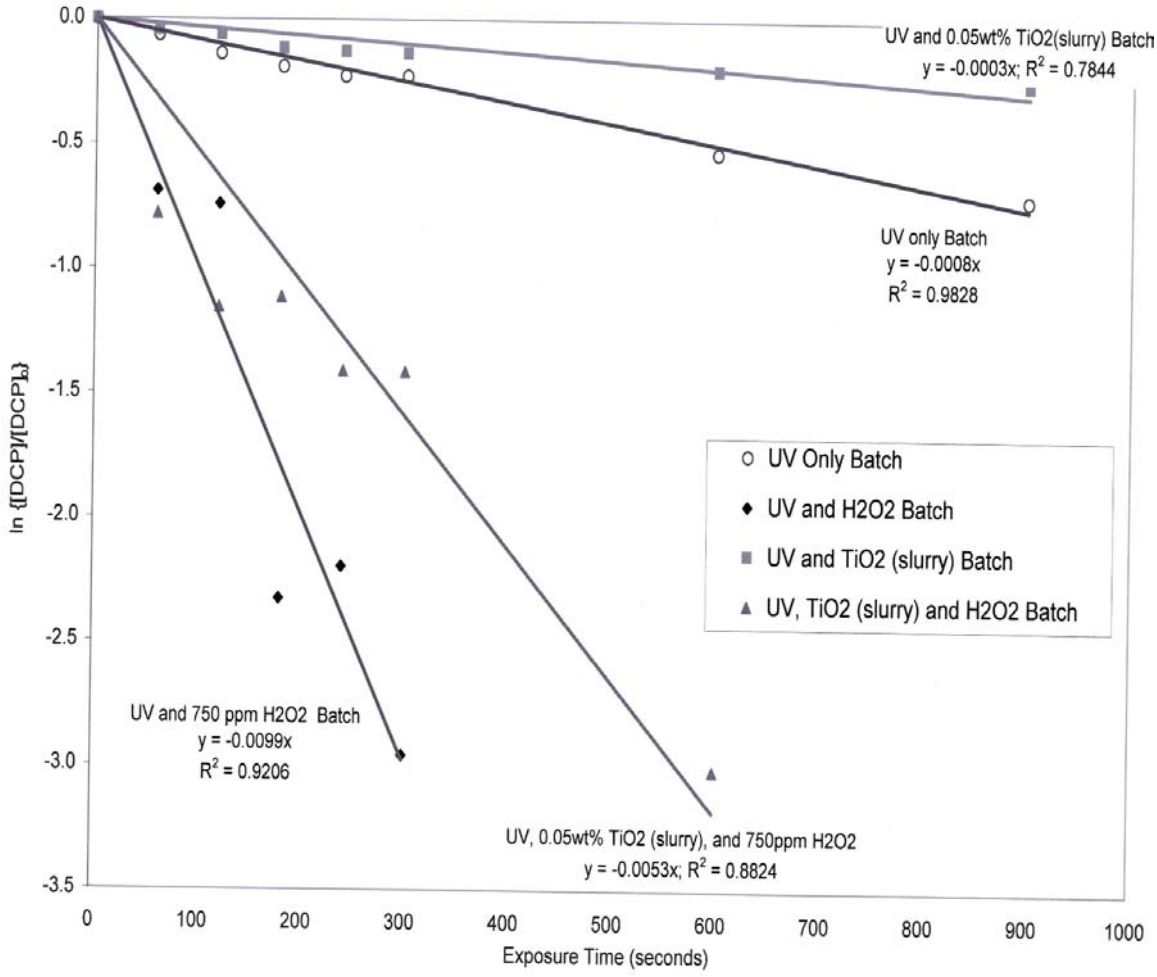

Figure D.1. Plots to Determine Pseudo-First Order Reaction Rates for the Photo-Oxidation of 2,4-Dichlorophenol in Batch UV Systems using 15 minutes of data.

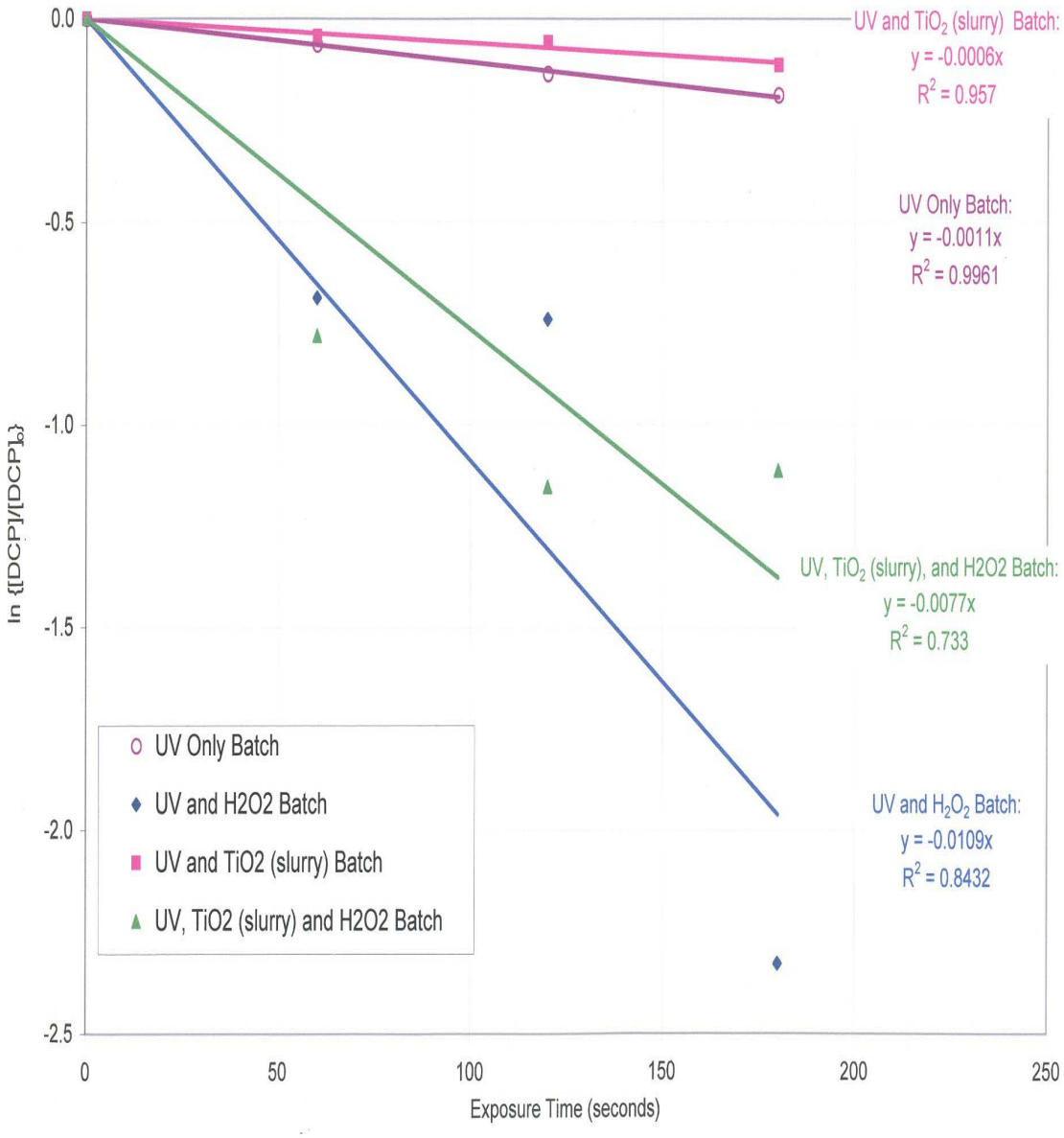

Figure D.2. Plots to Determine Pseudo-First Order Reaction Rates for the Photo-Oxidation of 2,4-Dichlorophenol in Batch UV Systems using 3 minutes of data.

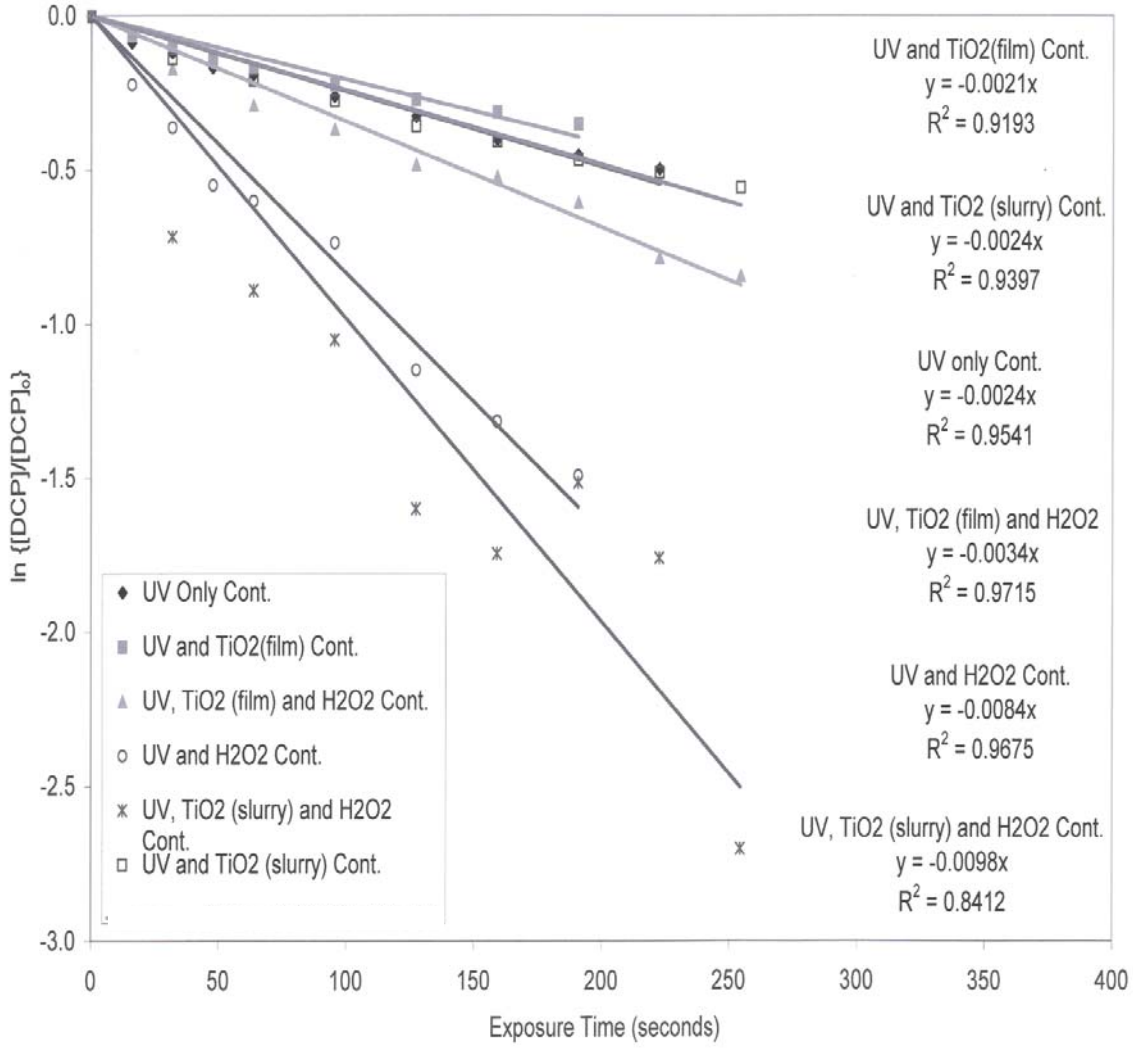

Figure D.3. Plots to Determine Pseudo-First Order Reaction Rates for the Photo-Oxidation of 2,4-Dichlorophenol Continuous UV Systems.

APPENDIX E: LANGMUIR-HINSHELWOOD KINETIC PLOTS

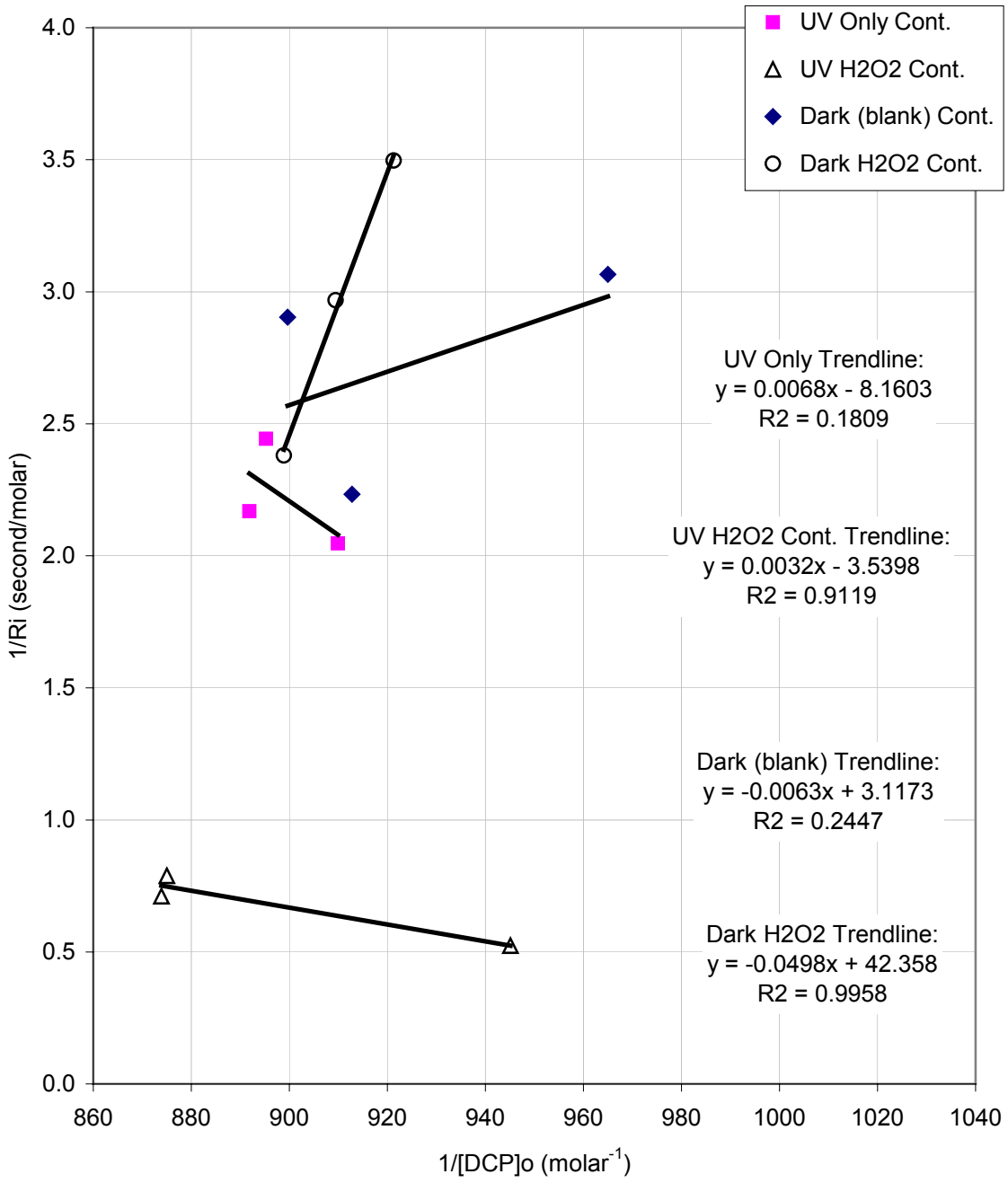

Figure E.1. Langmuir-Hinshelwood Kinetic Plots for Continuous dark (blank), dark H_2O_2, UV only, and UV/H_2O_2 Systems.

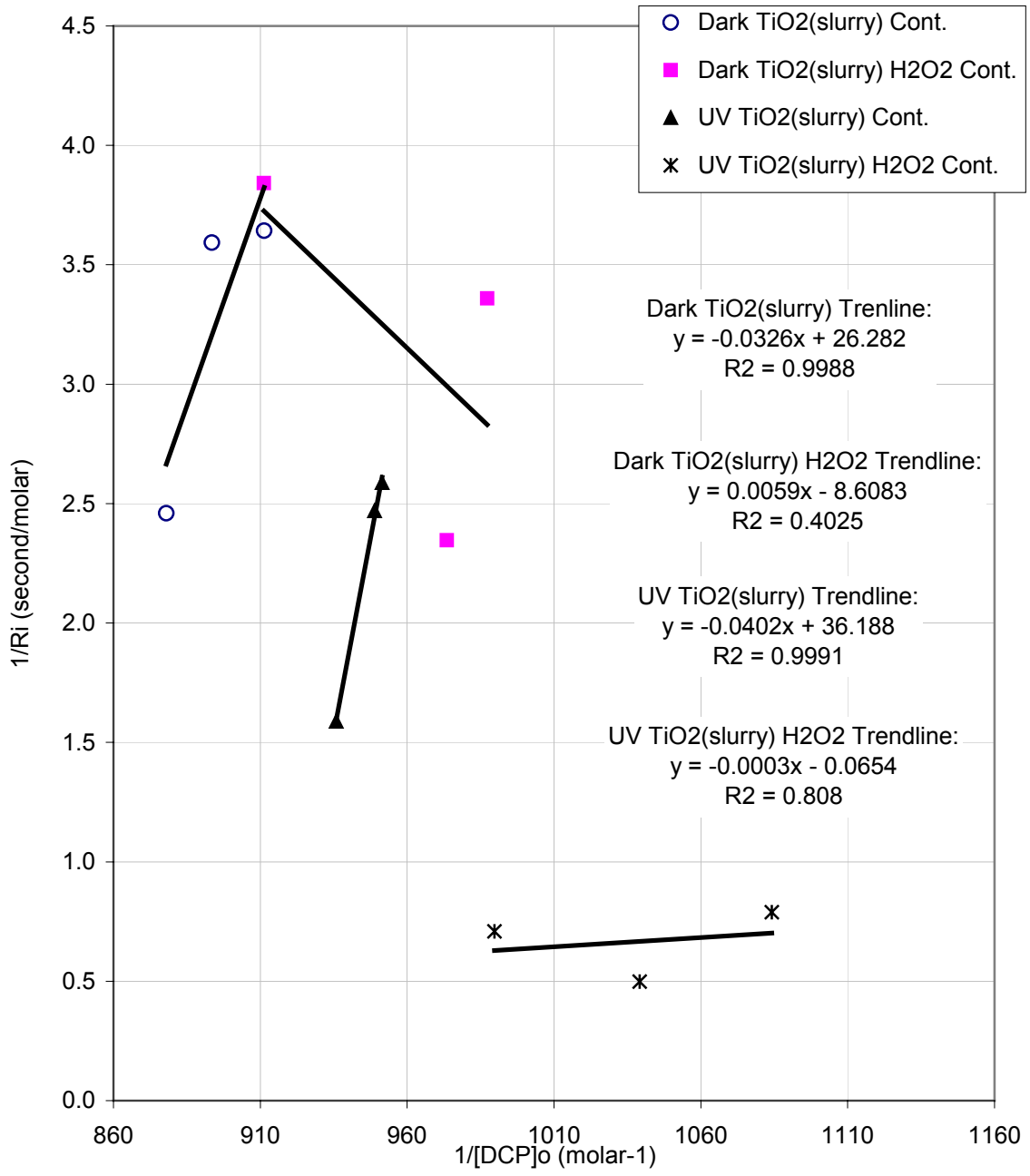

Figure E.2. Langmuir-Hinshelwood Kinetic Plots for Continuous Systems Utilizing TiO_2 in Suspension.

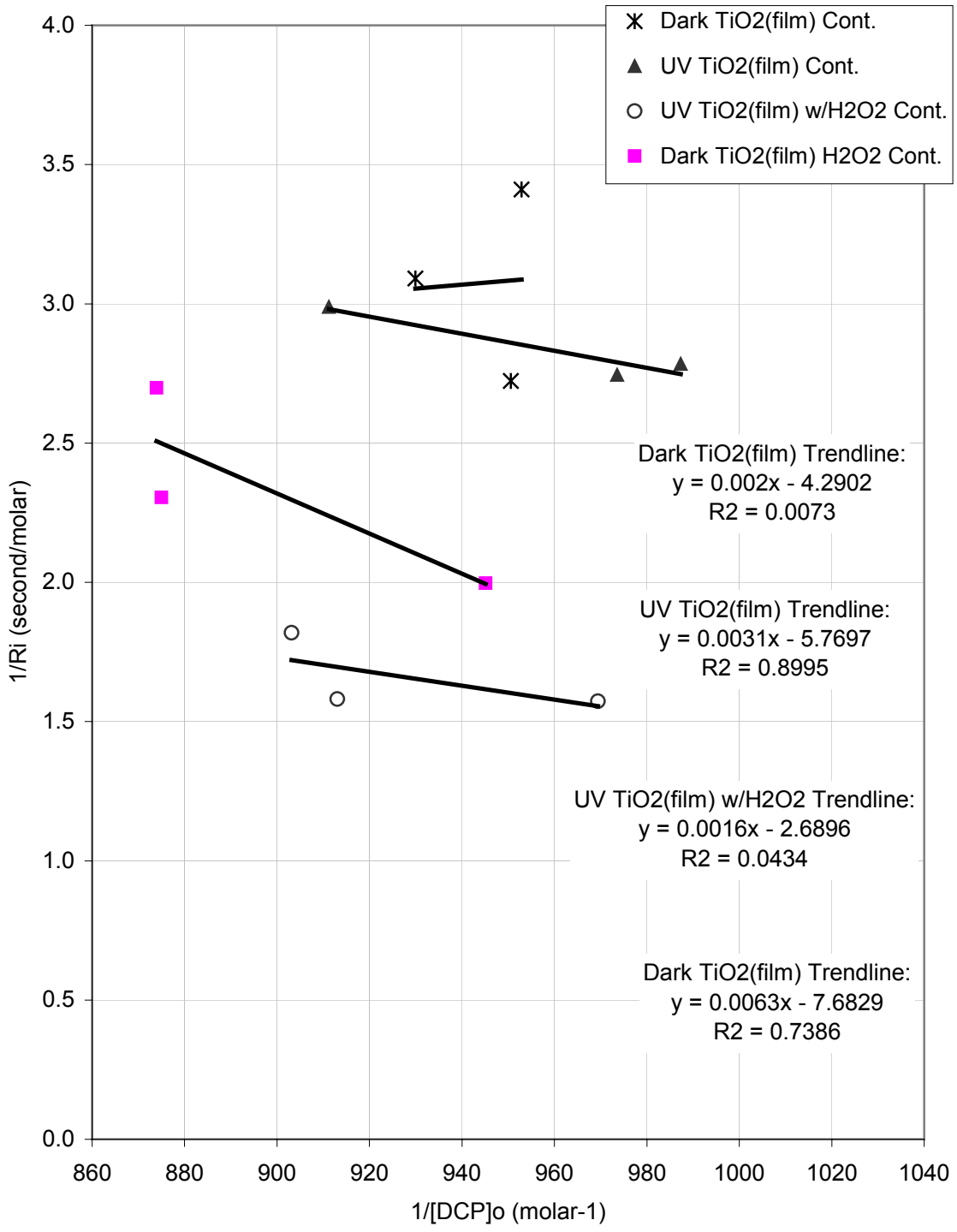

Figure E.3. Langmuir-Hinshelwood Kinetic Plots for Continuous Systems Utilizing TiO_2 in Thin Films of Mesoporous Silica.